E.O. Paton Electric Welding Institute of the National Academy of Sciences of Ukraine

International Scientific-Technical and Production Journal

The Paton WELDING JOURNAL

February 2013
No.2

Published since 2000

English translation of the monthly «Avtomaticheskaya Svarka» (Automatic Welding) journal published in Russian since 1948

Founders
E.O. Paton Electric Welding Institute of the NAS of Ukraine, International Association «Welding»

Publisher
International Association «Welding»

Translators:
A.A.Fomin, O.S.Kurochko, I.N.Kutianova, T.K.Vasilenko
Editor
N.A.Dmitrieva
Electron galley
D.I.Sereda, T.Yu.Snegiryova

Address
E.O. Paton Electric Welding Institute, International Association «Welding»
11, Bozhenko str., 03680, Kyiv, Ukraine
Tel.: (38044) 200 82 77
Fax: (38044) 200 81 45
E-mail: journal@paton.kiev.ua
www.paton.kiev.ua
URL: www.rucont.ru

State Registration Certificate
KV 4790 of 09.01.2001
ISSN 0957-798X

Subscriptions
$348, 12 issues per year, air postage and packaging included.
Back issues available.

CONTENTS

TECHNOLOGY OF HEAT TREATMENT OF PIPE JOINTS FROM STEEL OF K56 GRADE PRODUCED BY FLASH-BUTT WELDING

S.I. KUCHUK-YATSENKO[1], Yu.V. SHVETS[1], V.F. ZAGADARCHUK[1], V.I. SHVETS[1], V.I. KHOMENKO[2], S.I. ZHURAVLYOV[2] and A.Ya. SUDARKIN[2]

[1]E.O. Paton Electric Welding Institute, NASU
11 Bozhenko Str., 03680, Kiev, Ukraine. E-mail: office@paton.kiev.ua
[2]CJSC «Pskovelektrosvar»
3 Novatorov Str., 180680, Pskov, Russia. E-mail: info@pskovelectrosvar.ru

To determine the optimum mode of heat treatment of flash-butt welded joints of pipes from K56 steel the influence of soaking time and heat treatment temperature on impact toughness and yield limit was studied. Testing was performed in keeping with API 1104 and DNV-OS-F101 international standards. Metallographic examination of the influence of microstructure on strength properties of the joints in Neophot-32 light microscope and JAMP 2000F scanning electron microscope was conducted. Analysis of the obtained data allowed establishing the optimum heat treatment mode, at which the joints meet the normative requirements made of welds at construction of critical pipelines, including off-shore pipelines. 10 Ref., 11 Figures.

Keywords: *flash-butt welding, pipe steels, pipelines, welded joints, mechanical properties, microstructure, impact toughness, heat treatment, forced cooling*

Over the recent years construction of ultrahigh-capacity pipelines for gas and oil transportation was deployed in the Russian Federation. New generations of pipelines operate at higher pressures compared to traditional working pressure (gas pipelines — 100–200 atm, oil pipelines — 75–100 atm). Here, pipe wall thickness is increased (up to 39 mm) [1]. To save metal and lower the pipeline construction cost while preserving their reliability, requirements to mechanical properties of pipe metal, in particular, ductility properties, cold resistance and weldability are increased. In order to meet the high requirements made of pipes, metallurgical companies developed steels with ferritic-bainitic and bainitic structures.

At the same time higher requirements are now made of mechanical properties of circumferential pipe joints welded in site [2]. This pertains, primarily, to impact toughness properties at low testing temperatures.

Earlier we developed [3] the technology of flash-butt welding (FBW) of pipes from steels of K56 grade of 1219 mm diameter and 27 mm thickness, used for off-shore pipelines. Pipes were manufactured in keeping with TU 14-3-1573–96. Composition of pipe metal is as follows, wt.%: 0.06 C; 0.21 Si; 1.42 Mn; 0.12 Ni; 0.07 Mo; 0.04 V; 0.04 Al; 0.02 Ti; 0.05 Cr; 0.02 Nb; 0.004 S; 0.012 P. Such a composition implies lower content of carbon, and alloying by niobium, titanium and vanadium that in combination with the methods of thermomechanical treatment [4] ensures high strength and cold resistance required in pipeline operation.

Mechanical properties of pipe metal are as follows: σ_y = 484.4–493.5 MPa; σ_t = 546.7–556.8 MPa; KCV_{20} = 334.7–336.6 J/cm^2; KCV_{-40} = 333.0–336.6 J/cm^2; hardness $HV5$-1850–1950 MPa.

Required set of properties is achieved due to grain refinement, dispersion, dislocation, subgranular and solid solution strengthening [5]. Steel microstructure is a ferritic matrix with a small number of bainite and carbide inclusions (Figure 1). Size of ferrite grains elongated along the rolling direction is equal to 5–10 μm, that corresponds to point 10–11.

Steels of this type are thermally unstable. Welding heating leads to microstructural changes, which result in joint mechanical properties differing from those of the base metal.

Tensile testing showed that the ultimate strength of welded joints decreases by approximately 6 %, compared to base metal, and is equal to 520 MPa. Fracture runs at the distance of about 18–20 mm from the joint plane. According to microstructure (Figure 2) the fracture site corresponds to the section of high-temperature tempering, in which the joint hardness is minimum at approximately $HV5$-1700 MPa (Figure 3). It

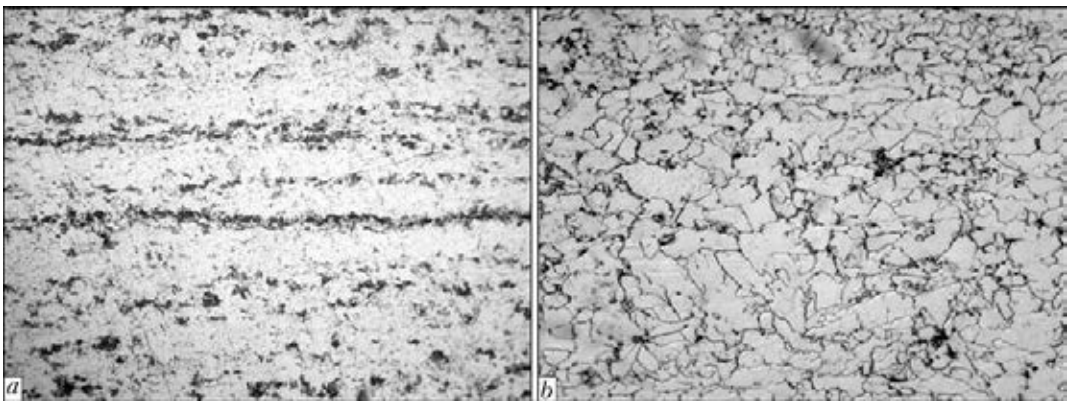

Figure 1. Pipe steel microstructures (*a* — ×100; *b* — ×400)

should be noted that directly in the butt joint zone after welding hardness is somewhat higher than that of base metal — approximately *HV*5-2100 MPa. Lowering of yield limit in the section of high-temperature tempering can be prevented by lowering the heat input in welding either by shortening the welding time, or by increasing the cooling rate.

Here bend testing showed that bend angle of all the welded joints was equal to 180 °C and the weld had no cracks. Impact bend testing turned out to be critical. Results of testing Charpy samples with a notch along the joint line show a slight lowering of impact toughness in the vicinity of the butt. While base metal impact toughness was 335.8 and 334.9 J/cm^2 at 20 and −20 °C, respectively, the average impact toughness in the section of the joint line decreased to 15.0 J/cm^2 at the temperature of 20 °C and to 8.1 J/cm^2 at −20 °C.

Achieved level of impact toughness does not meet the requirements of DNV-OS-F101 Off-Shore Standard [2].

As shown by metallographic examination, the low impact toughness is predetermined by metal microstructure in the joint zone. The structure consists of bainite with polygonal grains of proeutectoid ferrite along the boundaries of primary austenite grains (Figure 4, *a*), the size of which corresponds to point 3. Coarse grain and polygonal ferrite along the grain boundaries are known to be factors lowering the cold resistance [6].

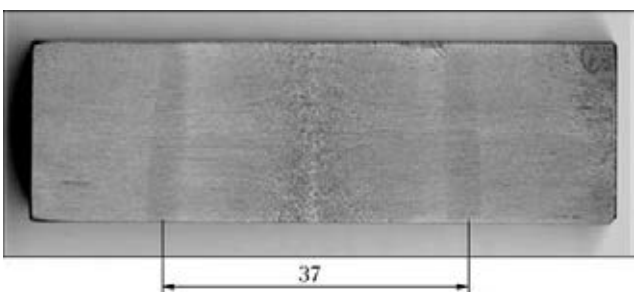

Figure 2. Macrostructure of pipe steel joints made by FBW

Increase of cooling rate after welding leads to reduction of the volume fraction of proeutectoid ferrite and greater dispersity of bainite (Figure 4, *b*). However, it only slightly increases the impact toughness from 6.9 up to 8.1 J/cm^2 at −40 °C.

It is known [7] that recrystallization at normalizing improves weld microstructure. It is believed to be rational to apply local high-temperature treatment in the butt area to improve the impact toughness.

Given below are the results of investigations on development of basic technology of heat treatment (HT) of FBW joints of pipes from steel 10G2FB (TU 14-3-1573–96).

Local heating of welded joints 320 mm wide with removed flash was performed with a single-turn enclosing inductor heater of 2.4 kHz frequency.

Temperature monitoring was performed by the following schematic: temperature sensor — sensor signal normalizer — analog-digital converter — computer. Multichannel modules with individual galvanic decoupling in the channels of HL-7B 30-06 type providing output signal of 0–10 V DC voltage at thermo-emf variation in the range of 0–50 mV were used as signal normalizers. Stand-alone twelve-digit analog-digital

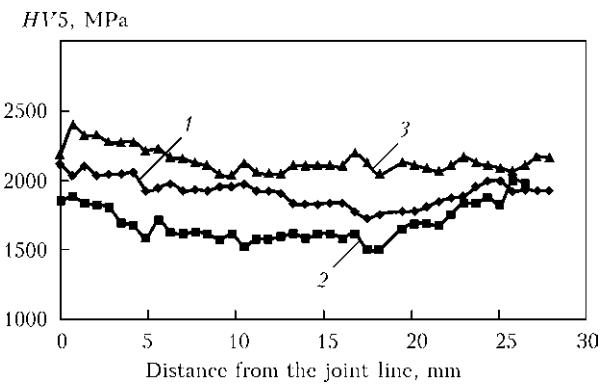

Figure 3. Distribution of *HV*5 hardness in the welded joint: *1* — after welding and cooling in air; *2* — after HT and cooling in air; *3* — after HT and cooling by water-air mixture

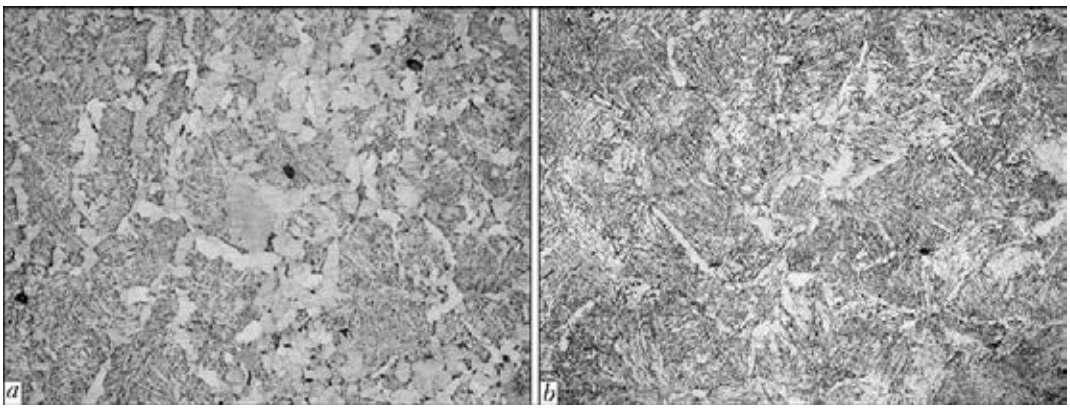

Figure 4. Microstructures (×100) of pipe steel welded joint after its cooling in air (*a*) and in water (*b*)

converter of ADS-12E type was connected to a notebook type computer vie a parallel interface. Temperature sensors were chromel-alumel thermocouples of 0.5 mm diameter, which were welded to samples by capacitor-type welding in the heating zone.

Cooling was performed either in air, or forcedly from two sides by an air-water sprayer.

Evaluation of impact toughness values of the joints after HT was conducted on Charpy samples with a sharp-notch in the joint plane, located normal to the pipe surface, at –20 °C temperature. Testing was performed in certified PWI laboratory for mechanical testing.

Metallographic examination was conducted in Neophot-32 light microscope after section etching in 4 % alcohol solution of nitric acid.

HT mode includes the following components: heating rate, heating temperature, time of soaking at constant temperature, rate of cooling after soaking.

Criterion for selection of the heating rate is producing a uniform temperature field by sample thickness. Conducted investigations revealed that uniform heating of butt joints up to 950 °C temperature across the entire thickness is achieved in 5 min.

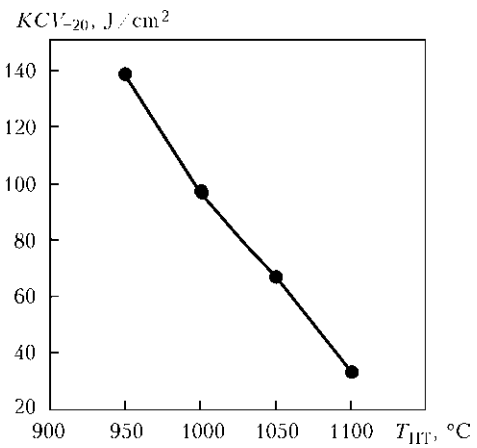

Figure 5. Dependence of average values of joint impact toughness on HT temperature

Lower limit of normalizing temperature was determined on the basis of dylatometric analysis of steel performed in Gleeble unit. According to dilatometric curves, at heating duration of 5 min complete austenitizing is achieved at temperature A_{c3} = 911 °C. Considering the experience of conducting the normalizing ensuring temperature rise by 30–40 °C above point A_{c3}, the lower temperature of normalizing was taken to be 950 °C.

At development of optimum HT mode normalizing temperatures in the range of 950–1100 °C were considered.

According to the results of testing the joints (Figure 5), average values of impact toughness KCV_{-20} decreased monotonically from 140 J/cm^2 at 950 °C to 38 J/cm^2 at 1100 °C with HT temperature rise.

Metallographic examination of the joint after HT showed that metal microstructure in the joint zone is a ferritic matrix with islet inclusions of residual austenite (Figure 6).

Ferritic matrix is granular and consists predominantly of polygonal mesoferrite, formation of which along the joint line, unlike the metal layers adjacent to the joint line, is caused by metal decarbonization in this section.

Structurally non-uniform sections with increased carbon content are observed in residual austenite (Figure 7). Evidently, residual austenite partially decomposes. The decomposition product is the structure described in [7–10] as granular bainite, which is a mechanical mixture of bainitic α-phase and carbides.

HT temperature increase leads to ferrite grains growing from 3–10 μm at 950 °C up to 10–30 μm at 1050 °C (see Figure 6, *a–c*). At 1100 °C temperature (Figure 6, *d*) growth of ferrite grains is somewhat suppressed. However, volume fraction of residual austenite in the matrix increases.

It is known [7] that increase of grain size and quantity of the second phase are exactly the factors, lowering the cold resistance. This accounts

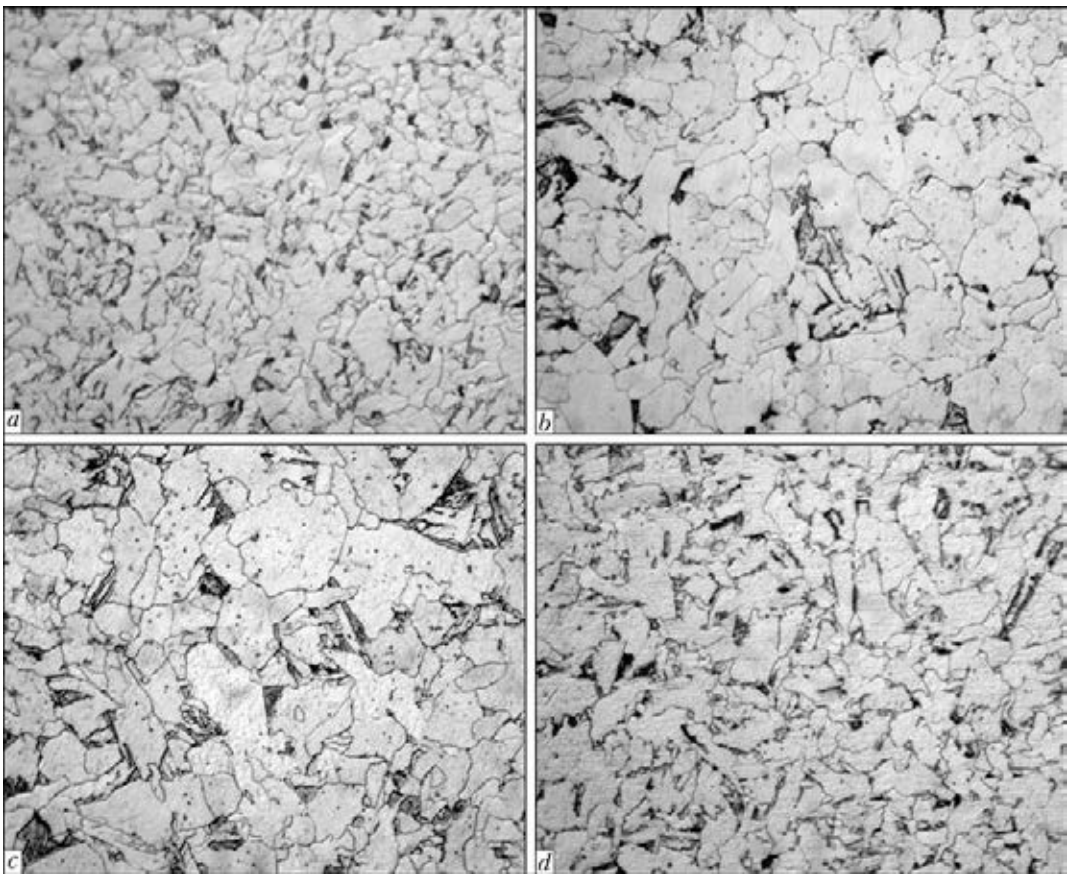

Figure 6. Microstructures (×1000) of metal in the zone of butt welded joints after HT at temperature of 950 (*a*), 1000 (*b*), 1050 (*c*) and 1100 (*d*) °C

for the shape of the curve of temperature dependence of impact toughness.

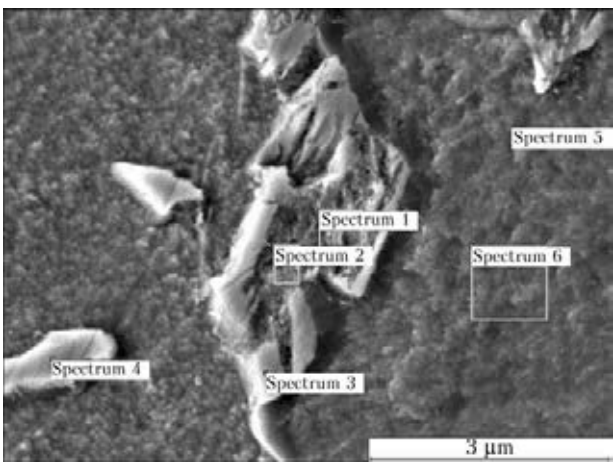

Spectrum number	C	O	V	Fe
1	2.37	2.23	0	95.41
2	3.20	2.35	0.86	93.59
3	1.81	1.33	0	96.86
4	1.48	1.27	0	97.25
5	1.01	0.88	0.43	97.68
6	1.24	1.13	0.13	97.50

Figure 7. Microstructure and chemical inhomogeneity of residual austenite, wt.%

1000 °C is the optimum HT temperature, allowing for the possible non-uniformity of the temperature field across the item thickness.

Figure 8 illustrates the influence of the time of sample soaking at normalizing temperature (1000 °C) on impact toughness value. Average value of impact toughness at 1 min soaking time was equal to 47 J/cm^2 (minimum values for individual samples do not exceed 30 J/cm^2).

Increase of soaking duration above 1 min leads to impact toughness increase. It is obvious that 1 min is insufficient for complete recrystallization of steel.

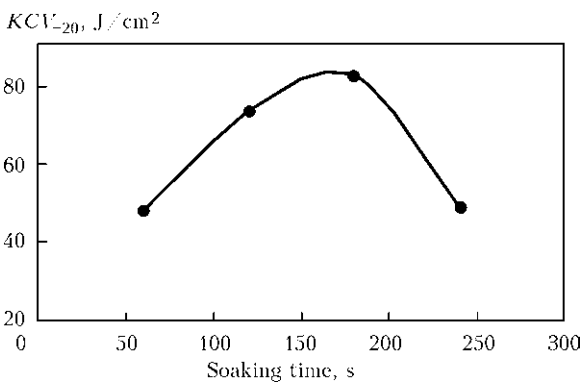

Figure 8. Dependence of average values of impact toughness on soaking at T_{HT} = 1000 °C

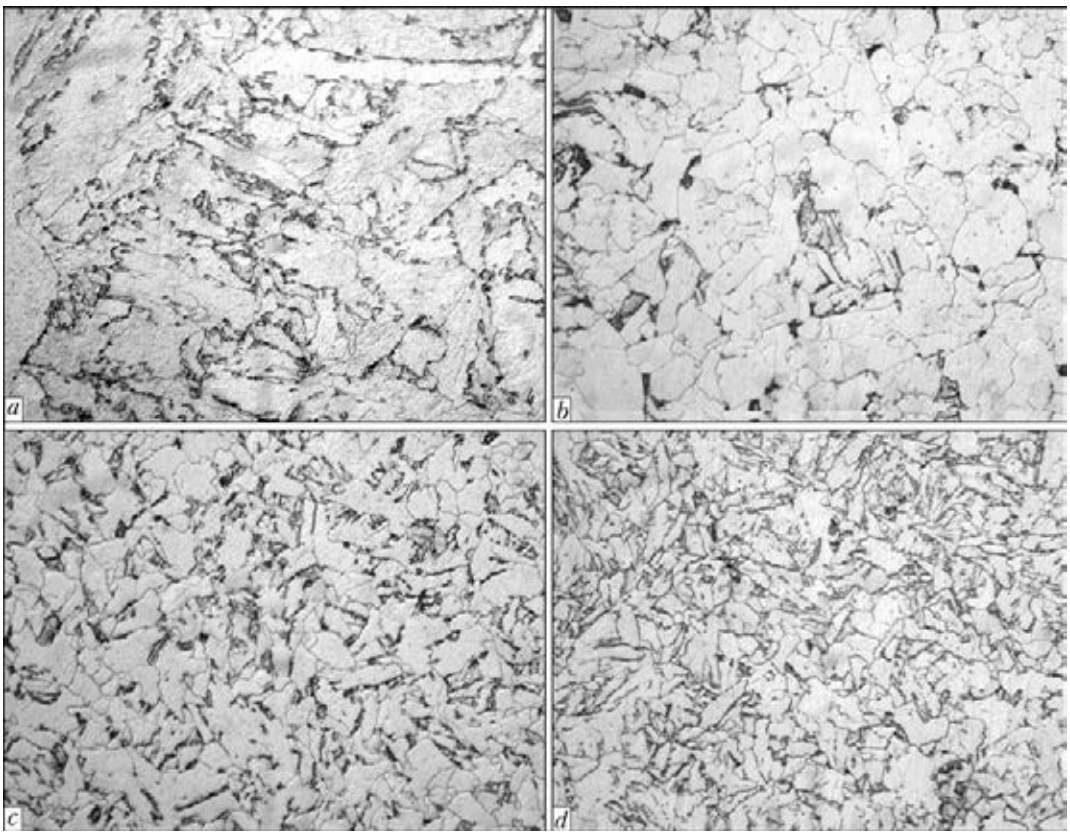

Figure 9. Microstructures (×1000) of metal in the zone of butt welded joints after HT at 1000 °C with soaking for 1 (*a*), 2 (*b*), 3 (*c*) and 4 (*d*) min

Dependence of impact toughness on soaking time is of an extreme nature. The highest and most stable KCV_{-20} values were obtained in the range of 2.5–3.0 min, and were equal to more than 80 J/cm^2. Increase of soaking duration above 3 min leads to impact toughness lowering and at 4 min soaking the impact toughness was equal to about 50 J/cm^2.

An abrupt lowering of impact toughness at soaking time longer than 3 min is due to a change in metal microstructure. Thus, while at 2 min soaking the matrix mostly consists of polygonal mesoferrite (Figure 9, *b*), at 4 min soaking feathery-acicular ferrite (Figure 9, *d*) prevails, which is identified as the product of shear transformation, unlike mesoferrite, forming by the diffusion mechanism. Residual austenite is located along ferrite needles.

Formation of such a microstructure occurs, probably, due to austenitic matrix enrichment in carbon and, consequently, inhibition of mesoferrite formation and increase of the fraction of residual austenite.

Joint line enrichment in carbon is possible as a result, on the one hand, of homogenizing of its concentration in the joint at HT (after welding the joint line is depleted in carbon) and, on the other hand, as a result of decomposition of thermally unstable vanadium carbides. Both the processes develop in time that is reflected on the curve of impact toughness dependence on HT duration.

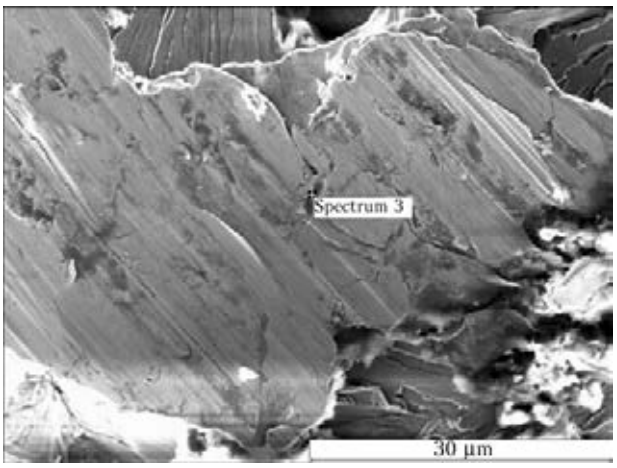

Figure 10. Fragment of joint fracture surface

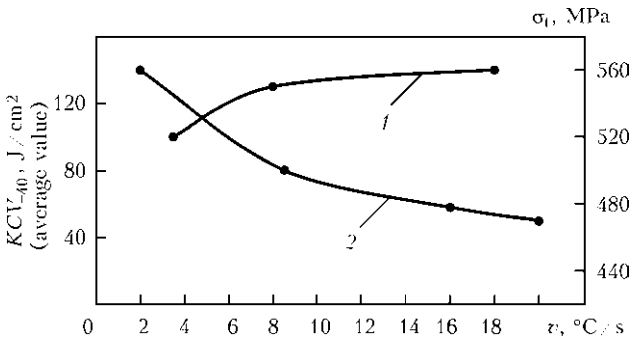

Figure 11. Dependence of tensile strength (*1*) and impact toughness (*2*) on cooling rate at HT

Indirect confirmation of diffusion-induced redistribution of carbon in the matrix was obtained at investigation of joint fractures. Fracture surface showed sections with high carbon content. In spectrum 3 (Figure 10) element content is as follows, at.%: 58.78 C; 5.79 O; 35.44 Fe.

Rate of cooling after HT has a dual influence on the joint properties: on the one hand, its increase leads to improvement of the joint strength properties and, on the other hand, toughness properties decrease (Figure 11). Optimum cooling rate, in terms of ensuring the set of mechanical properties, is in the range of 8–12 °C/s. At such cooling rates the indices of welded joint ultimate strength are preserved on the level of base metal strength.

Proceeding from analysis of the above data and allowing for the possible non-uniform heating of large-diameter pipes under the conditions of the actual construction, the following mode of pipe HT can be realized: heating temperature of 1000 °C, soaking time of 2.5–3.0 min, cooling by water-air mixture.

The above results of mechanical testing of the joints after basic HT show that they meet the requirements made of circumferential pipe joints [2].

Conclusions

1. Basic technology of HT of FBW joints on thick-walled pipes from steels of K56 grade was developed, which ensures compliance to the requirements of DNV-OS-F101 and API 1104 made of mechanical properties of welds for underwater pipelines.

2. Optimum temperature of welded joint normalizing is equal to 950–1000 °C, soaking duration at this temperature is equal to 2.5–3.0 min, cooling rate should be within 8–12 °C/s.

3. Rate of heating at HT does not have any essential influence on joint toughness values.

1. Morozov, Yu.D., Matrosov, M.Yu., Nastich, S.Yu. et al. (2008) High-strength pipe steels of new generation with ferrite-bainite structure. *Metallurg,* **8**, 39–42.
2. (2000) *DNV-OS-F101*: Offshore standard. Submarine pipeline systems. Jan. 2000.
3. Kuchuk-Yatsenko, S.I., Shvets, Yu.V., Zagadarchuk, V.F. et al. (2012) Flash-butt welding of thick-walled pipes from high-strength steels of K56 strength class. *The Paton Welding J.*, **5**, 2–7.
4. Pogorzhelsky, V.I., Litvinenko, V.I., Matrosov, Yu.I. et al. (1979) *Controlled rolling*. Moscow: Metallurgiya.
5. Heisterkamp, F., Hunna, K., Matrosov, Yu.I. et al. (1999) *Niobium-containing low-alloy steels*. Moscow: Intermet Engineering.
6. Livshits, L.S., Khakimov, A.N. (1989) *Metals science of welding and heat treatment of welded joints*. Moscow: Mashinostroenie.
7. Grabin, V.F., Denisenko, A.V. (1978) *Metals science of welding of low- and medium-alloy steels*. Kiev: Naukova Dumka.
8. Svishchenko, V.V. (1995) *Structure and mechanism of formation of granular bainite*: Transact. of I.I. Polzunov Altaj STU. Barnaul: AltGTU.
9. Kremnev, L.S., Svishchenko, V.V., Cheprasov, D.P. (1997) Structure and mechanism of granular bainite formation in 20Kh2NAch steel. *Metallovedenie i Termich. Obrab. Metallov*, **9**, 6–9.
10. Svishchenko, V.V., Cheprasov, D.P., Shabalin, V.N. et al. (2008) Formation of intermediate structure of granular morphology in low-carbon low-alloy steel under the conditions of step-isothermal decomposition of austenite. *Polzunovsky Almanakh*, **3**.

Received 29.11.2012

METHODS OF CONTROL OF SILICON OXIDE ACTIVITY IN SLAG MELTS

I.A. GONCHAROV[1], **V.I. GALINICH**[1], **D.D. MISHCHENKO**[1], **R.N. SHEVCHUK**[1], **A.N. DUCHENKO**[1] and **V.S. SUDAVTSOVA**[2]

[1]E.O. Paton Electric Welding Institute, NASU
11 Bozhenko Str., 03680, Kiev, Ukraine. E-mail: office@paton.kiev.ua
[2]3 Krzhizhanovskogo Str., 03142, Kiev, Ukraine. E-mail: post@ipms.kiev.ua

Silicon oxide is included into composition of fluxes for welding of carbon and low-alloy steels. To predict the metallurgical and welding-technological properties of fluxes, it is important to know their activity in slag melt. The aim of the present work is to develop the methods of in-process evaluation of activity (effective concentration) of silicon oxide SiO_2 in slag melts and to define the methods of its control. The design of unique electrolytic sensor has been developed. The application of alloy, containing 5 wt.% Si as the second electrode allowed increasing the heat resistance of the sensor up to 1500 °C. Using the designed sensor, the procedure was suggested for determination of SiO_2 activity in slag melts by using the method of electromotive forces, which guarantees the accuracy in measurement of electromotive forces within 1–2 mV ranges. This procedure can be applied in metallurgy directly in the melting process, as well as in the development of welding consumables. It was found that increase in MgO content in slag melt of $MgO–Al_2O_3–SiO_2–CaF_2$ system causes the reduction in silicon oxide activity, that can be explained by the formation of refractory and thermodynamically stable silicates and aluminates of magnesium. The effect of additions (1 wt.%) of metals on the SiO_2 activity in melts of $MgO–Al_2O_3–SiO_2–CaF_2$ system was determined. The feasibility of control of thermodynamic activity of silicon oxide in slags in welding and, respectively, the processes of silicon reduction and formation of non-metallic inclusions in welds is shown. 5 Ref., 3 Tables, 1 Figure.

Keywords: *arc welding, high-strength steels, slag melts, thermodynamic properties, activity of SiO_2, electrolytic sensor, methods of control*

The oxide and oxide-fluoride melts are widely used in metallurgy and welding. To predict the metallurgical and technological properties of slags in molten state, it is important to know their thermodynamic properties, in particular the activity of components of slag melts. The main component, included into composition of fluxes for welding of carbon and low-alloy steels, is silicon oxide. It is this component that defines the degree of polymerization of melt and, respectively, its structurally dependent properties. The complex of these properties defines the technological parameters of fluxes in the process of welding. At the same time, the presence of silicon oxide in the flux composition is a cause of proceeding of a number of redox reactions during welding, such as silicon reduction and formation of silicate non-metallic inclusions, non-desirable from the point of view of producing the optimum microstructures and mechanical properties in welding of advanced high-strength low-alloy steels. The advanced welding consumables are, as a rule, complex multi-component systems. Moreover, not only the melt components have an influence on the activity of slag melt components during welding, but also metals, included into composition of steel, wire and flux.

The aim of the present work is to develop the methods of in-process evaluation of activity (effective concentration) of silicon oxide SiO_2 in slag melts and to define the methods of its control.

The most accurate method of determination of activities of components in alloys is the method of electromotive forces (EMF) [1]. Its principle is as follows: to investigate the activity of one of components of oxide systems, a concentration element is developed without transfer of ions of the type

$$M|MO_x\|MO_x\text{–other components of slag being investigated}|M,$$

where M, MO_x are the metal and lower oxide of this metal. The developed concentration element for measurement of activity of silicon oxide SiO_2 in melt of $MgO–Al_2O_3–SiO_2–CaF_2$ system [2] is written schematically as follows:

$$(+)(Fe–Si)|SiO_2\|MgO–Al_2O_3–SiO_2–CaF_2|(Fe–Si)(–),$$

where (–) and (+) are the negative and positive poles.

In operation of this concentration element the following processes are proceeding at the electrodes:

$$(-)(\text{Fe–Si}) - 4e = Si^{4+}$$
$$(\text{in melt of } MgO–Al_2O_3–SiO_2–CaF_2) + Fe$$
$$(+)\ Si^{4+}\ (\text{in quartz glass}) + 4e = (\text{Fe–Si}).$$

Common process:

$$Si^{4+}\ (\text{in quartz glass}) =$$
$$= Si^{4+}\ (\text{in melt of } MgO–Al_2O_3–SiO_2–CaF_2).$$

Activity of SiO_2 was calculated using the known equation

$$E = RT/4F \ln a_{SiO_2}/a^{fl}_{SiO_2},$$

where E is the EMF of concentration element; R is the gas constant; a_{SiO_2}, $a^{fl}_{SiO_2}$ are the activities of silicon oxide SiO_2, respectively, in quartz glass and liquid glass of $MgO–Al_2O_3–SiO_2–CaF_2$ system.

At T = 1673 K $E = -0.036 \ln a^{fl}_{SiO_2}$, hence $a^{fl}_{SiO_2} = e^{-E/0.036}$.

This cell can be manufactured in the following way. In a graphite block two depressions are drilled for electrode of Fe–Si (ferrosilicon). From the bottom or on the side the tungsten current taps are connected. The cell in this form is heated up to 1500 °C in inert atmosphere and subjected to holding for 30–60 min. The fused ferrosilicon will have a good contact with current taps and walls of depressions. Then, a quartz glass is poured on the surface of one Fe–Si electrode, the slag being investigated is poured on the second electrode surface. Determination of SiO_2 activity by using this procedure is a complex task. Moreover, during the experiment the interaction of oxides and Fe–Si with graphite takes place. In this connection the need arises in its replacement by other more inert materials, such as boron alumonitride.

Therefore, the task was put forward to design a unique electrolytic sensor for in-process determination of SiO_2 activity in oxide and oxide-fluoride melts. Special electrodes were manufactured, which had at the beginning the pure Si, SiC or $MoSi_2$ as a Si-containing component. It was found during special experiments that a double electrical layer is slowly formed on the surfaces of SiC and $MoSi_2$, as the silicon is strongly bonded with other atoms of carbon or molybdenum. Sensor with electrode of pure silicon as a metallic component allowed making measurements only up to 1400 °C. Therefore, basing on the state diagram of Fe–Si system the alloy was selected by us, containing 5 wt.% Si and melting at temperature of 1500 °C, and also the ferresilicon-containing electrodes were manufactured using the technology described below. The fine-grain crushed silicon was mixed with powdered carbonyl iron of OSCh grade and poured into a quartz ampoule of 5 mm diameter and 4 cm length. Then, the tungsten rod of 40–50 cm length was put into this mixture. The junction was sealed with a paste of aluminium oxide and liquid glass to provide the more quality contact between the tungsten rod and alloy and to increase the junction strength. The second electrode of the concentration element represented a rod of ferrosilicon (5 wt.% Si), fastened to the tungsten current tap by a thin molybdenum wire. For this, a groove was cut in the electrode upper part by a diamond disc to insert the 1 mm diameter tungsten wire. The place of junction was pasted by a mixture of a powdered aluminium oxide with liquid glass. The tungsten current taps were insulated by inserting them into porcelain tubes. Electrodes were isolated one from another by a corundum plate and tied by a molybdenum wire. Scheme of the concentrated element, which was used for in-process determination of SiO_2 activity in oxide and oxide-fluoride melts, is given in the Figure.

The slag being investigated (8 g mass) was poured into a corundum round-bottomed crucible which was placed into the Tamman furnace. After

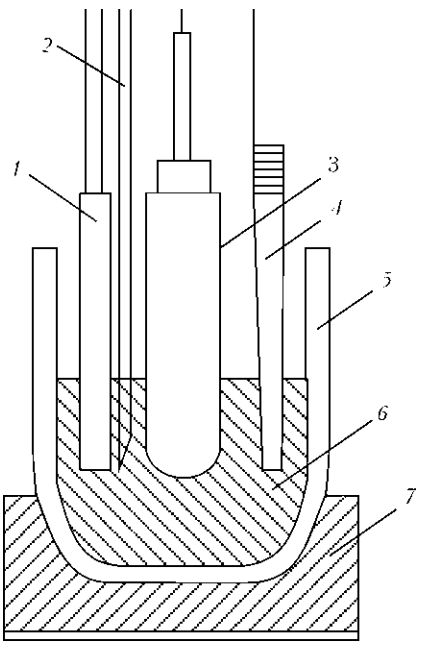

Scheme of a concentration element: *1* — thermocouple VR5-20; *2* — mixer; *3* — rod of Fe–Si connected with tungsten current tap in case of SiO_2; *4* — rod of Fe–Si connected with tungsten current tap; *5* — corundum crucible; *6* — slag being investigated; *7* — support of niobium plate and boron alumonitride

Table 1. Activity of SiO_2 in model slags of $MgO–Al_2O_3–SiO_2–CaF_2$ system

SiO_2, wt.%/mole fraction	Al_2O_3, wt.%/mole fraction	CaF_2, wt.%/mole fraction	MgO, wt.%/mole fraction	E, mV	a_{SiO_2}, mole %
40/0.507	40/0.298	20/0.195	0/0	20	0.573
38/0.462	38/0.272	19.2/0.179	4.8/0.087	47	0.270
36/0.418	36/0.246	18/0.161	10/0.174	49	0.250
34/0.380	34/0.223	17/0.146	15/0.251	75	0.123

heating up to 1400 °C it was subjected to holding for 3–5 min at this temperature (for homogenization). Then, two electrodes, above-described, were immersed slowly into the melt. After heating of electrodes up to preset temperatures the value of EMF was preserved constant within 1–2 mV ranges.

The accuracy and propriety of the developed procedure were checked on slags of $CaO–SiO_2$ system, well-studied earlier. It was occurred that activities of SiO_2, determined by us, are correlated with literature data within the errors of experiment [2]. This gave the grounds to start the determination of activity of silicon oxide SiO_2 in model slags of $MgO–Al_2O_3–SiO_2–CaF_2$ system, to which a whole number of fluxes for welding of high-strength low-alloy steels is referred. The developed procedure was applied for investigation of dependence of MgO effect on SiO_2 activity. The obtained results are given in Table 1.

It is seen from Table 1 that the MgO adding into slags of $MgO–Al_2O_3–SiO_2–CaF_2$ system causes a significant decrease of silicon oxide activity. This can be explained by the formation of complex compounds close by composition to Al_2MgO_4 and Mg_2SiO_4 [3], which are very refractory and thermodynamically stable.

During welding the components of fluxes are coming into interaction with alloying elements, included into composition of electrode wire and steel. In addition the agglomerated fluxes, as a rule, contain the alloying elements. To study this interaction, the powdered alloys in the amount of 1 wt.% of ferrosilicon FS75 (75 wt.% Si), ferrotitanium FTi70 (70 wt.% Ti), silicocalcium SK30 (30 wt.% Ca), ferromanganese FMn90 (90 wt.% Mn) and metal manganese Mn998 (99.8 wt.% Mn) were added to the oxide fluoride melt (34 wt.% SiO_2, 34 wt.% Al_2O_3, 17 wt.% MgO, 15 wt.% CaF_2) using a cup with a corundum tube.

Table 2. Effect of additions of ferroalloys and metal manganese on SiO_2 activity in melt

Melt	E, mV	a_{SiO_2}, mole %
Flux	75.5	0.123
Flux + Fe–Mn	114.0	0.042
Flux + Mn	141.7	0.020
Flux + Fe–Si	161.0	0.011
Flux + Fe–Ti	277.5	0.001
Flux + Ca–Si	332.5	0.0001

The results of measurements of EMF, obtained by using the above-described procedure, and appropriate values of activity of silicon oxide in slag melt are given in Table 2. It is seen from Table 2 that the activity of SiO_2 in melt of $MgO–Al_2O_3–SiO_2–CaF_2$ system with adding of ferroalloys is decreased. This can be explained by reaction proceeding between SiO_2 and metals.

To explain the effect of different metals on SiO_2 activity in the studied oxide melt, the thermodynamic probability of these processes was evaluated. For this, the change of Gibbs energy ΔG for each reaction given below (at 298 and 1673 K) was calculated:

1. $[Mn] + (SiO_2) \rightarrow (MnO_2) + [Si]$
2. $3[Mn] + 2(SiO_2) \rightarrow (Mn_3O_4) + 2[Si]$
3. $2[Mn] + (SiO_2) \rightarrow 2(MnO) + [Si]$
4. $4[Ti] + 3(SiO_2) \rightarrow 2(Ti_2O_3) + 3[Si]$
5. $[Ti] + (SiO_2) \rightarrow (TiO_2) + [Si]$
6. $2[Fe] + (SiO_2) \rightarrow 2(FeO) + [Si]$
7. $4[Fe] + 3(SiO_2) \rightarrow 2(Fe_2O_3) + 3[Si]$
8. $3[Fe] + 2(SiO_2) \rightarrow (Fe_3O_4) + 2[Si]$
9. $[Si] + (SiO_2) \rightarrow 2\{SiO\}$
10. $2[Ca] + (SiO_2) \rightarrow 2(CaO) + [Si]$,

where ( ), [ ], { } are the liquid, solid or gaseous state of substances.

To calculate ΔG at 298 K the following formula was applied:

$$\Delta G = \sum_i v_i (\Delta G_i)^{\text{prod}}_{\text{form}} - \sum_i v_i (\Delta G_i)^{\text{reag}}_{\text{form}}.$$

Thus, for reaction 1 we have

$$\Delta G^0_{298} = \Delta G^0_{MnO_2,\ 298} + \Delta G^0_{SiO,\ 298} - \Delta G^0_{Mn,\ 298}. \quad (1)$$

To calculate ΔG at 1673 K, we assume in the first rough approximation that $\Delta C_p = 0$. Then, the change of Gibbs energy for temperature 1673 K is equal to

Table 3. Calculated thermodynamic functions for reactions of metals with SiO_2

Number of reaction	ΔH^0_{298}, kJ/mole	ΔS^0_{298}, kJ/mole	ΔC_p, kJ/mole	ΔG^0_{298}, kJ/mole	ΔG^0_{1673}, kJ/mole (*I* approx.)	ΔG^0_{1673}, kJ/mole (*II* approx.)
1	337	−2.55	2.14	333.91	332.76	329.91
2	329	42.85	46.49	310.22	257.38	319.37
3	87.9	33.08	7.76	64.70	32.57	42.913
4	−463	−35.38	17.50	−471.90	−403.90	−380.60
5	−83	−3.97	4.36	−85.59	−76.68	−70.87
6	325	29.74	23.76	305.42	275.13	306.81
7	929	−0.46	31.60	913	930.22	972.35
8	598	17.26	23.37	666.99	568.97	600.13
9	635	351.10	15.57	524.35	47.16	67.92
10	−363	−25.38	7.50	−3316	−303.90	−280.60

$$\Delta G^0_{1673} = \Delta H^0_{298} - T\Delta S^0_{298}. \quad (2)$$

To calculate the change of enthalpy of reaction 1 the following formula is applied:

$$\Delta H^0_{298} = \sum_i v_i(\Delta H^0_{298}). \quad (3)$$

For reaction 1 this formula acquires the form

$$\Delta H^0_{298} = \Delta H^0_{MnO_2,\ 298} + \Delta H^0_{Si,\ 298} - \Delta H^0_{SiO_2,\ 298} - \Delta H^0_{Mn,\ 298}, \quad (4)$$

where $\Delta H^0_{MnO_2,\ 298}$, $\Delta G^0_{MnO_2,\ 298}$ are the enthalpy and Gibbs energy of MnO_2 formation.

Similarly for change of entropy of given reaction

$$\Delta S^0_{298} = S^0_{MnO_2,\ 298} + S^0_{Si,\ 298} - S^0_{SiO_2,\ 298} - S^0_{Mn,\ 298}. \quad (5)$$

Equation (2) gives the accurate enough results within wide range of temperatures. However, in many cases this is stipulated not by the fact that ΔH and ΔS are slightly depended on temperature, but a partial mutual compensation of effect of changes of these functions.

In the second approximation (Uhlich) the temperature dependence of thermodynamic functions is taken constant, i.e. the change of heat capacity of products and reagents of reaction ΔC_p is constant and equal to change of heat capacity of all the substances at room temperature:

$$\Delta G^0_T = \Delta H^0_{298} - T\Delta S^0_{298} + \Delta C_{p,\ 298}(T - 298 - T \ln T/298). \quad (6)$$

As it is not important for us the precise value ΔG, but its sequence and sign, we shall apply the approximated methods of calculation of ΔG using equations (2) and (6). When calculating, the literature data were used [4]. The data for manganese were taken for α-form, stable under normal conditions. The results of calculations are given in Table 3.

For reactions 4, 5 and 10, ΔG^0_{1673} is negative. This proves the interaction of titanium and calcium with SiO_2, moreover, the proceeding of reactions 4 and 10 is more probable. This is well correlated with experimental data, obtained by us, on decrease of SiO_2 activity at adding the ferrotitanium and silicocalcium into slag melt of $MgO–Al_2O_3–SiO_2–CaF_2$ system. Results of calculations of Gibbs energy, given in Table 3, confirm that titanium and calcium, included into composition of ferroalloys, interact with silicon oxide by the above-mentioned scheme. To explain the decrease in SiO_2, obtained experimentally at adding of other ferroalloys, it is necessary to use during calculation the partial molar Gibbs energies of metals, accounting for their activity, as well as the fact that when contacting the slag these metals are in a molten state. For this, we shall apply the modified equation

$$\Delta G = \sum_i a_i v_i(\Delta G_i)^{prod}_{form} - \sum_i a_i v_j(\Delta G_j)^{reag}_{form}, \quad (7)$$

where ΔG_i, ΔG_j are the partial molar Gibbs energies of components of final and initial melts.

In its turn

$$\Delta G_{i(j)} = RT \ln a_{i(j)}. \quad (8)$$

Activities of components of ferroalloys and slags $a_{i(j)}$ were used from [1, 5]:

11. $(Mn)_{Fe} + (SiO_2) \rightarrow (Si)_{Fe} + 2[MnO]$, $\Delta G = -460$ kJ/mole
12. $[Mn] + (SiO_2) \rightarrow (Si) + 2(MnO)$, $\Delta G = -371$ kJ/mole
13. $(Ti)_{Fe} + (SiO_2) \rightarrow (Si)_{Fe} + [TiO_2]$, $\Delta G = -878$ kJ/mole
14. $(Si)_{Fe} + (SiO_2) \rightarrow 2\{SiO\}$, $\Delta G = -86$ kJ/mole.

The values of Gibbs energies of reactions 11–14 are negative, thus proving their self-proceed-

ing in a straight direction. This is well correlated with data, according to which the activity of SiO_2 is significantly decreased at adding of the mentioned ferroalloys into the slag being investigated.

Therefore, with adding of some metals into complex oxide melts it is possible to control the activity of its components, in particular SiO_2 and, thus, the metallurgical properties of flux during welding. With decrease of SiO_2 in slag melt it is possible to suppress the proceeding of reactions of silicon reduction and formation of silicate non-metallic inclusions, undesirable from the point of view of metallurgy of low-alloy steel welding.

Conclusions

1. Activities of SiO_2 in slag melts of $MgO–Al_2O_3–SiO_2–CaF_2$ system were determined by the EMF method using the designed electrolytic sensor.

2. It was found that the increase in MgO content in slag melt of $MgO–Al_2O_3–SiO_2–CaF_2$ system causes the decrease in activity of the silicon oxide, that can be explained by the formation of refractory and thermodynamic stable silicates and aluminates of magnesium.

3. The effect of additions of metals on SiO_2 activity in melts of $MgO–Al_2O_3–SiO_2–CaF_2$ system was studied. It was found that adding of 1 % of silicocalcium, ferrotitanium, ferrosilicon, ferromanganese and metal manganese into melt of $MgO–Al_2O_3–SiO_2–CaF_2$ system leads to the jumpy drop of silicon oxide activity. The highest decrease (by 2–3 orders) is attained at adding of silicocalcium and ferrotitanium.

1. Sudavtsova, V.S., Makara, V.A., Galinich, V.I. (2005) *Thermodynamics of metallurgical and welding melts*. Pt 1: Iron- and aluminium-based alloys. Kiev: Logos.
2. Taylor, J.R., Dinsdale, A.T. (1990) Thermodynamic and phase diagram data for the $CaO–SiO_2$ system. *Calphad*, 14(**1**), 71–88.
3. Goncharov, I.A., Sokolsky, V.E., Davidenko, A.O. et al. (2012) Formation of spinel in melt of the $MgO–Al_2O_3–SiO_2–CaF_2$ system agglomerated welding flux and its effect on viscosity of slag. *The Paton Welding J.*, **12**, 18–25.
4. (1979) *Thermodynamic properties of individual materials*: Refer. Book. Ed. by V.P. Glushko. Vol. 2, Book 2. Moscow: Nauka.
5. Podgaetsky, V.V., Kuzmenko, V.G. (1988) *Welding slags*. Kiev: Naukova Dumka.

Received 17.12.2012

NEWS

Trenchless Laying of Pipelines

The principle of trenchless well driving consists in the use of compressed air to provide a reciprocal movement of the pneumatic hammer striker, whose impact on the casing is transferred to a reamer to cause an axial movement of the latter. A series of machines of this type were developed for punching of holes with a diameter of up to 630 mm.

For trenchless replacement of pipes, a special reamer is mounted on the impact mechanism (pneumatic hammer) located in the working well. This reamer provides destruction of an old pipe and expansion of soil to match its external diameter. A new pipeline, which is lengthened by sections from the working well, is pulled into the formed channel in movement of the reamer. The possibility exists of the continuous feed of a one-piece spiral-welded pipe made in site (in the well) from strip-type polyethylene billets. The reamer and a new pipe are pulled by using a cable and hoist from the receiving well. Length of a replaced section is up to 50 m.

Application:

- making of through, blind horizontal, inclined and vertical passages in puddled soils (e.g. in street or road intersections, etc.);
- trenchless replacement of old brittle material sewer pipes by polyethylene ones;
- removal of failed service lines from earth;
- installation of concrete and reinforced concrete grouted piles, cleaning of functioning service lines.

The trenchless technology allows several times saving of the funds, compared to traditional trench laying of pipelines, and preserves the outward appearance of territories within the work zone (this is particularly important for big cities with heavy traffic, and for reconstruction or overhaul of active underground service lines in urban development areas).

The speed of laying of a new pipeline is 6 m/h at a diameter of plastic pipes of 225 or 315 mm.

Vibrations of earth in trenching are similar to those occurring in foundation piling, i.e. they are not in excess of those specified by standards.

MATHEMATICAL MODELLING OF STRESS-STRAIN STATE OF WELDED STRINGER PANELS FROM TITANIUM ALLOY VT20

O.V. MAKHNENKO, A.F. MUZHICHENKO and **I.I. PRUDKY**
E.O. Paton Electric Welding Institute, NASU
11 Bozhenko Str., 03680, Kiev, Ukraine. E-mail:office@paton.kiev.ua

Improvement of methods for prediction of stress-strain state of welded joints in thin-sheet structures is a relevant problem. This, in particular, refers to stringer panels from VT20 titanium alloy which have high requirements on providing of high accuracy and strength at cyclic loads. Mathematical 3D modelling of stresses and deformations in small specimens (400 × 100–200 × 2.5 mm) with one stiffening rib and full size stringer panels (1100 × 550 × 2.5 mm) with four stiffening ribs was carried out under conditions of automatic non-consumable electrode welding by slot weld. Effect of preliminary elastic extension of plate and stiffening ribs on residual stress-strain state of panels was investigated. Computational investigations of stress-strain state for different variants of welding of the specimens showed that small width of panel specimens (100 mm) is not sufficient for determination of extension effect on residual stresses, and application of 200 mm width specimens is relevant for this purpose. The results of numerical calculations of stress-strain state for different variants of welding of stringer panels show principal possibility of performance at present time of such calculations in 3D problem statement for large welded structure with numerous welds, but at significant time consumption for calculation. 20 Ref., 3 Tables, 9 Figures.

Keywords: *welded stringer panels, titanium alloy VT20, welding stresses and deformations, method of preliminary elastic extension, mathematical modelling*

Prediction of welding deformations and stresses can be considered as an important factor of technological preparation of welded structure manufacture for selection of efficient method, mode and sequence of welding as well as geometry of stiffening ribs. Finally, all these factors are oriented on reduction of welding deformations in thin-sheet structures (as a rule the limits are set in specification).

Approximate engineering methods of calculation, based on knowledge of value of weld shrinkage function and application of methods of elasticity theory, obtained a wide distribution in predicting of stress-strain state of the welded panel structures. Analytical methods [1–3] or finite element method (FEM) [4] are used at that for problem solving. More general approaches of thermoplastic analysis in combination with FEM for 2D problem statement, i.e. at assumption of plane stressed state or plane deformation [5], are used for investigation purposes. Such a simplification of the model allows rapidly reducing the requirements to computational capabilities of the system and decreasing time for calculation.

Attempts of 3D modelling of panel welding with the help of FEM and methods of thermoplasticity theory are made at present time in the developed countries. The next researchers take the leading positions in development of specified problem. Thus, F. Boitout (ESI Group, France) carries out extensive computational investigation applicable to the welded structures, including in modelling of panel welding [6]. Investigations on optimization of welding process of light welded panels for minimization of the general deformations were performed by D. Camilleri and T. Gray (University of Strathclyde, Glasgow, Great Britain) [7]. Systematic computational investigations on the welded structures, including evaluation of the welding stresses and deformations, are made under the leadership of H. Murakawa (JWRI, Japan) [8–10]. P. Michaleris (Pennsylvania State University, USA) using 3D model studied deformations of shell-plate of the panel from welding of stiffening rib resulting in buckling failure [11]. Investigations carried out in recent time at the E.O. Paton Electric Welding Institute are also related with study of deformations and stresses in welding and thermal straightening of thin-sheet structures of panel type [12–14].

Mathematical 3D model using FEM and methods of thermoplasticity theory was developed for determination of stress-strain state of thin-sheet stringer panels in welding of longitudinal slot welds on the T-joints considering capabilities of current computer techniques and numerical methods of solving of boundary-value

problem. It is used for performance of computational investigation of effect of different technological factors on level of residual stresses and deformations of welded stringer panels from VT20 alloy. This model allows also studying the torsion deformations caused by non-simultaneous performance of welds, besides the main types of deformations, i.e. transverse and longitudinal shrinkage, buckling and angular strains. 3D model in contrast to 2D model allows the effect of sequence of welding process on residual stresses and deformations to be determined.

Mathematical model of welding of small panel specimen (400 × 100 × 2.5 mm) with one stiffening rib was developed for preliminary evaluation of the stress-strain state of thin-sheet panels at different variants of technology of automatic welding. Table 1 gives reference data [15–18] on thermophysical and mechanical properties of VT20 alloy which were used in the calculation. Melting temperature of alloy makes $T_m = 1668 \pm 5$ °C.

The developed computational model is based on numerical solution of the corresponding problems of thermoplasticity by means of tracing in time of development of temperature fields and connected with them kinetics of elastic-plastic deformations up to residual ones (complete smoothing of temperature) [5] in performance of the slot weld of panel specimen by moving heat source.

Modelling of the heat source is made in the following way. $\eta_s = 0.6$ coefficient of heating efficiency was set for automatic TIG welding by immersed arc based on comparison of calculation and experimental data by dimensions penetration zone. Rate of energy input in welding

$$q_{h.i} = \eta_s \frac{UI}{v_w}, \quad (1)$$

where U is the voltage, V; I is the welding current, A; v_w is the welding speed, mm/s.

Power of heating W is traditionally distributed according to Gauss's law on the surface and depth of heated metal, i.e. in arbitrary point x, y, z of welded elements depending on welding speed v_w along the x-direction, i.e. in the Cartesian coordinates system in movement of the source on $z = z_0 = 0$ surface

$$W(x, y, z) = W_0 \exp\left\{-K_x[(-v_w t)^2 + y^2] - K_z z^2\right\}, \quad (2)$$

where K_x is the coefficient of heat concentration on surface, i.e. in x- and y-directions, and K_z — on thickness (Figure 1). The latter parameters were selected from conditions $K_x = 12/B^2$ [19], where B is the width of weld pool. W_0 parameter is determined from energy balance:

$$W_0 = 2\pi \int_0^\infty \int_0^\delta \exp\left[-K_x \rho^2 - K_z z^2\right] \rho d\rho dz = q_s \quad (3)$$

or

$$W_0 = \frac{2q_{eff}}{\frac{\pi}{K_x}\sqrt{\frac{\pi}{K_z}}},$$

where $\rho^2 = (-tv_w)^2 + y^2$; t is the time.

Heat rejection is performed on mechanism of heat conduction, i.e. determined by differential equation of heat conductance in the Cartesian coordinates system:

$$\frac{\partial}{\partial x}\left(\lambda \frac{\partial T}{\partial x}\right) + \frac{\partial}{\partial y}\left(\lambda \frac{\partial T}{\partial y}\right) + \frac{\partial}{\partial z}\left(\lambda \frac{\partial T}{\partial z}\right) + W(x, y, z) = c\gamma \frac{\partial T}{\partial t}. \quad (4)$$

Symmetry condition is fulfilled at $y = 0$ (fusion line)

$$\frac{\partial T}{\partial y} = 0 \quad (5)$$

on panel surfaces $z = 0$, $z = \delta$

$$\frac{\partial T}{\partial z} = \pm \alpha_y (T - T_0), \quad (6)$$

where T_0 is the initial uniform temperature, equal ambient temperature; α_y is the coefficient of surface heat emission.

Stress fields and deformation fields as well as displacement vector U_j ($j = x, y, z$) in each point (x, y, z) in instant of time t can be calculated knowing temperature field $T(x, y, z, t)$ in different points (x, y, z) of the welded elements of panel. A solution is found by means of successive tracing of development of elastic-plastic state in time t starting from initial $t = 0$, $\sigma_{ij} = 0$, $\varepsilon_{ij} = 0$ and $T = T_0$. The solution on each tracing step t is based on a previous solution step in moment $t - \Delta t$, where Δt — tracing step by time t. Temperature field $T(x, y, z, t)$ is the disturbing factor.

Theory of Prandtl–Reiss plastic flow associated by Mises flow rule is used for solution of the thermoplasticity problem. Linearized problem on each step of tracing was solved using FEM. Physical non-linearity is realized in iteration way. At that, dependence of physical-mechanical properties of VT20 alloy on temperature (see Table 1) was considered in the computational model. Packet of computer programs «Weldpredictions» [20] developed at the E.O.

Table 1. Thermophysical and mechanical properties of VT20 titanium alloy depending on temperature at $\nu = 0.35$

T, °C	λ, W/(mm·°C)	c, J/(kg·deg)	$E \cdot 10^{-5}$, MPa	$\alpha \cdot 10^{6}$, 1/°C	σ_y, MPa
20	8	0.549	1.20	8	850
100	8.80	0.565	1.20	8.20	726
200	10.20	0.587	1.20	9.10	601
300	10.90	0.628	1.14	9.80	478
400	12.20	0.670	1.04	9.90	478
500	13.80	0.712	0.96	10.20	478
600	15.10	0.755	0.84	10.40	478
700	15.17	0.782	0.75	10.50	478
800	15.17	0.795	0.70	10.60	361
900	15.17	0.809	0.60	10.70	244
1000	15.02	0.808	0.50	10.70	128
1156	15.40	0.830	0.50	10.70	32
1157	15.30	0.770	0.54	9.50	32
1200	16.70	0.791	0.50	9.70	21
1400	18.30	0.827	0.50	10.99	21
1600	21.20	0.910	0.50	12.56	21
1800	23.70	0.997	0.50	12.56	21
1944	25.30	1.065	0.50	12.56	21
2000	25.30	1.230	0.50	12.56	21

Note. E — modulus of elasticity of material; ν — Poisson's ratio; α — coefficient of temperature expansion; λ — heat conduction coefficient; c — specific heat capacity; σ_y — yield strength.

Paton Electric Welding Institute is used for problem solution.

Computational investigation of stress-strain state of small specimens of panel (400 × 100 × × 2.5 and 400 × 200 × 2.5 mm) with one stiffening rib at different variants of preliminary extension in welding was carried out based on the developed mathematical model. Data in Figure 2 show that the preliminary extension of the panels has little effect on level of residual stresses of small specimen 100 mm width. The main influence is provided by rigid fixing of the specimens in welding. This results in significant reduction of maximum residual stresses in comparison with welding in a free state. A conclusion can be made analysis of calculation data that 100 mm width of small specimens of panels is not sufficient for evaluation of influence efficiency of the preliminary extension on residual stresses in the full-sized panels.

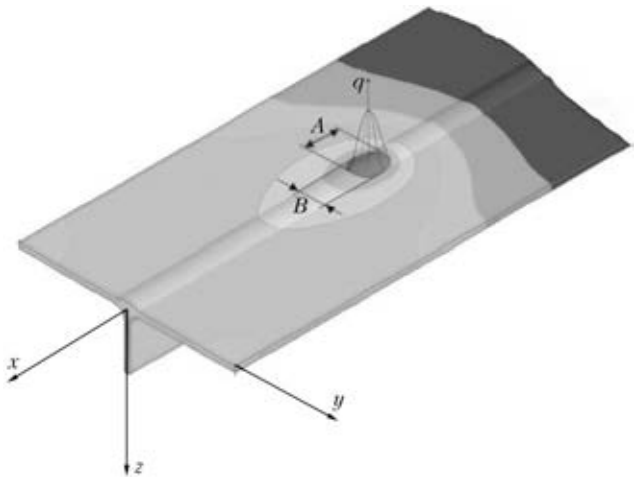

Figure 1. Scheme of heat source in welding of panel specimen by slot weld: A — length of weld pool; B — width of weld pool; q — Gaussian distribution of heat power

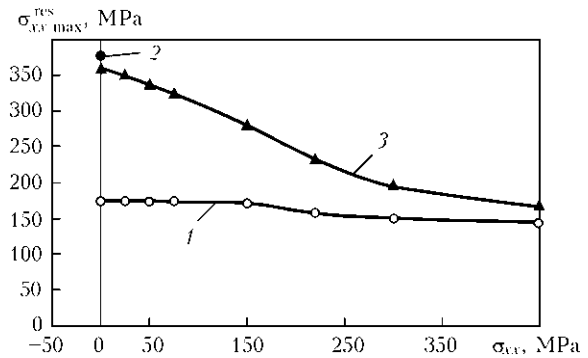

Figure 2. Dependence of maximum residual longitudinal stresses $\sigma^{res}_{xx\,max}$ on preliminary extension σ_{xx}: *1* — welding in a free state; *2*, *3* — welding with extension at B = 200 and 100 mm, respectively

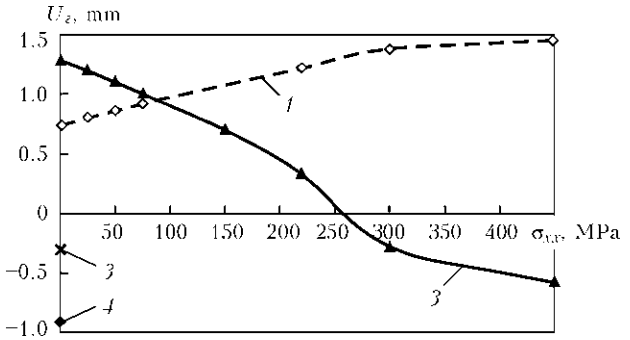

Figure 3. Dependence of residual buckling U_z on preliminary extension σ_{xx}: *1*, *2* — welding at extension B = 200 and 100 mm, respectively; *3*, *4* — welding in a free state at B = 200 and 100 mm, respectively

Effect of preliminary extension on maximum residual stresses (see Figure 2) significantly increases and principle change of influence of preliminary extension on residual buckling of the panel takes place (Figure 3) if width of panel specimen achieves 200 mm. At that, the preliminary extension of sheet and rib of panel specimen on 250 MPa level is an optimum from point of view of minimization of residual stresses (2 times reduction) and buckling deformations (close to zero).

Figure 4 shows good matching of experimental (curve *1*) and calculation (curve *2*) data in case of welding without preliminary elastic extension except for weld zone. In the latter experimental determination of residual stresses by means of deformation measuring is not accurate enough since can be performed only from one side of the specimen where the stiffening rib is absent. Calculation data (curve *5*) are confirmed by experimental ones (curve *2*) in welding of the specimen with 220 MPa preliminary elastic extension of plate.

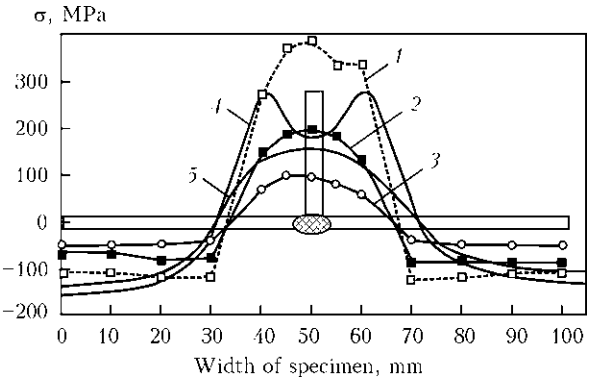

Figure 4. Experiment (*1–3*) and calculation (*4*, *5*) data on residual longitudinal stresses in welding of specimen in fixture with extension (*1*), under conditions of preliminary longitudinal elastic extension at σ = 220 and 450 MPa, respectively (*2*, *3*), in fixture without extension (*4*) and under conditions of preliminary longitudinal elastic extension at σ = 220 MPa (*5*)

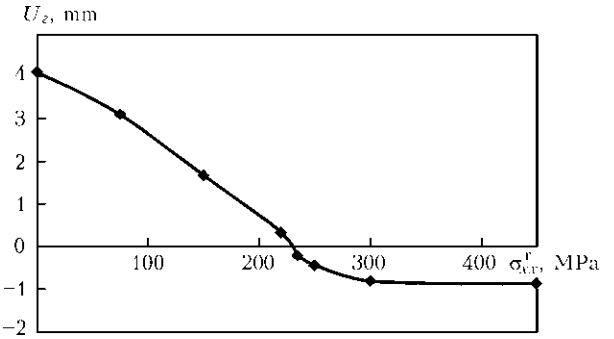

Figure 5. Dependence of residual buckling U_z on preliminary extension of rib σ^r_{xx} at plate extension σ^p_{xx} = 220 MPa

Computational experiments were carried out for determination of effect of the preliminary extension of stiffening rib on maximum residual longitudinal stresses in the specimen of stringer panel (400 × 200 × 2.5 mm) at 220 MPa plate preliminary extension. Preliminary extension of the stiffening rib has significant influence on residual buckling of specimen of stringer panel, as can be seen from calculation data (Figure 5). Minimum buckling is provided at value of stiffening rib preliminary extension close to preliminary extension of the plate (σ^r_{xx} = σ^p_{xx} = = 220 MPa). Thus, if preliminary extension of the plate is 220 MPa, extension of the stiffening rib is reasonable to be at the same level or somewhat higher (230–240 MPa) for reduction of buckling deformations.

Calculation results (Figure 6) show small dependence of maximum residual longitudinal stresses of specimen of the stringer panel (400 × × 200 × 2.5 mm) on preliminary stiffening rib extension if plate preliminary extension makes 220 MPa. It should be noted that obtained calculation data on welding of stringer panels have experimental confirmation.

A model for determination of stress-strain state in welding of 1100 × 550 × 2.5 mm stringer panel with four stiffening ribs was created based

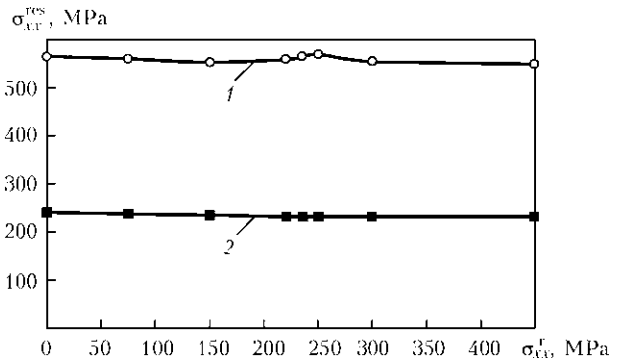

Figure 6. Dependence of maximum residual longitudinal stresses σ^{res}_{xx} on preliminary extension of rib σ^r_{xx} after welding (*1*) and extension removal (*2*) at plate extension σ^p_{xx} = = 220 MPa

on the developed mathematical model for small specimen of stringer panel.

Computational algorithm of determination of stress-strain state during stringer panel welding includes three main successive steps of modelling:

1. Setting of preliminary elastic extension σ by means of fixing of one transverse edge of plate and ribs and displacement of the second edge in longitudinal direction by $\Delta = 1100\sigma/E$ (mm) value, fixing of transverse edges from sheet plane as well as fixing of longitudinal edges of ribs in direction from plate plain;

2. Modelling of welding (by slot weld) of four longitudinal ribs in set sequence and specified welding direction using movable heat source;

3. Release of welded panel by means of removal of all fixtures.

The first and third steps of modelling were carried out per one time step and they are, respectively, connected with loading and unloading of model of stringer panel in the elastic field.

In a process of movement of welding heat source the finite elements are fastened between themselves in the range of penetration zone, simulating fusion of stiffening rib and plate between themselves.

Calculation of stress-strain state of the stringer panels was carried out at different preliminary extension and set asymmetrical sequence of welding (Figure 7). The welds were performed in sequence from one end of the panel to another and only in one direction for showing maximum effect of non-simultaneous weld performance on distribution of the residual stresses and deformations.

Table 2 demonstrates the results of calculation of maximum residual longitudinal stresses and residual buckling of the panel (1100 × 550 × × 2.5 mm) depending on general preliminary extension.

Time of calculation of the stress-stain state in welding of stringer panels is sufficiently long. Calculation of one variant took on average 15 days using modern personal computer with quadcore processor. This work presents the results for

Table 2. Maximum residual longitudinal stresses and residual buckling of panel depending on general preliminary extension

Plate/rib		$\sigma^{res}_{x.x\,max}$, MPa		σ^{res}_{z}, mm
σ, MPa	Δ, mm	After welding	After fixing removal	
0/0	0/0	550	316	15.1
80/80	0.73/0.73	550	313	12.5
220/220	2.02/2.02	550	223	7.6
300/300	2.75/2.75	550	195	5.2

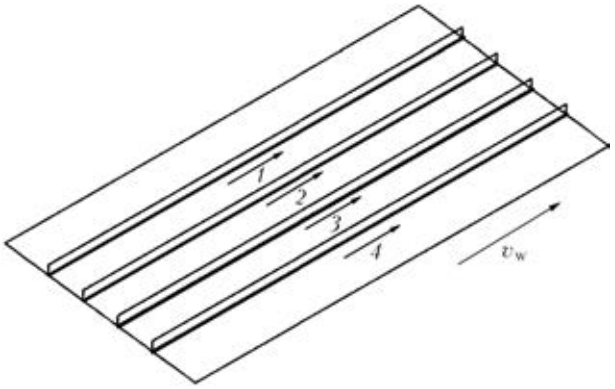

Figure 7. Scheme of weld performance sequence in modelling of welding of stringer panel

only four variants of stringer panel welding. It allows showing the principal possibility of performance at present time of such calculations in 3D problem statement for sufficiently large welded structures with numerous welds.

Distribution of the residual longitudinal stresses σ_{xx} (Figure 8, *a*) on the surface of stringer panel after welding of all welds (immersed-arc welding at $v_w = 13$ m/h, $I = 250$ A, $U = 11.5$ V) under conditions of fixing with preliminary extension ($\sigma_{xx} = 220$ MPa) was obtained on the second step of modelling. Maximum longitudinal extension residual stresses of 450–550 MPa level appear in average section of the panel, and they achieve up to 650 MPa in zone of end effects of welding.

Significant redistribution of the longitudinal residual stresses (Figure 8, *b*) takes place after removal of fixing from welding panel. Maximum

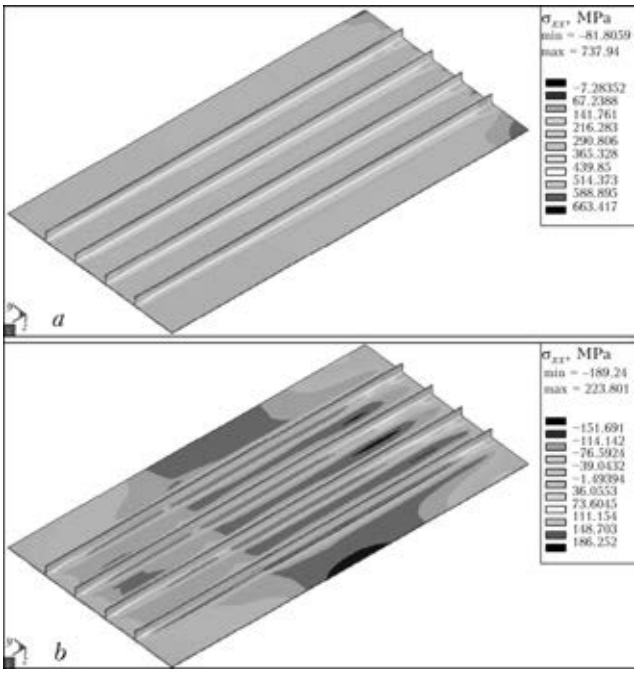

Figure 8. Distribution of residual longitudinal stresses σ_{xx} after welding and complete cooling of all four ribs (*a*) and after fixing removal (*b*)

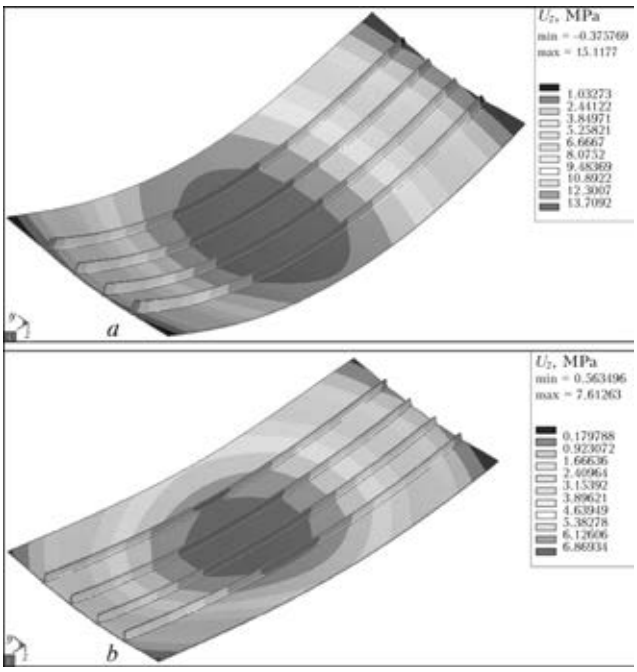

Figure 9. Residual buckling of stringer panel during welding in fixing without preliminary extension ($U_{z\,\max}$ = 15.1 mm) (*a*) and with preliminary extension σ_{xx} = 220 MPa ($U_{z\,\max}$ = = 7.6 mm) (*b*)

longitudinal residual extension stresses reduce up to 220 MPa in the average section of panel. Noticeable asymmetry of distribution of residual stresses related with non-simultaneous weld performance is observed. The values of residual stresses in the average section of panel in zone of last weld approximately 40 MPa higher than in zone of previous welds for which maximum longitudinal extension stresses do not exceed 180 MPa.

Residual deformations also appear on the third step of modelling. In considered case of welding with σ_{xx} = 220 MPa preliminary extension the maximum residual buckling deformations achieve 7.6 mm (Figure 9, *b*) that is significantly lower of 15.1 mm value of buckling for welding of fixed stringer panel without preliminary extension (Figure 9, *a*). Nevertheless, the values of buckling for cases of welding with σ_{xx} = 220 and 300 MPa preliminary extension appeared to be higher as a result of calculation then were predicted (calculation of small specimens of panels). Besides, insignificant asymmetry of distribution of residual buckling with displacement of the maximum towards the last weld related with non-simultaneous performance of weld runs is also observed. At that, any noticeable torsion deformations of stringer panel are absent. This can be seen on similar values of displacements from angle plain of the panel. Therefore, fixing of stringer panel in welding for elimination of displacements from plane and ends of the panel in longitudinal direction is efficient for prevention of residual torsion deformations.

Residual buckling deformations in a form of violation in plain were measured as pointers of longitudinal buckling on line of the ribs W_{r1}, W_{r2}, W_{r3}, W_{r4}, and as pointers of buckling of the end and average cross sections W_{c1}, W_{c2}, W_{c3}, W_{c4}, and as a torsion angle α of the cross sections relatively to each other. The results of measurements are given in Table 3.

Comparison of calculation and experiment data (see Table 3) shows that the method provides a character of distribution of residual deformations similar to measurement results, however, the values of longitudinal buckling are overestimated (maximum calculation buckling is 7.6 mm and experimental one makes 5.0 mm). Besides, the calculation angle α is sufficiently lower than its experimental values (calculation α = 0.2° and experimental — 1.6°). Probably, the input data (parameters of preliminary elastic extension) in calculation performance had insufficiently correspondence to the same parameters at experiment, either the real conditions of welding of stringer panels were not completely considered by developed mathematical model and the latter requires further improvement and experimental check.

In conclusion note that the results of modelling of stress-strain state for different variants of

Table 3. Experiment and calculation data on residual buckling deformations and torsion deformation of welded stringer panels

Number of panel	W_{r1}, mm	W_{r2}, mm	W_{r3}, mm	W_{r4}, mm	W_{c1}, mm	W_{c2}, mm	W_{c3}, mm	α, deg
1	2.5	3.5	2.0	2.0	3.0	5.0	3.5	2.5
2	2.0	2.5	3.0	3.0	4.0	4.5	4.0	3.0
3	1.5	2.0	2.0	1.5	2.5	3.5	2.0	1.0
4	1.5	2.0	1.5	1.5	1.5	2.0	2.0	1.0
5	1.0	1.0	1.5	1.5	1.5	1.5	3.5	1.5
6	0.5	1.5	1.0	0.5	1.0	2.0	1.0	0.5
Average experimental data	1.5	2.1	1.8	1.7	2.3	3.1	2.7	1.6
Calculation data	6.9	7.4	7.5	7.1	5.0	7.6	5.5	0.2

welding small specimens of stringer panels 400 × × 100 × 2.5 mm and 400 × 200 × 2.5 mm with one stiffening rib showed:

• 100 mm width of the panel specimen is not enough for determination of efficiency of extension influence on residual stresses;

• significant effect of the preliminary extension on maximum residual stresses and buckling of the panel is noticeable at 200 mm width of the specimen and, at that, preliminary extension of sheet and rib of the panel specimen on 250 MPa level is optimum from point of view of minimization of residual stresses (2 times reduction) and buckling deformations (close to zero);

• preliminary rib extension has significant influence on residual buckling of stringer panel specimen of 400 × 200 × 2.5 mm size as well as on the fact that the minimum buckling is provided at rib extension close to plate preliminary extension ($\sigma^{r}_{xx} = \sigma^{p}_{xx}$ = 220 MPa), i.e. at plate preliminary extension on 220 MPa level for the rib extension at the same level or somewhat above (230–240 MPa) is reasonable to be provided buckling deformation reduction. At that, maximum residual longitudinal stresses of stringer panel specimen have small dependence on preliminary rib extension.

The results obtained in modelling of stress-strain state for different variants of welding of 1100 × 550 × 2.5 mm size stringer panels with four stiffening ribs showed:

• principle possibility of performance at present time of such calculations in 3D problem statement for sufficiently large welded structure with numerous welds, but considering long enough time for calculation;

• high efficiency of preliminary elastic extension method on reduction of a level of residual stresses and buckling deformations of the stringer panels;

• efficiency of fixing of stringer panel in welding for elimination of displacements from plane and ends of the panel in longitudinal direction to prevent appearance of residual torsion deformations.

1. Kuzminov, S.A. (1974) *Welding deformations of ship hull structures*. Leningrad: Sudostroenie.
2. Vinokurov, V.A. (1968) *Welding strains and stresses*. Moscow: Mashinostroenie.
3. Talypov, G.B. (1974) *Welding strains and stresses*. Leningrad: Mashinostroenie.
4. Luo, Yy., Deng, D., Xie, L. et al. (2004) Prediction of deformation for large welded structures based on inherent strain. *Transact. of JWRI*, 33(**1**), 65–70.
5. Makhnenko, V.I. (1976) *Computational methods of investigation of welded stress and strain kinetics*. Kiev: Naukova Dumka.
6. Boitout, F., Dry, D., Gooroochurn, Y. et al. (2005) Distortion control for large maritime and automotive structures coupling with stamping simulation SYSWELD V2004. In: *Proc. of SYSWELD Forum* (Weimar, Sept. 2005), 107–120.
7. Camilleri, D., Gray, T. (2006) Optimization of welded lightweight multiple-stiffener plate structures to minimize unwanted shape distortion. *Welding and Cutting*, **6**, 320–327.
8. Deng, D., Ma, N., Murakawa, H. (2011) Finite element analysis of welding distortion in a large thin-plate. *Transact. of JWRI*, 40(**1**), 89–100.
9. Ma, N.-X., Ueda, Y., Murakawa, H. et al. (1995) FEM analysis of 3-D welding residual stresses and angular distortion in T-type fillet welds. *Ibid*., 24(**2**), 115–122.
10. Gu, S.M., Murakawa, H., Ueda, Y. et al. (1996) Simulation of welding deformation for accurate ship assembly: Report 3. *Ibid*., 25(**1**), 69–79.
11. Deo, M.V., Michaleris, P. (2003) Mitigation of welding induced buckling distortion using transient thermal tensioning. *Sci. and Technol. of Welding and Joining*, 8(**1**), 49–54.
12. Lobanov, L.M., Makhnenko, O.V., Seyffarth, P. (1997) Computational prediction of welding deformations in production of flat sections for reduction of fit-up operations volume. *Avtomatich. Svarka*, **1**, 21–24.
13. Paton, B.E., Lobanov, L.M., Tsybulkin, G.A. et al. (2003) Automated thermal straightening of welded thin-sheet structures. *The Paton Welding J*., **7**, 2–6.
14. Makhnenko, O.V., Muzhichenko, A.F., Seyffarth, P. (2009) Application of mathematical modeling in thermal straightening of shipbuilding panels. *Ibid*., **1**, 6–11.
15. (1967) *Physical properties of steels and alloys used in power engineering*: Refer. Book. Ed. by B.E. Nejmark. Moscow-Leningrad: Energiya.
16. (2005) *GOST 22178–76*: Sheets of titanium and titanium alloys. Technical requirements. Introd. 01.07.2005. Moscow: Standartinform.
17. (1997) *GOST 19807–91*: Titanium and titanium wrought alloys. Grades. Moscow: Standart.
18. Zinoviev, V.E. (1989) *Thermophysical properties of metals at high temperatures*: Refer. Book. Moscow: Metallurgiya.
19. Rykalin, N.N. (1951) *Calculations of thermal processes in welding*. Moscow: Mashgiz.
20. Makhnenko, V.I., Velikoivanenko, E.A., Pochinok, V.E. et al. (1999) Numerical methods for the prediction of welding stress and distortions. In: *Weld. and Surf. Rev*., Vol. 13, Pt 1. Amsterdam: Harwood Acad. Publ.

Received 19.09.2012

INFLUENCE OF LOCAL HEAT TREATMENT AT EBW OF TITANIUM ALLOYS WITH SILICIDE STRENGTHENING ON MECHANICAL PROPERTIES OF WELD METAL

E.L. VRZHIZHEVSKY, V.K. SABOKAR, S.V. AKHONIN and **I.K. PETRICHENKO**
E.O. Paton Electric Welding Institute, NASU
11 Bozhenko Str., 03680, Kiev, Ukraine. E-mail: office@paton.kiev.ua

Disadvantages of EBW of complex-alloyed titanium alloys include high rates of weld metal heating and cooling, leading to lowering of ductility properties. Research objective consisted in determination of the influence of preheating and local heat treatment by the electron beam on prevention of formation of defects in the form of cracks and improvement of ductility properties of welded joints of high-temperature titanium alloys. Research purpose was determination of preheating temperature to prevent the negative influence of high temperature gradient characteristic for EBW. In this case a smoother temperature gradient in welding is ensured that prevents cracking. After welding the joints were subjected to local annealing at the temperature of 900 °C for 10 min. All the welded joints were subjected to X-ray testing and metallographic examinations. It was revealed that varying the heating parameters at local heat treatment by the electron beam allows controlling the rate of phase and structural transformations in titanium alloys with silicide strengthening and, thus, changing the structure and, therefore, also the properties of welded joints that allows storing the welded structures for a long time before conducting total furnace treatment. The proposed approach can be used in manufacture of axial-flow compressors for gas turbine engines and power units. 6 Ref., 1 Table, 7 Figures.

Keywords: *electron beam welding, complex-alloyed titanium alloys, weld metal, local heat treatment, mechanical properties, prospects for application*

High-temperature titanium alloys are structural materials in manufacture of aircraft engine parts. Beginning from mid-1970s, EBW of parts from these alloys became widely accepted, allowing their narrow-gap joining with minimum distortion that is required in welding of axial-flow compressors. Disadvantages of EBW of high-temperature complex-alloyed titanium alloys include high rates of heating and cooling of weld metal and HAZ, leading to an abrupt lowering of ductility properties [1] that may cause defect formation in the form of transverse cracks at cooling after welding (Figure 1). Therefore, in welding of such structures it is rational to apply local heat treatment (LHT) directly in the chamber of EBW machine [2]. This technology allows prevention of cracking and improvement of ductility properties of welded joint metal for items of a small mass.

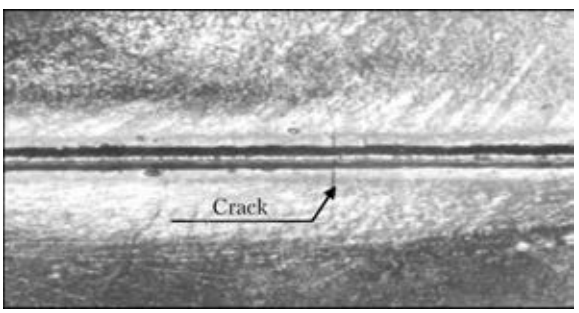

Figure 1. Appearance of EBW weld with a characteristic defect in the form of a crack

This work is a study of EB LHT influence on mechanical properties of weld metal in test titanium alloys with silicide strengthening of Ti–6.08Al–2.18Sn–3.88Zr–0.39Mo–1.14V–0.65Si (alloy 1) and Ti–5.5Al–3.02Sn–4.58Zr–0.1Mo–0.8Nb–0.59V–0.6Si (alloy 2) composition. Ingots were melted out in skull EB installation ISV-004 [3]. After rolling the produced alloys were annealed by the modes recommended for pseudo-α-alloys [4]. Experiments were conducted on flat samples of 150 × 70 × 13 mm size. EBW was performed in one pass with through-thickness penetration in UL 144 machine fitted with ELA 60/60 power unit. At LHT the width of the heated section was determined so that it covered the weld and HAZ. Figure 2 gives the appearance of a rectangular scan in the focused condition. At LHT beam current, focusing, impact duration and scanning frequency of the beam were selected from the

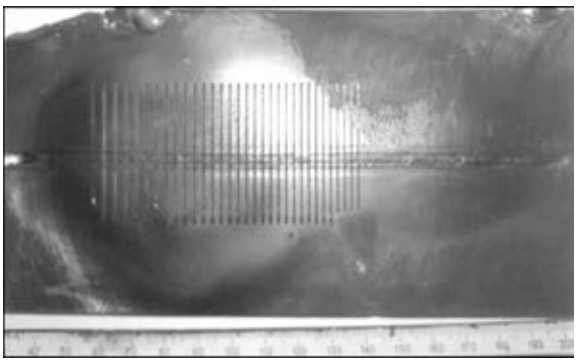

Figure 2. Appearance of rectangular scan used for LHT

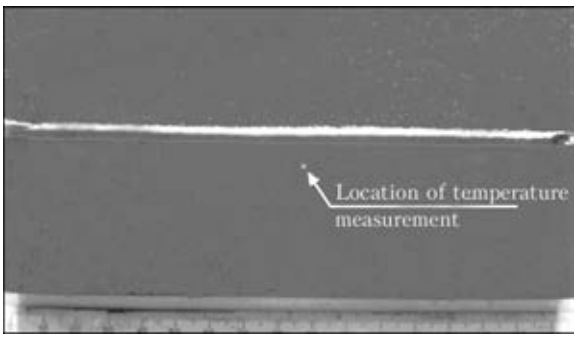

Figure 3. Location of thermocouple for temperature measurement at LHT

condition of ensuring temperature on the level of 750–950 °C in the treated section.

Temperature monitoring was performed using thermocouples fastened from the weld root side (Figure 3). Such a procedure is published in [5].

As was mentioned above, high heating and cooling rate, characteristic for EBW, is one of its disadvantages. In order to eliminate this negative influence, the impact of preheating on mechanical properties of the metal of welds of test titanium alloys 1 and 2 was studied. Such a method was not applied earlier in EBW of titanium alloys unlike subsequent LHT by the electron beam [6].

Preheating temperature was selected from the condition of ensuring a lowering of the level of welded sample deformations. We have tried out three preheating temperatures: 200, 300 and 400 °C, which ensured a smoother temperature gradient in welding. Mechanical testing of welded joints was conducted after each welding cycle with preheating. Test data are summarized in the Table. Conducted testing showed that the optimum preheating temperature of titanium alloys 1 and 2 is equal to 200 °C (Figure 4). Further increase of preheating temperatures to 300 and 400 °C leads to lowering of welded joint ductility (see the Table).

After welding of joints on titanium alloys 1 and 2, local annealing was performed at the temperature of 900 °C for 10 min (Figure 5). Welded joint macrostructure did not change after LHT. All the welded joints were subjected to X-ray testing and metallographic examination. No cracks were detected in welded joints, as LHT promoted relieving of welding stresses which are

Mechanical properties of weld metal of titanium with silicide strengthening*

Material	Preheating temperature for 5 min, °C	LHT temperature, °C, and duration, min	Yield point, MPa	Tensile strength, MPa	Impact toughness, J/cm^2	Notes
Alloy 1	–	–	1106.4	1208.2	9.05	Base metal
	Without HT	–	–	1309.7	–	Brittle fracture
	200	–	–	1187.6	5.40	–
	200	900, 10	810.5	1182.0	5.28	–
	300	–	–	1167.7	5.10	–
	300	900, 10	743.3	1088.9	4.97	–
	400	–	–	1192.0	3.88	–
	400	900, 10	789.8	1132.9	3.35	–
Alloy 2	–	–	1136.0	1273.6	10.4	Base metal
	Without HT	–	–	1190.6	–	Brittle fracture
	200	–	–	1140.1	4.91	–
	200	900, 10	1024.1	1042.9	4.40	–
	300	–	–	1167.8	3.28	–
	300	900, 10	1010.0	1167.8	3.16	–
	400	–	–	1040.8	3.13	–
	400	900, 10	1006.1	1168.0	3.48	–

*Average values after testing three samples are given.

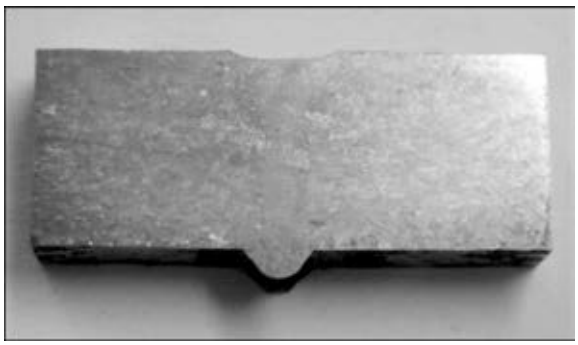

Figure 4. Macrosection of welded joint of alloy 1 made by EBW with 200 °C preheating

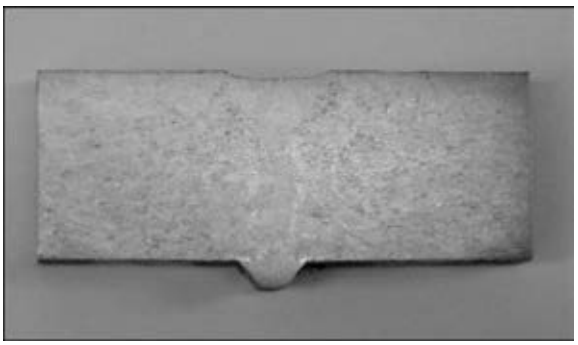

Figure 5. Macrosection of welded joint of alloy 1 made by EBW with 200 °C preheating and post-weld LHT

the main cause for cracking. As was noted in [2], varying the heating parameters at LHT by the electron beam allows not only eliminating welding stresses, but also controlling the rate of running of phase and structural transformations in titanium alloys and, thus, favorably changing the structure and properties of welded joints and ensuring complete absence of defects in them.

Technology of welding with post-weld LHT allows prevention of welded joint cracking up to performance of general furnace treatment.

Studied alloy 1 belongs to the group of pseudo-α-alloys of titanium, and has the coefficient of β-phase stabilization K_β = 0.1. In as-rolled condition the alloy has a plate-like structure (Figure 6, *a*), in which silicide particles are located relatively uniformly within primary β-grains both along the boundaries, and in the volume of α′-plates. Annealing stimulates the diffusion processes, the result of which is silicide concentration along the boundaries of α-plates (Figure 6, *b*).

Microstructures of a welded joint of alloy 1 are shown in Figure 7. Weld metal consists of aimed in the heat removal direction primary β-grains with plate-like α′-phase in the grain volume. In the weld upper part, the grains grow with 45° inclination to weld axis (Figure 7, *a*),

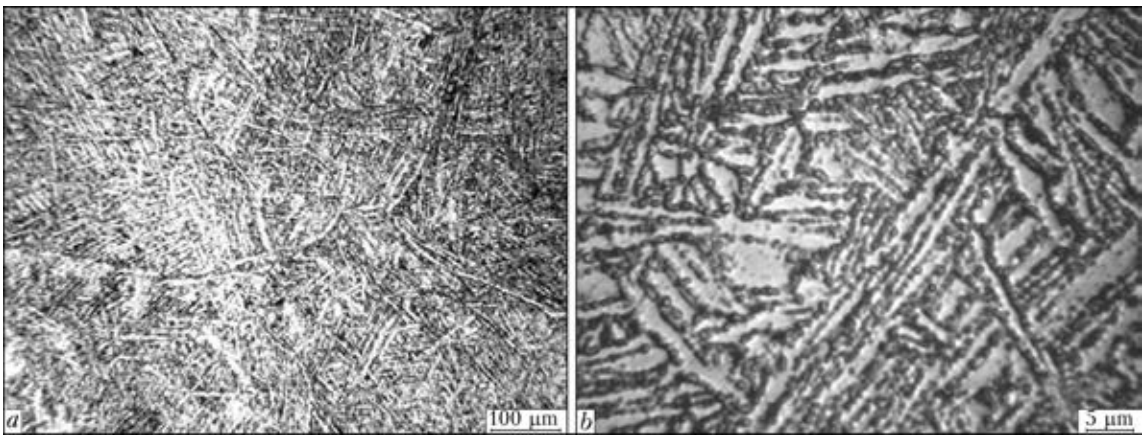

Figure 6. Microstructures of base metal of alloy 1

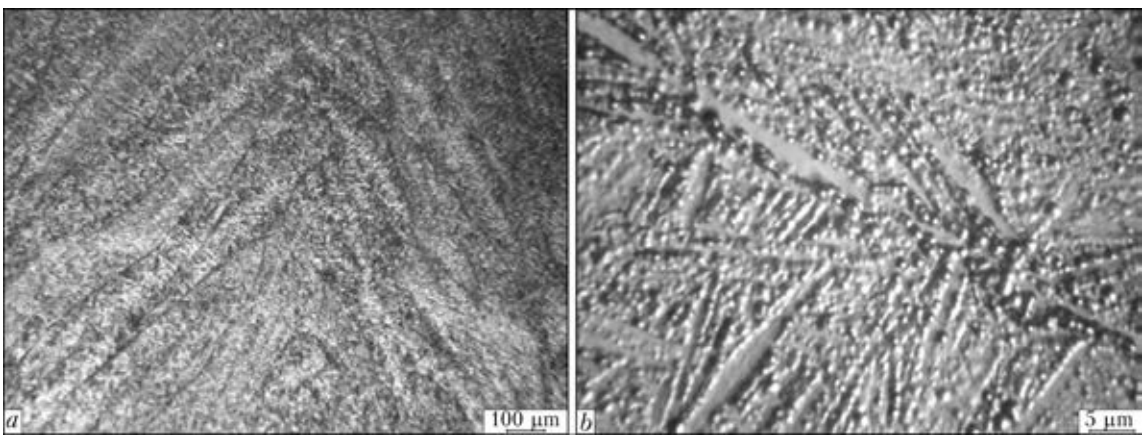

Figure 7. Microstructures of weld metal of alloy 1 after EBW with preheating at 200 C and post-weld LHT

and in the grain middle they intergrow at an angle of about 180°. After welding silicide particles are localized both along the boundaries of primary β-grains, and in α-plate volume. After annealing silicide particles are mainly located on α-plate boundaries (Figure 7, *b*).

It should be noted that microstructures of welded joints of alloys 1 and 2 are similar, irrespective of the difference in their composition. In addition, these two alloys have approximately the same silicon content.

Thus, conducted investigations showed that EBW of titanium alloys with silicide strengthening with preheating and post-weld LHT prevents cracking of welded joints during cooling after welding and provides satisfactory ductility properties. Proposed procedure ensures sound formation of welded joints before performance of the corresponding furnace treatment.

1. Gurevich, S.M., Zamkov, V.N., Blashchuk, V.E. et al. (1986) *Metallurgy and technology of welding of titanium and its alloys*. Kiev: Naukova Dumka.
2. Lyasotskaya, V.S. (2003) *Heat treatment of titanium alloy welded joints*. Moscow: Ekomet.
3. Levitsky, N.I., Matviets, E.A., Lapshuk, T.V. et al. (2012) Production of multicomponent titanium alloys by the method of electron beam skull melting. *Metall i Litio Ukrainy*, **4**, 6–9.
4. Iliin, A.A., Kolachev, B.A., Polkin, I.S. (2009) *Titanium alloys. Composition, structure, properties*: Refer. Book. Moscow: VILS–MATI.
5. Lysenkov, Yu.T., Vlasov, G.A., Ovchinnikov, V.V. (1980) Improvement of properties of VT20 alloy welded joints by local electron beam heat treatment. *Svarochn. Proizvodstvo*, **4**, 7–8.
6. Lyasotskaya, V.S., Lysenkov, Yu.T., Biryukov, I.M. et al. (1981) Improvement of properties of VT20 alloy welded joints by local electron beam heat treatment. *Ibid*., **11**, 19–20.

Received 18.10.2012

NEWS

Technology of Ultrasonic Welding of Products of Polystyrene

The most effective method of joining products of polystyrene is the ultrasonic welding (USW). The given process allows producing the quality joint during fractions of seconds, eliminating here the process of adhesion or mechanical assembly of parts and structures of polystyrene.

At the E.O. Paton Electric Welding Institute a large scientific and industrial experience has been gained on USW of products made of polystyrene. The developed technologies are easily adapted to a definite type of polymer, shape or geometry of product and envisage:

- optimizing of main parameters of USW conditions;
- selection of method of introducing the ultrasonic oscillations (welding in near and far field);
- calculation and recommendation for selection of type of edge preparation, their geometry and sizes;
- recommendations for selection of type of filling materials and dyes, their concentration with account for their light and weather stability, spreading capacity and weldability of polymer by an ultrasound;
- selection of sequence of operations in a working cycle and method of dosing of mechanical energy being exerted, providing the preset quality of welded joints;
- selection of waveguide-tool, its design, manufacture and final optimizing.

The developed technologies provide strength of welded joints, close to the strength of parent metal, high efficiency of process, its ecology.

USW technology can be applied for manufacture of products and structures of polystyrene and copolymers of styrene and methyl methacrylate, which are used in auto-, avia- and machine building, light, food and chemical industry, radio electronics, medicine, agriculture.

The developed technological processes of USW provide:

- high quality of welded joints, reduction in labor intensity of operations and saving the energy consumption by a possibility of using the new criteria of dosing the input energy and automation of the welding process;
- decrease in cost of purchase, i.e. the cost of technology is 2–5 times lower than the cost of foreign analogs;
- elimination of processes of adhesion by dichloroethane, toluene, butyl acetate and other substances, harmful for the human organism.

Efficiency: up to 60 welds per minute.

This development has been implemented at a number of enterprises of Ukraine and Russia.

INVESTIGATION OF DISPERSION OF DISSIMILAR WIRE MATERIALS DURING ELECTRIC ARC SPRAYING

Yu.S. BORISOV, N.V. VIGILYANSKAYA, I.A. DEMIANOV, A.P. GRISHCHENKO and **A.P. MURASHOV**
E.O. Paton Electric Welding Institute, NASU
11 Bozhenko Str., 03680, Kiev, Ukraine. E-mail: office@paton.kiev.ua

The process of combined spraying of steel and copper wires under the electric arc spraying conditions was investigated. The effect of spraying parameters on the process of spraying of dissimilar wires was established, this making it possible to control particle size distribution of the spraying products in electric arc spraying of pseudo-alloy coatings and, hence, structure and properties of the resulting coatings. 2 mm diameter wires, i.e. copper wire of the M1 grade and steel wire Sv-08A, were used as spraying consumables. Investigations were carried out by using electric arc metalliser EM-14M. The regression equations describing dependence of the mean size of particles on the electric power, compressed air pressure and spraying distance were derived by using mathematical experimental design. It was found that the mean size of particles depends primarily on the compressed air pressure. Combining the maximal values of the power (9.6 kW) and compressed air pressure (7 atm) during spraying results in formation of particles of the minimal size: 37 μm in spraying of copper wire, 54 μm in spraying of steel wire Sv-08A, and 52 μm in their combined spraying. Combining the minimal values of the power (1.7 kW) and compressed air pressure (6 atm) leads to formation of particles of the maximal size: 54 μm in spraying of copper wire, 85 μm in spraying of steel wire Sv-08A, and 85 μm in their combined spraying. It was found that the pseudo-alloy particles consisting of particles of the steel melt with a copper shell on their surface are formed during the process of combined spraying of copper and steel wires as a result of inter-phase interaction of their melts. 24 Ref., 1 Table, 6 Figures.

Keywords: *electric arc spraying, steel and copper wire, melt dispersion, inter-phase interaction, pseudo-alloy, particle size distribution, microstructure of particles*

One of the key factors of the process of thermal spraying of coatings is size of spraying material particles. In many respects, it determines conditions of heating and acceleration of the particles, development of the process of their interaction with the environment and, eventually, shape and size of the particles forming the coating layer that are deformed at collision with the substrate surface [1, 2]. Thickness of these particles (splats) determines their cooling rate, which is related to the probability of formation of non-equilibrium structures (amorphous, oversaturated solid solutions, etc) in a coating [3]. Particle size distribution of a spraying material also affects homogeneity of properties of a coating and degree of heterogeneity of its structure.

Under conditions of using powders for thermal spraying, this factor is determined by the chosen particle size distribution of a source material. The basic difference of the wire thermal spraying method from the powder one consists in the fact that formation of a flow of the spraying material particles occurs directly during the coating deposition process in dispersion of the applied wire melt. This predetermines the importance of investigation of the dispersion process, the results of which are required to control formation of coatings and monitor their properties.

Electric arc spraying is characterised by a large number of factors allowing the values of velocity, temperature and, particularly, sizes of the spraying particles [4] and, hence, properties of the coating to be controlled.

Dispersion of the wire melts in electric arc spraying of coatings. A coating in electric arc spraying is formed from the molten metal drops moving in a carrier gas jet (Figure 1). Heating and melting of a spraying material occur due to heat of the electric arc burning between the consumable wires, i.e. electrodes, which the molten metal is formed from. The molten metal is blown off from the electrode tips, refined under the effect of gas-dynamic and electromagnetic forces, and moves in the form of drops towards the substrate surface.

The processes of formation and detachment of molten metal from the electrode tips were analysed in studies [4–11]. The authors considered the main forces acting on a molten metal drop forming at the wire tip. The molten metal at the electrode tips is kept by the surface tension forces. As the metal is accumulated, under the effect of electrodynamic forces it is pushed out

to the peripheral parts of the electrodes, where detachment and transfer of the particles take place under the effect of a gas flow. The force that drives detachment of a drop depends on the velocity of the jet, whereas the force that holds the drop is proportional to its diameter and surface tension of the wire material melt. The balance of these forces can be written down in the form of the following equation [9]:

$$0.5C_d S\rho_g(W_g - W_p)^2 = \pi d_b \sigma, \qquad (1)$$

where C_d is the drag coefficient; $S = \pi d^2_{max}/4$ is the cross section area of the drop, m^2; ρ is the density, kg/m^3; σ is the surface tension, N/m; d_b is the detachment bridge, m; W is the velocity, m/s; and indices p and g refer to the drops and gas, respectively.

Changing the spraying parameters (wire feed speed, current and voltage at the electrodes, compressed air pressure) leads to changes in the wire melting mechanism. If there is a dynamic balance between the average speed of movement of the melting front and electrode feed speed, arcing is stable. In such a mode the gas flow provides evacuation and spraying of the molten metal from the electrodes up to their collision and short circuiting. Then the molten metal is again accumulated at the electrode tips, the arc column contracts, and the cycle is repeated. Along with periodic ejection of metal portions from the inter-electrode gap, there occurs also a continuous jet-like running off of the overheated metal from the electrode surfaces. This is a result of reduction of surface tension forces at high overheating of the molten metal, leading, consequently, to its inability to hold the fused layer on the electrode surfaces. Under the effect of the gas jet this fused layer is washed away from the electrode surfaces and sprayed [12].

The maximal size of drops torn off from the wire was estimated based on the condition of equality of surface tension forces and a drag force for arc metallising [13]:

$$d_{max} = 1/(W_g - W_p)\sqrt{8\sigma d_b/(C_d\rho_g)}. \qquad (2)$$

Solution of the inverse problem allows determining the required conditions, such as the velocity of the jet in spraying of a certain-diameter wire.

The experimental data [8] show that variations of the electric parameters of the process make it possible to vary not only the temperature of spraying particles, but also their size distribution. As indicated in studies [5, 6, 14, 15], the main parameters affecting the particle size distribution in arc metallising are the voltage at the arc electrodes and the compressed air pressure.

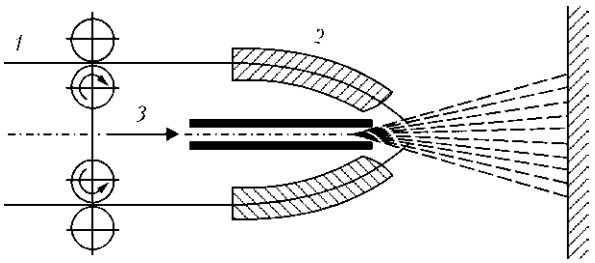

Figure 1. Flow diagram of the electric arc spraying process: *1* — wires; *2* — guides; *3* — compressed air

The degree of dispersion of the spraying material is also affected by the energy of the air jet, which in turn depends on the diameter of an air nozzle and can be expressed in the form of the following formula [5]:

$$d_{mean} = K_1(3.75/R_0 + 0.29)\sqrt{G/\gamma\mu_2} \text{ [mm]}, \qquad (3)$$

where K_1 is the size coefficient; R_0 is the radius of the air nozzle; G is the device productivity, kg/s; γ is the density of the spraying material, kg/m^3; and μ_2 is the spraying uniformity coefficient.

Physical-chemical processes occurring in molten metal during melting of the electrode by the arc, sizes of particles of the melt being sprayed, and properties of the coatings also depend on the intensity of melting of the electrodes and mass of the molten metal at their tips. Study [7] suggests formulae for approximate calculation of mass of the molten metal formed at the electrode tips in the inter-electrode gap during melting of solid and flux-cored wires. They allow for such factors of the electric arc metallising process as the arc current, electrode feed speed, frequency of molten metal ejections, and electrode diameters.

In spraying of pseudo-alloy coatings, two wires of dissimilar metals are fed to the electric arc metallisers. Therefore, the sprayed layer is a dispersed mixture of two spraying materials. When spraying two dissimilar wires, melting may occur non-uniformly because of a difference in values of the melting temperatures. No experimental investigation results are available on the character of melting of particles in simultaneous spraying of two dissimilar wires. Data on the effect of working parameters of a metalliser on the process of spraying of dissimilar wires will make it possible to define the methods to control particle size distribution of the spraying products in electric arc spraying of pseudo-alloy coatings and, hence, structure and properties of the resulting coatings.

Mathematical experimental design matrix

Mode number	Power W, kW	Compressed air pressure P, atm	Spraying distance H, mm
1	9.6	7	200
2	9.6	6	60
3	4.4	7	60
4	4.4	6	200
5	3.8	7	60
6	3.8	6	200
7	1.7	7	200
8	1.7	6	60

The present study was aimed at investigation of the process of combined spraying of copper and steel wires under conditions of electric arc metallising, as well as the effect of the process parameters on particle size distribution in the melts and microstructure of the spraying products.

Experimental procedure. 2 mm diameter wires, i.e. copper wire of the M1 grade and steel wire Sv-08A, were used as working materials for investigation of the spraying process. The process was performed by using twin-wire electric-arc metalliser EM-14M. The method of mathematical experimental design was used to study the character of relationship between the wire spraying conditions and particle size distribution [16]. The following parameters were chosen as the variable factors for optimisation: arc power, compressed air pressure, and spraying distance. The choice was based on the fact that these factors exert the substantial effect on the wire spraying process [5, 6, 10]. The experimental conditions are summarized in the experimental design matrix (Table).

Boundary conditions for the factors were chosen on the basis of analysis of previous experiments and experience with electric arc spraying of coatings by using wire materials [17–19]. In addition to the above variable factors, there were also the constant factors, such as the angle of inclination of the jet to the substrate — 90°, and the angle between the electrodes — 30°.

To investigate size and structure of the particles formed in spraying of dissimilar wires, the particles were collected by spraying of the wires in water. Then the particles were separated by using a magnetic plate.

Microstructure of the particles was examined with metallographic microscope «Neophot-32». Particle size distribution of the spraying products was measured by using image processing software «Atlas».

Results of analysis of spraying products. Figure 2 shows histograms of dependence of the mean size of particles on the spraying parameters determined in separate spraying of copper and steel wires, as well as in their simultaneous spraying. It follows from them that the degree of dispersion of sprayed copper is lower than that of steel and pseudo-alloy. This seems to be related to the fact that copper has the lowest surface tension coefficient (surface tension of copper is 1.35 N/m, and that of steel is 1.85 N/m [20]).

The following regression equations were derived as a result of mathematical processing of the measurement results. They express dependence of the particle size on the spraying conditions:

$$d_{\text{p}}^{\text{mean}}(\text{Cu}) = 46 - 0.31W - 0.62P + 0.004H;$$

$$d_{\text{p}}^{\text{mean}}(\text{Fe}) = 73 - 0.15W - 0.96P + 0.004H;$$

$$d_{\text{p}}^{\text{mean}}(\text{Cu} - \text{Fe}) = 73 - 0.74W - 1.21P + 0.01H.$$

Analysis of the regression equations allowed evaluating the effect of the variable factors of the process on the mean size of the particles for each of the materials.

The regression equations are indicative of the fact that it is the compressed air pressure that exerts the highest effect on the size of the parti-

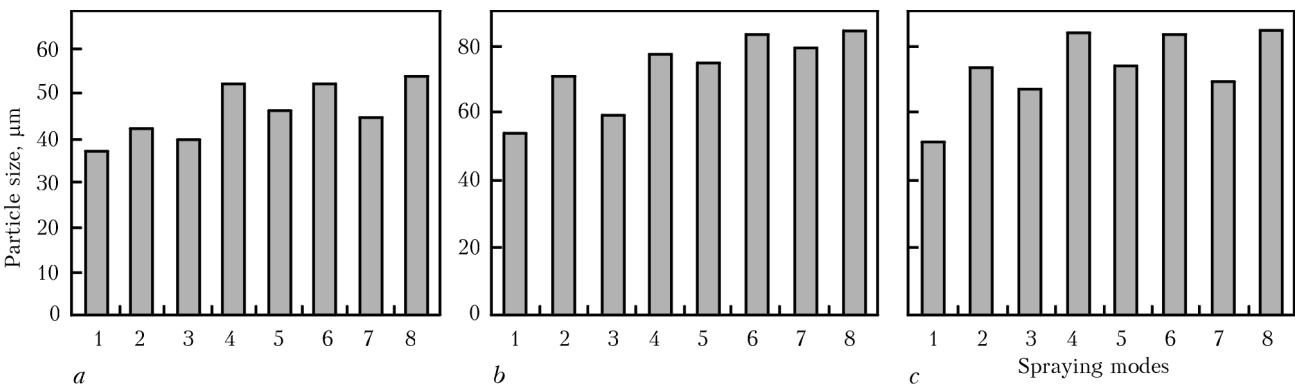

Figure 2. Dependence of mean size of particles on spraying modes: *a* — copper particles; *b* — steel particles; *c* — steel–copper pseudo-alloy particles

cles. Increasing the power and compressed air pressure leads to decrease in particle diameters. The minimal size of the particles was obtained in spraying by combining the maximal values of the power and compressed air pressure (mode 1). Combination of the maximal values of the power and compressed air pressure leads to formation of particles with the maximal sizes (mode 8).

Considering the turbulent character of the jet in electric arc spraying [13], the formed drops of the copper and iron melts may collide while moving in the jet, this determining the probability of development of the inter-phase interaction processes with phenomena of mutual mixing and formation of solid solutions in the copper–iron system. As seen from the copper–iron constitutional diagram (Figure 3), iron and copper have limited mutual solubility [21].

There are two ranges of possible interaction — at the initial stage of melting and detachment of drops from the copper and steel wire tips, and during their flight to the substrate surface.

To evaluate the possibility of interaction of particles in the spraying jet, conditional volume concentration β′ of the spraying material particles in the spraying jet was calculated, and the probability of collision of the particles in the jet was estimated [22]. Conditional volume concentration β′ is a ratio of the volume of the spraying material to that of the fed gas (compressed air):

$$\beta' = V_w / V_g, \quad (4)$$

where V_g is the volume of the compressed air equal to 1.2 m^3/min, and V_w is the volume of the fed wire, m^3/min, equal to

$$V_w = \pi 2r^2 v_w, \quad (5)$$

where r = 0.001 m is the radius of the wire, and v_w = 4.5 m/min is the wire feed speed.

As shown by calculation of β′ from formula (4), the conditional volume concentration of particles of the spraying material melt in the jet during metallising is $0.28 \cdot 10^{-4}$. However, it expresses the averaged distribution of the dispersed material in the jet. The distribution of particles of the material melt across the jet is non-uniform. In the first approximation it can be described by the Gaussian distribution, which is observed in the distribution of the particles that form a coating [23, 24]:

$$Y_i = Y_0 \exp - (r_i^2 / 2\delta^2), \quad (6)$$

where Y_i is the density of the flow of particles at point r_i in the jet section; Y_0 is the density of the flow of particles at the jet axis; r_i is the current radius of the jet section, and δ is the standard deviation.

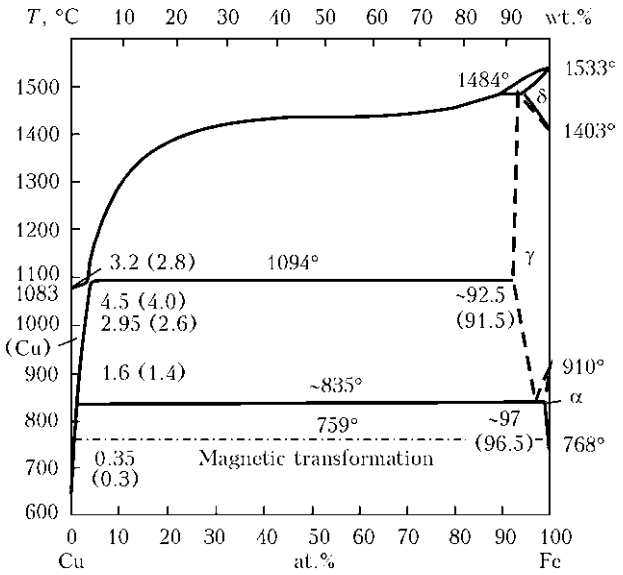

Figure 3. Copper–iron constitutional diagram

Integration of function Y_i with respect to dr yields the total density of the flow of the dispersed material in the jet section:

$$\int_{-\infty}^{+\infty} Y_i dr = Y_0 \sqrt{2\pi\delta}. \quad (7)$$

The total density of the flow can be determined through replacing the Gauss figure by the equidimensional rectangle with base $4r_{disp}$ ($r_{disp} = \sqrt{2\delta}$ is the dispersion radius) and height equal to the average concentration of the dispersed medium in the jet.

Replacing r_{disp} by $\sqrt{2\delta}$ yields

$$Y_0 / Y_{av} = 4/\sqrt{\pi} = 2.26. \quad (8)$$

Therefore, maximal conditional concentrations β′ of the particles of the material melt in the jet during spraying observed in the near-axis zone may amount to $0.64 \cdot 10^{-4}$, while the actual volume concentration of the particles of the material melt in the jet is $\beta' < 0.5 \cdot 10^{-4}$.

Calculation of the ratio of the average distance between the particles in the gas jet to their size allows evaluating the probability of collision of the particles, their coagulation in the molten state, and the resulting variation in composition and size of the spraying material particles [23]. The ratio of distance l between the particles to particle size d_p is as follows:

$$\frac{l}{d_p} = \frac{1}{\sqrt[3]{1.91\beta'} - d_p} - 1. \quad (9)$$

Figure 4 shows results of the calculation of value l/d_p at a particle diameter of 140 μm de-

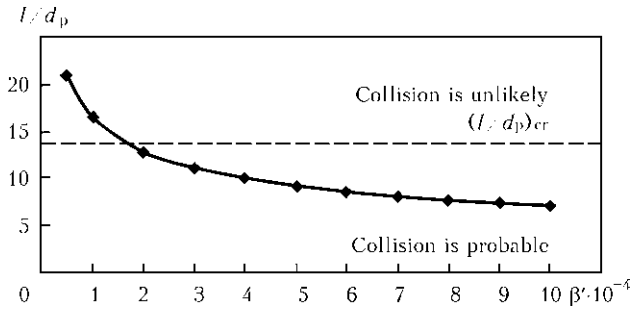

Figure 4. Dependence of inter-particle distance on concentration of dispersed phase

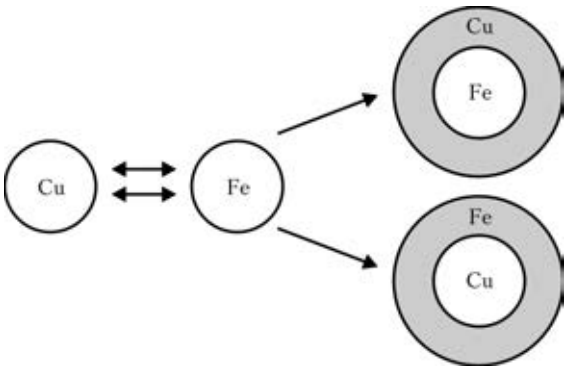

Figure 5. Types of interaction of copper and steel particles

pending on β′. It follows from these results that at the concentrations of the material particles less than $0.64 \cdot 10^{-4}$ the processes of collision and coagulation of the particles moving in the jet are unlikely.

Initially, the use of this procedure for evaluation of the possibility of interaction of particles within the jet showed that the particles of steel and copper during their flight within the jet should not collide and interact between each other. Nevertheless, results of magnetic separation of the entire mass of the dispersion product in combined spraying of the copper and steel wires indicated that practically all the particles of the collected powder are characterised by magnetic properties, this evidencing the presence of a magnetic material, i.e. iron, in each of them. In this connection, a necessity arose for analysis of the process of contact inter-phase interaction

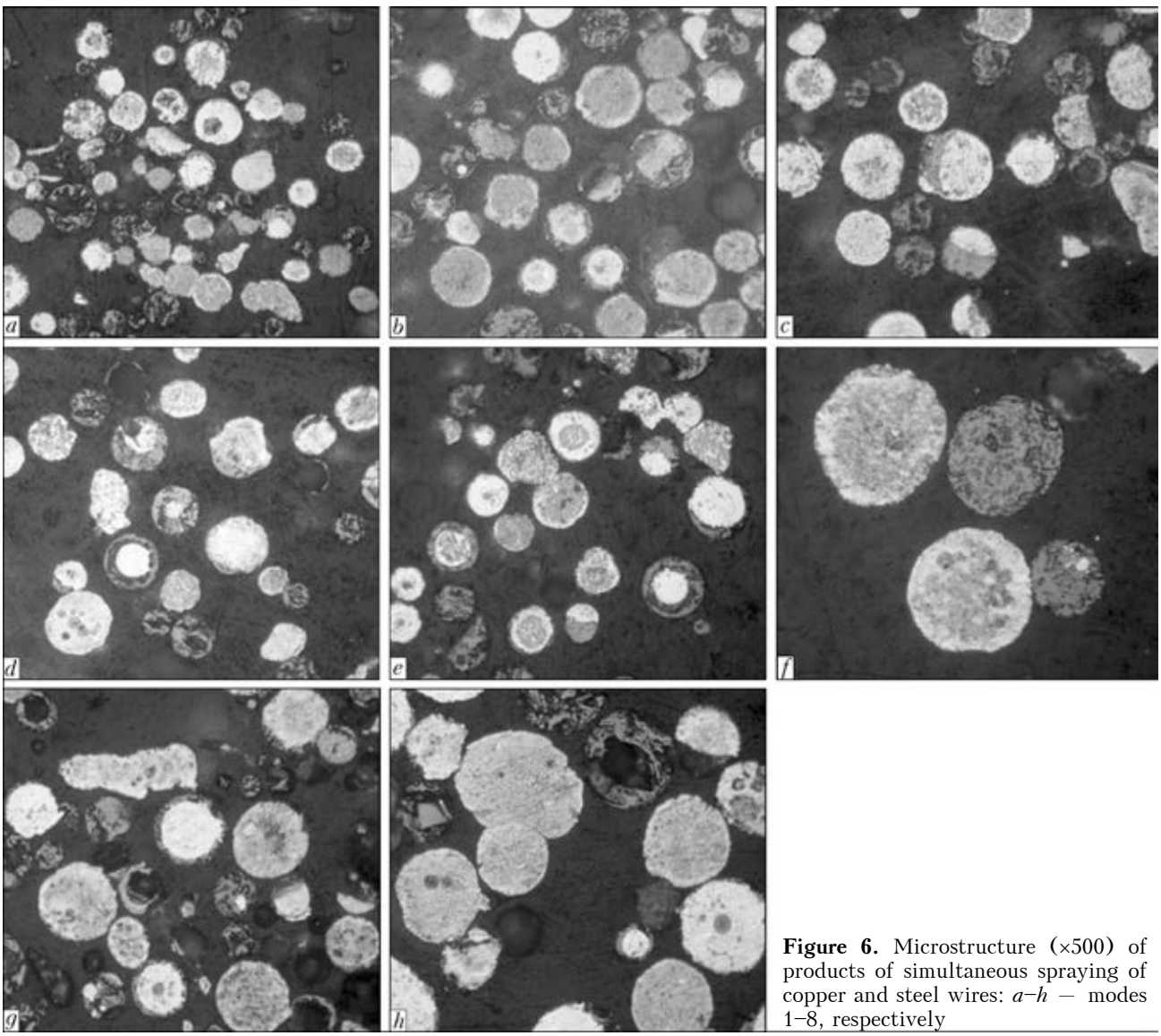

Figure 6. Microstructure (×500) of products of simultaneous spraying of copper and steel wires: *a–h* — modes 1–8, respectively

of particles of the copper and steel melts in case of their collision.

Calculation of the surface energy of the melt of sprayed steel and copper particles allows predicting the most probable type of contact interaction of the particles depending on their diameter. Free energy F of the surface of a liquid drop is proportional to its surface area [24]:

$$F = \sigma S, \quad (10)$$

where $S = 4\pi r^2$ is the surface area of a spherical particle with radius r, and σ is the coefficient of surface tension of the liquid.

A change in the free energy of a particle after interaction can be determined from the following formula:

$$\Delta F = F' - F, \quad (11)$$

where $F' = F_1' + F_2'$ is the energy of the particle after interaction, and $F = F_1 + F_2$ is the energy of the particle before interaction.

Figure 5 shows types of probable interactions of the steel and copper particles.

In case of capture of the steel particle by the copper one, a change in the free energy is $\Delta F = 3.6 \cdot 10^{-8}$ J, and in case of capture of the copper particle by the steel one this change is $\Delta F = 4.9 \cdot 10^{-8}$ J. Results of this calculation of the surface energy of the particles allow a conclusion that the most probable process of interaction of the steel and copper particles will occur in a direction of capture of the steel drops by the copper melt.

Analysis of microstructure of the particles showed that during the spraying process in all technological modes the copper and steel particles merge and form the pseudo-alloy particles. As seen from Figure 6, the steel and copper wire spraying products contain individual steel particles, whereas all copper particles have the form of pseudo-alloy copper–steel particles, which are the copper particles of the spherical and drop-like shapes with the fine or coarse steel particles embedded into them.

Based on the above evaluation of the probability of collision of particles in their flight within the jet, it can be assumed that the pseudo-alloy copper–steel particles form at the initial stage of melting and detachment of the melt drops from the wire tips.

Conclusions

1. The regression equations describing dependence of the mean size of particles on the values of the electric power, compressed air pressure and spraying distance were derived by using mathematical experimental design for investigation of the process of dispersion of the melts of steel and copper wires under the electric arc spraying conditions.

2. It was established that with the electric power varied within 1.7–9.6 kW, compressed air pressure — within 6–7 atm, and spraying distance — 60–200 mm, the mean size of the spraying particles in case of separate spraying of the copper wire varies within 37–54 μm, and that in case of steel wire Sv-08A — within 54–85 μm. In case of combined spraying of these wires under the said conditions the formed particles have a size of 52 to 85 μm.

3. The mean size of the particles depends primarily on the pressure of compressed air — as it increases, diameter of the particles decreases. In case of spraying by combining the maximal values of the power (9.6 kW) and compressed air pressure (7 atm), the formed particles have a minimal size: 37 μm in spraying of the copper wire, 54 μm in case of spraying wire Sv-08A, and 52 μm in their combined spraying. Combining the minimal values of the power (1.7 kW) and compressed air pressure (6 atm) leads to formation of particles with the maximal size: 54 μm in spraying of the copper wire, 85 μm in spraying of steel wire Sv-08A, and 85 μm in their combined spraying (pseudo-alloy particles).

4. It was found that electric arc spraying of copper by using copper and steel wires leads to inter-phase interaction of particles of the melts, which results in formation of a copper shell on the surface of the steel melt particles to form particles with a pseudo-alloy structure. Calculation-theoretical analysis of the interaction process shows that the most probable range of this interaction is the initial stage of the process of dispersion of the wire melts.

1. Baldaev, L.Kh., Borisov, V.N., Vakhalin, V.A. (2007) *Thermal spraying*: Manual. Ed. by L.Kh. Baldaev. Moscow: Market DS.
2. Kudinov, V.V., Bobrov, G.V. (1992) *Spraying of coatings: theory, technology and equipment*: Manual. Ed. by B.S. Mitin. Moscow: Metallurgiya.
3. Borisov, Yu.S., Korzhik, V.N. (1995) Amorphous thermal coatings. Theory and practice (Review). *Avtomatich. Svarka*, **4**, 3–11.
4. Vakhalin, V.A., Kudinov, V.V., Belashchenko, V.E. (1981) Investigation of effective efficiency of heating of electrodes and material utilisation factor in arc metallising. *Fizika i Khimiya Obrab. Materialov*, **8**, 65–69.
5. Kats, N.V., Antoshin, E.V., Vadivasov, D.G. (1966) *Spray metallising*. Moscow: Mashinostroenie.
6. Troitsky, A.F. (1960) *Principles of metallising by spraying*. Tashkent: Gosizdat UzSSR.
7. Royanov, V.A. (1990) Melting of electrodes in arc metallising. *Svarochn. Proizvodstvo*, **2**, 35–38.
8. Ageev, V.A., Belashchenko, V.E., Feldman, I.E. et al. (1989) Analysis of methods for control of parame-

ters of spraying particles in electric arc metallising. *Ibid*., **12**, 30–32.
9. Korobov, Yu.S. (2004) Estimation of forces affecting the spray metal in electric arc metallising. *The Paton Welding J*., **7**, 21–25.
10. Vakhalin, V.A., Kudinov, V.V., Maslennikov, S.B. et al. (1981) Process of melting and spraying of electrode material in electric arc metallising. *Fizika i Khimiya Obrab. Materialov*, **3**, 58–63.
11. Korobov, Yu.S., Boronenkov, V.N. (1998) Calculation of parameters of motion, heating and oxidation of particles in electric arc metallising. *Svarochn. Proizvodstvo*, **3**, 9–13.
12. Kuznetsov, V.D., Pashchenko, V.M. (1999) *Physical-chemical principles of coating formation*: Manual. Kyiv: NMTs VO.
13. Boronenkov, V.N., Korobov, Yu.S. (2012) *Fundamentals of arc metallising. Physical-chemical principles*. Ekaterinburg: UralGU.
14. Newbery, A.P., Granta, P.S., Neiser, R.A. (2005) The velocity and temperature of steel droplets during electric arc spraying. *Surface and Coatings Technology*, 195(**1**), 91–101.
15. Planch, M.P., Liao, H., Coddet, C. (2004) Relationships between inflight particle characteristics and coating microstructure with a twin wire arc spray process and different working conditions. *Ibid*., 182 (**2/3**), 215–226.
16. Novik, F.S., Arsov, Ya.B. (1980) *Optimisation of metal technology process by experimental design methods*. Moscow: Mashinostroenie.
17. Kats, N.V., Antoshin, E.V., Vadivasov, D.G. et al. (1966) *Spray metallising*. Moscow: Mashinostroenie.
18. Shashkov, A.N. (1960) *Antifriction pseudo-alloys*. Moscow: Mashgiz.
19. Krasnichenko, L.V., Smolyaninov, A.I., Podkovich, E.G. et al. (1966) Complex metallising pseudo-alloys as bearing materials. In: *Application of new materials in agricultural machine-building*: Transact. Rostov-na-Donu: Risknm, 3–20.
20. (1985) *Properties of elements*: Refer. Book. Ed. by M.E. Dritsa. Moscow: Metallurgiya.
21. Hansen, M., Anderko, K. (1962) *Structures of binary alloys*. Vol. 2. Moscow: Metallurgizdat.
22. Detlaf, A.A., Yavorsky, B.M. (1973) *Course of physics. Mechanics. Fundamentals of molecular physics and thermodynamics*: Manual. Vol. 1. Moscow: Vysshaya Shkola.
23. Borisov, Yu.S. (1982) *Theoretical and technological principles of deposition of plasma coatings from composite powders*: Syn. of Thesis for Dr. of Techn. Sci. Degree. Kiev.
24. Formation of sprayed layer. *http://*www.hvof.org-/theory/forming

Received 26.11.2012

NEWS

Testing of Welded Vessels Using Internal Pressure at Static and Low-Cycle Loadings

On the base of Test Laboratory of the E.O. Paton Electric Welding Institute, certified by the National Body on accreditation, a hydraulic complex, put into the State Register of Ukraine, is functioning.

The complex is designed for evaluation of strength of welded structures, operating under the pressure, in the process of their designing, manufacture and service.

In the solution of this problem the procedures are used, based on the fact that the integral characteristic of suitability of any structure to service is the safety factor which is set by a single loading up to their fracture. For structures, operating at alternating loads, the procedures of tests envisage the establishment of safety factor after conductance of cyclic loadings using value and duration specified for the service conditions.

Studies of stress-strain state and strength of high-pressure vessels are carried out at internal static and low-cycle loading. Certification tests of vessels can be performed.

FLUX ARC BRAZING OF ALUMINIUM TO GALVANISED STEEL

V.F. KHORUNOV and **O.M. SABADASH**
E.O. Paton Electric Welding Institute, NASU
11 Bozhenko Str., 03680, Kiev, Ukraine. E-mail: office@paton.kiev.ua

The study was dedicated to investigation of the processes occurring in DC flux arc brazing of overlap joints between thin-sheet aluminium and galvanised steel. Aluminium AD1, galvanised steel 08Yu, and reactive flux of the $KF–AlF_3–K_2SiF_6–KZnF_3$ system were used in the experiments. It was shown that reactive flux of the K–Al–SiF system used for brazing without passage of the filler alloy through arc gap improves conditions of formation of the overlap joints (wetting, spreading and filling of capillary gaps by the aluminium-silicon filler alloy) between aluminium and galvanised steel due to rapid destruction of the oxide film and formation of layers of low-melting point metal melts in the brazing location due to reactions of the flux with the materials being brazed. It was found that in brazing under conditions of arc heating the rate of spreading of the filler alloy on galvanised steel is approximately 3 times as high as on aluminium. The non-equilibrium contact angle on galvanised steel is 28–33°, and on aluminium — 8–10°. The data are given on structure of the brazed joints, composition of individual phases and chemical heterogeneity of the joints. According to the X-ray spectral microanalysis results, the 2–5 μm thick variable-composition Al–Fe–Si system transition layer containing small amounts of manganese (from steel) and zinc (from coating) forms at the contact boundary with steel. It was shown that the brazed joints between alloy AD1 and galvanised steel 08Yu produced by using the aluminium-silicon filler alloy have strength equal to that of the aluminium alloy. The overlap joints tolerate bending to an angle of 180°, while in multiple inflections (5–6 times) fracture occurs in aluminium. 23 Ref., 2 Tables, 5 Figures.

Keywords: *aluminium, galvanised steel, arc brazing, reactive flux, spreading of filler alloy, reaction layer, brazed joints*

Reduction of weight of structures with simultaneous improvement of their mechanical characteristics is one of the key challenges in building of low-consumption and reliable flying vehicles and ground-based equipment. Thin-sheet aluminium–steel structures are characterised by high design strength and corrosion resistance. They are 2 times as light as the steel ones, and are applied under severe conditions of alternating loads, temperatures and aggressive environment. An example is motor car construction, where decrease in weight allows extending service life, achieving substantial saving of fuel, and diminishing the negative effect on the environment. One of the main ways of reducing weight of a car body is application of high-strength ultralow-carbon steels [1] with aluminium or zinc corrosion-resistant coatings, and aluminium alloys. Meeting this challenge involves a number of complicated problems. Steel and aluminium differ greatly in their physical-mechanical characteristics (melting point, thermal expansion coefficient, strength) and chemical properties (ultimate solubility of iron in solid aluminium corresponds to 0.03–0.05 at the eutectic temperature [2, 3]), this leading to certain difficulties in providing the strong joints.

Solid-state welding of aluminium alloys to steel by the explosion [4] and friction [5] methods finds a limited application because of specifics of thin-sheet structures. In the fusion welding processes, interaction of steel with aluminium in the liquid phase is a cause of formation of a transition layer consisting of brittle intermetallic phases of the Al–Fe system, low strength, porosity and cracking of the welded joints. To avoid formation of solidification cracks in welding of 3–4 mm thick sheets, the content of brittle phases in the weld pool should not exceed 10 wt.% [6]. Alternatives to fusion arc welding can be the modern processes of TIG welding [7], laser welding [8, 9], modified MIG braze-welding (CMT-process) [10–12] with local melting of aluminium, or high-temperature brazing (laser brazing [13], MIG process [14], constricted arc process [15]), which are characterised by decreased heat input. Low level of the thermal-deformation effect in the brazing location, owing to a low heat input, and high corrosion resistance of the joints due to preservation of the zinc coating are the main advantages of arc brazing. The causes preventing a wide application of arc brazing for fabrication of strong sheet structures are related primarily to difficulties in ensuring a high quality

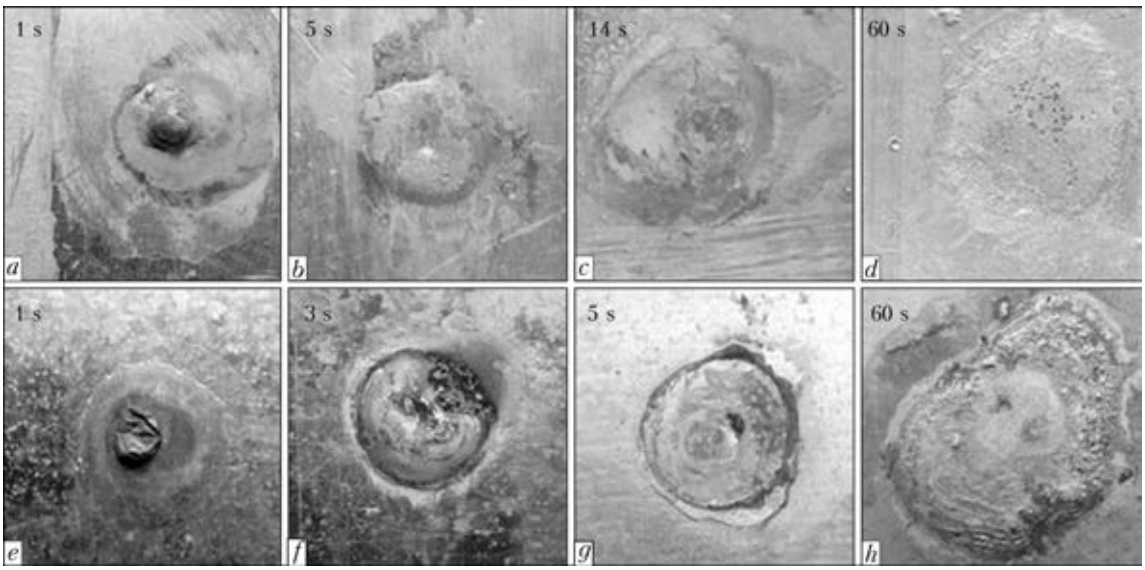

Figure 1. Drops of solidified filler alloy Al–12Si on aluminium AD1 (*a–d*) and galvanised steel 08Yu (*e–h*): *a–d* — AD1; *e–g* — 08Yu (arc brazing in argon atmosphere, I_b = 25 A, T_b = 600–615 °C, Kemppi system MASTERTIG MSL$^{(TM)}$ 2300 ACDC (Finland)); *h* — steel (furnace brazing in nitrogen atmosphere, T_b = 600 ± 3 °C)

of the joints. This can be achieved by using welding machines with feedback and low heat input [16].

Aluminium filler alloys of the Al–Si system are used for different types of the joints (overlap, T-, butt joints) between galvanised sheet steel and aluminium. In spreading of aluminium [17] or aluminium-silicon melts [18] on carbon steel, the transition layer of the Al–Fe–Si metal system forms as a result of reaction diffusion at the contact boundary, inhibiting spreading and leading to its complete termination. At the same time, it is a known fact that in high-temperature brazing of aluminium [19] and its alloys to stainless steel [20, 21] the reactive mixtures of the $KF–AlF_3$ salt system, containing additions of potassium hexafluosilicate and potassium-zinc fluoride, actively destroy (dissolve) oxides and form (from reduced silicon and zinc contained in fluorides) a layer of low-melting point alloy Al–Si(Zn) on aluminium, which improves spreading and capillary properties of the finished filler alloy.

Activation of the processes of wetting, spreading and improvement of capillary properties of the aluminium filler alloys can also be achieved in arc brazing due to the use of reactive fluoride fluxes of the $KF–AlF_3$ salt system. In this study, the experiments were carried out by using non-corrosive flux FAF 540 developed by the E.O. Paton Electric Welding Institute [22].

Under the TIG process conditions, wetting of the materials being brazed (aluminium AD1 and galvanised steel 08Yu) with a liquid filler alloy and reactivity of flux FAF 540 of the $KF–AlF_3–K_2SiF_6–KZnF_3$ salt system were evaluated from the area of spreading of the filler alloy addition (with weight of 0.17 g) of aluminium-silicon alloy (Al–12 % Si). The argon-arc torch was placed at the centre of a sample, so that the arc was ignited on the filler alloy addition. The brazing temperature range of 600–615 °C was set by the values of the straight polarity direct current and holding time. The rate of feeding of a shielding gas (argon of grade A) to the brazing zone was 6–9 l/min.

Substantial differences in physical-chemical properties of aluminium and steel, presence of a zinc coating on steel, local heating, and short-time interaction of liquid and solid phases during the brazing process exert a considerable effect on spreading of the filler alloy.

It was established that at the relatively equal time ranges and arc heating parameters the speed of motion of perimeter of a filler alloy drop and, hence, the area of spreading of the filler alloy on galvanised steel are higher than those on aluminium (Figure 1).

The kinetics of spreading of the filler alloy is related to the complex processes of chemical interaction of the salt and metal melts at the contact boundary with aluminium and galvanised steel. Destruction of the surface oxide film (as a result of chemical interaction with the salt melt) and distribution of the filler alloy over the overheated (approximately by 200 °C higher than the melting point) zinc melt improve wetting with the liquid filler alloy and its spreading on galvanised steel. In this case, fluidity of the filler alloy changes but insignificantly in dissolution in it of the entire coating metal. According to study [23], fluidity of aluminium alloys with 7–11 % Si and 8–15 % Zn is identical to that of

commercial silumins, and their mechanical properties are higher and depend on the zinc content, whereas formation of the Al–Fe–Si metal system transition layer at the interface with steel, as noted above, inhibits and stops spreading of the filler alloy.

The maximal area of spreading of the filler alloy on the surface of galvanised steel is S_{sp} = = 540 mm^2 during time t = 5 s at the set arc heating parameters (current I_b = 25 A, voltage $U_b = 12 \pm 0.3$ V). At the same brazing parameters the comparable area of spreading ($S_{sp} = 560$ mm^2) of the filler alloy on aluminium can be achieved at a longer (about 3 times) time and a local penetration of this material (Figure 2).

At a constant intensity of heat transfer of the heat source, because of high thermal diffusivity and heat capacity of aluminium, more heat is required to provide the equal area of spreading of the filler alloy compared to steel. Under non-isothermal conditions, spreading of the filler alloy on aluminium is restricted to region of existence of a thin layer of the metal melt over which the filler alloy is distributed. Therefore, the area of spreading of the filler alloy in non-equilibrium arc heating is much smaller (see Figure 2) than during the equilibrium process of brazing in furnace with a high uniformity of the temperature field and maximum permissible temperature gradient of ±5 °C over the aluminium part. The non-equilibrium contact angle on galvanised steel is 28–33°, and that on aluminium is 8–10°.

The most common type of joints on thin-sheet structures of aluminium and galvanised steel are the overlap joints. Mechanical properties of this type of the joints increase with increase in overlapping (edge lapping) of the thin sheets, and with improvement of the quality of filling the gap with the filler alloy and obligatory formation of fillets of a concave shape. Flux arc brazing of the overlapped aluminium to galvanised steel samples was performed on the 1 mm thick sheets with a set edge lapping of 2–6 mm. Filler wire AK12 and non-corrosive flux FAF 540 were used

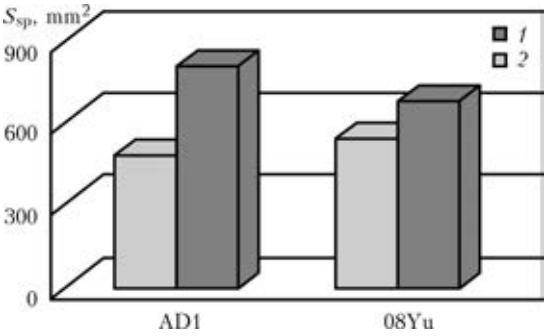

Figure 2. Area of spreading S_{sp} of filler alloy of the Al–12Si system in flux arc (*1*) and furnace (*2*) brazing

as brazing consumables. The aluminium sheets before brazing were subjected to etching in water solutions of alkali (15 % NaON) and a mixture of acids (2 vol.% HF and 20 vol.% HNO_3), and the steel sheets were degreased with acetone. A layer of flux (50 % water suspension) was applied to the aluminium sheet at the brazing location. Brazing of the overlap joints between aluminium and galvanised steel was carried out on the preliminarily prepared sheets. The effect of the arc brazing parameters was evaluated from the quality of formation, microstructure and chemical heterogeneity of the seams, tolerance of the brazed samples to bending to an angle of 180° and inflections, and tensile strength of the brazed joints at room temperature.

Investigations of straight polarity direct current flux arc brazing of aluminium to galvanised steel allowed defining the optimal parameters for the process of formation of the overlap joints (Table 1).

Characteristic peculiarity of the arc brazing procedure is ignition of the short arc and guiding it over the melt of a thin reaction layer on the surface of aluminium at a distance of approximately 2–3 mm from the joint, which makes it possible to diminish the thermal effect on the materials being brazed and retain integrity of the zinc coating. The filler wire is fed ahead of the arc at sufficiently small angles, so that it is melted in a thin layer of the metal melt. Optimal conditions of formation of the brazed seam are

Table 1. Approximate parameters of flux arc brazing of thin-sheet (1 mm) aluminium AD1 to galvanised steel 08Yu

D_f, mm	I_b, A	U_b, V	v_b, mm/s	TIG process flow diagram
1.6	47–50	9–11	12.0	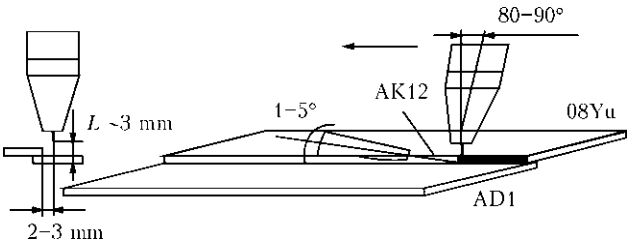
1.2	24–26	8–10	1.5–2.0	

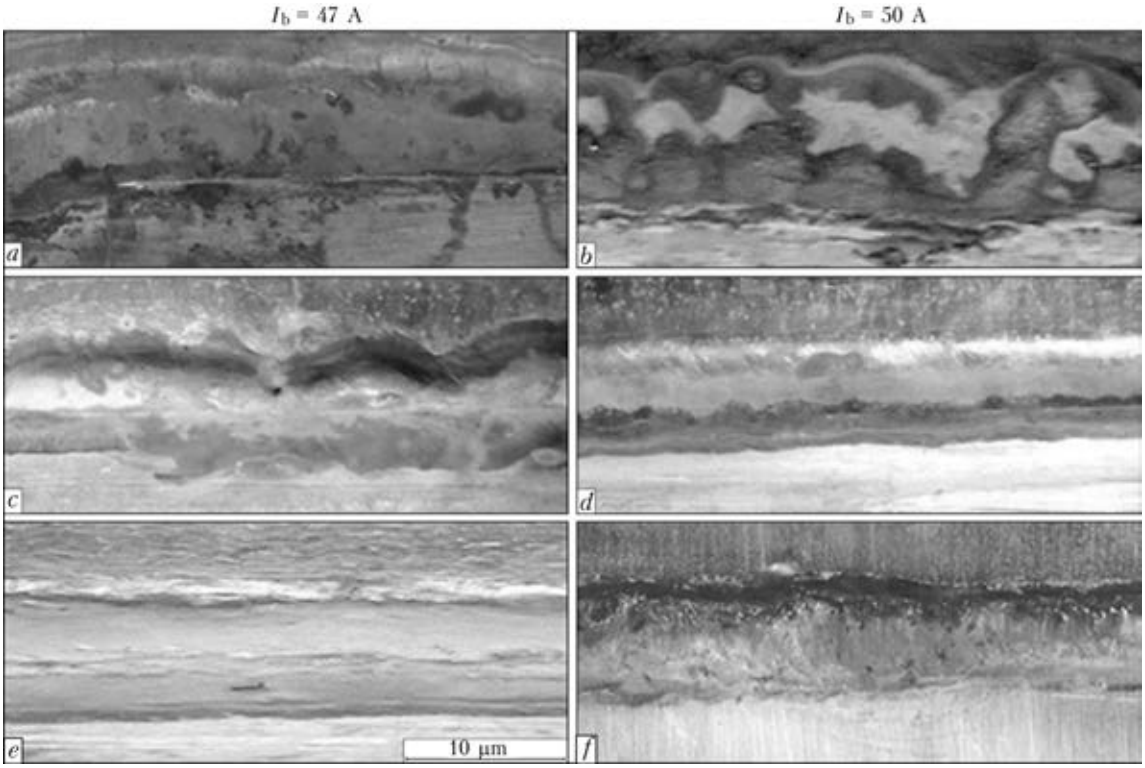

Figure 3. Appearance of the joints (×2) between galvanised steel 08Yu and aluminium AD1 produced in arc brazing (v_b =12 mm/s: *a*, *b* — excess of flux (G_f = 30 g/m^2); *c*, *d* — shortage of flux; *e*, *f* — optimal flux consumption (G_f = = 7–10 g/m^2)

achieved in melting of the filler in a relatively small volume of molten metal of the reaction layer, spreading of the excessive melt into the zone of a higher temperature and rapid filling of the brazing gap under the effect of capillary forces. This critical condition provides the stable process of formation of the brazed joint at the identical temperatures maintained at edges of the sheets of the materials joined. Reliability of shielding during the brazing process is ensured at a flow rate of the A grade argon equal to 8–10 l/min and torch nozzle diameter of 10–12 mm.

To ensure good formation of the seams (Figure 3, *a*, *f*) the consumption of flux is strictly limited and chosen depending on the brazing parameters.

Violation of the stable process of melting of the filler wire related to a change in the con-

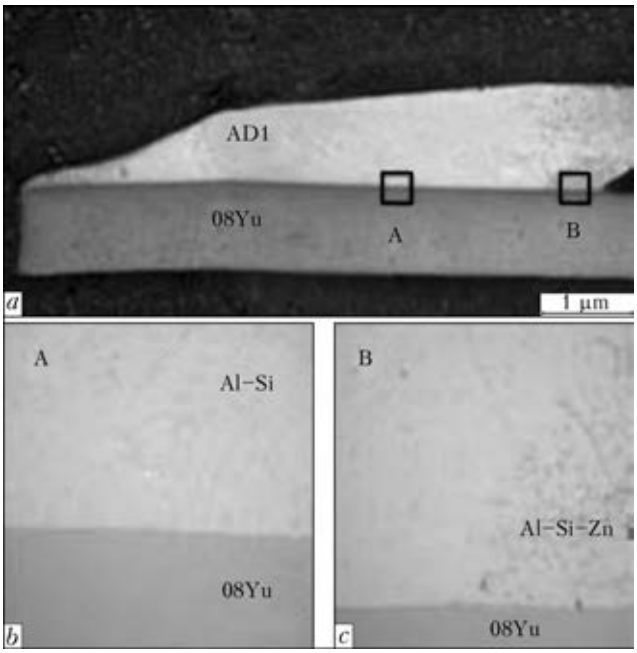

Figure 4. Macro- (*a* — ×10) and microstructure (*b*, *c* — ×400) of the brazed joint between aluminium AD1 and galvanised steel 08Yu

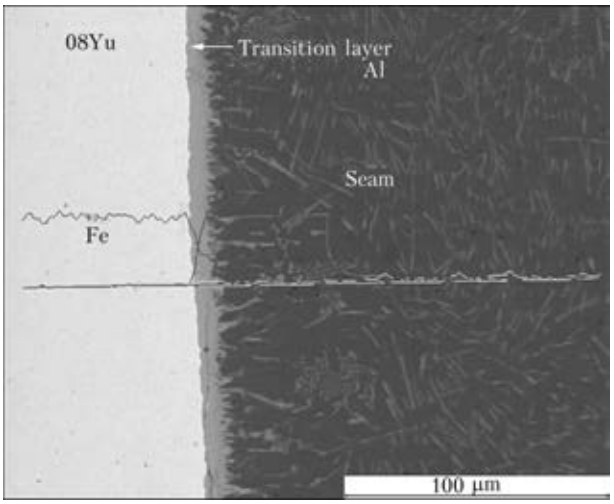

Figure 5. Microstructure (×350) and distribution of elements in the brazed joint of aluminium AD1 to galvanised steel 08Yu (microscope CamScan)

Table 2. Content of elements (wt.% in microvolumes) in the brazed joint between alloy AD1 and galvanised steel 08Yu

Joint region	Al	Si	Mn	Fe	Zn
08Yu	–	–	0.32	99.68	–
Transition layer (~5 μm)	65.58–59.93	5.11–4.75	0.12–0.09	29.20–34.89	0–0.35
Seam (matrix)	93.57–94.30	4.56–4.04	–	1.39–1.24	0.48–0.42

sumption of flux (deviation from the optimal consumption) leads to a non-rational distribution of the filler alloy in the brazed joint: rolls of metal onto the edge (Figure 3, *a*, *b*), lacks of penetration (Figure 3, *c*, *d*) and other defects of the brazed joints. The overlap steel-aluminium joints produced by arc brazing at the optimal parameters are characterised by complete filling of the variable gap with the filler alloy at a lap width of 5–6 mm. In this case the brazed seams are usually of a segmented shape and have a smooth surface and smooth transitions to aluminium and steel (Figure 4). On the reverse side of the joint (fillet region) the filler alloy forms a concave meniscus with a radius of less than 0.5 mm. The smooth surface of the seam with smooth fillets leads to decrease in the concentration of stresses, which is particularly important for making rigid structural connections on the above dissimilar metals.

The brazed joints between aluminium AD1 and galvanised steel 08Yu produced under non-isothermal conditions (TIG process, I_b = 24 A, v_b = 1.5 mm/s) have a heterogeneous structure (Figures 4 and 5).

The contact boundary with aluminium is meandering, having traces of a deep (about 180 μm) intergranular penetration of the eutectic phase (Al + Si) into the aluminium alloy being brazed. The central part of the seam is occupied by the aluminium-based α-solid solution with the lamellar dispersed eutectic (Al + Si) located in its interlayers between the grains (in Figure 4, *a* — gray cells, in Figure 5 — light cells). Investigation of chemical composition of the fillet (Figure 4, *c*) revealed the trend to alloying the brazed seam with zinc (formation of alloy of the Al–Si–Zn system) and growth of its content to 20 wt.% in the peripheral regions bordering with the zinc coating. According to the results of X-ray spectral microanalysis, the variable-composition Al–Fe–Si system transition layer from 2 to 5 μm thick, which contains small amounts of manganese (from steel) and zinc (from the coating), forms at the contact boundary with steel (Figure 5; Table 2).

No diffusion porosity and flux inclusions were detected in the transition layer region and in the aluminium to galvanised steel brazed joints. Marked structural changes in steel were not revealed either.

The overlap brazed joints tolerate bending to an angle of 180°, and in multiple inflections (5–6 times) the fracture occurs in aluminium. Tensile tests at room temperature showed that the brazed joints between alloy AD1 and galvanised steel 08Yu produced by using the aluminium-zinc filler alloy have strength equal to that of the aluminium alloy.

Conclusions

1. Reactive layers of the melts (aluminium-silicon and zinc) provide substantial improvement of capillary properties of the filler alloy, thus making it possible to join thin-sheet aluminium to galvanised steel with a large (up to 6 thicknesses) overlap.

2. The investigation results allowed establishing the arc brazing parameters that provide rapid destruction (dissolution) of oxides, stable melting, spreading and complete filling of the gap with the filler alloy.

3. The 2–5 μm wide intermetallic layer of the Al–Fe–Si system forms under non-equilibrium conditions at the contact boundary with steel. Zinc in the brazed seam is contained mostly in the aluminium solid solution.

4. As shown by the short-time shear tests, the overlap brazed joints have strength equal to that of the aluminium alloy.

1. Kuroda, M., Uenishi, A., Yoshida, H. et al. (2006) Ductility of interstitial-free steel under high strain rate tension: Experiments and macroscopic modeling with a physically-based consideration. *Int. J. Solids and Struct.*, **43**, 4465–4483.
2. Mondolfo, L.F. (1979) *Structure and properties of aluminium alloys*. Moscow: Metallurgiya.
3. (1997) *Constitutional diagrams of binary metal systems*: Refer. Book. Vol. 2. Ed. by N.P. Lyakishev. Moscow: Mashinostroenie.
4. Han, J.H., Ahn, J.P., Shin, M.C. (2003) Effect of interlayer thickness on shear deformation behavior of AA5083 aluminum alloy/SS41 steel plates manufactured by explosive welding. *J. Mat. Sci.*, **38**, 13–18.
5. Fukumoto, S., Tsubakino, H., Okita, K. et al. (1999) Friction welding process of 5052 aluminium alloy to 304 stainless steel. *Mat. Sci. and Techn.*, **15**, 1080–1086.
6. Ryabov, V.R., Rabkin, D.M. (1984) *Welding of dissimilar metals and alloys*. Moscow: Mashinostroenie.

7. Bruckner, J. (2003) Arc joining of steel with aluminium. *The Paton Welding J.*, **10/11**, 180–182.
8. Mathieu, A., Shabadi, R., Deschamps, A. et al. (2007) Dissimilar material joining using laser (aluminum to steel using zinc-based filler wire). *Optics & Laser Technology*, **39**(April), 652–661.
9. Hui-Chi Chen, Pinkerton, A.J., Lin Li et al. (2011) Gap-free fibre laser welding of Zn-coated steel on Al alloy for light-weight automotive applications. *Mater. and Design*, **32**, 495–504.
10. Zhanga, H.T., Feng, J.C., He, P. et al. (2009) The arc characteristics and metal transfer behaviour of cold metal transfer and its use in joining aluminium to zinc-coated steel. *Mater. Sci. and Eng. A*, **499**, 111–113.
11. Zhang, H.T., Feng, J.C., He, P. et al. (2007) Interfacial microstructure and mechanical properties of aluminium-zinc-coated steel joints made by a modified metal inert gas welding-brazing process. *Materials Characterization*, **58**, 588–592.
12. Kim, Y., Park, K., Kim, S. et al. (2012) Dissimilar metal joining of steel to aluminum using the arc heat source. *Mater. Sci. Forum*, **706–712**, 2974–2979.
13. Mathieu, A., Pontevicci, S., Viala, J.-C. et al. (2006) Laser brazing of a steel/aluminium assembly with hot filler wire (88 % Al, 12 % Si). *Mater. Sci. and Eng. A*, **435/436**, 19–28.
14. Taichi, M., Kazuhiro, N., Tong, H. et al. (2003) Dissimilar metal joining of aluminum to steel by MIG arc brazing using flux cored wire. *ISIJ Int.*, 43(**10**), 1596–1602.
15. Draugelates, U., Bouaifi, B., Helmich, A. et al. (2002) Plasma arc brazing: a low-energy joining technique for sheet metal. *Welding J.*, 81(**3**), 38–42.
16. Siewert, T., Samardzic, I., Klaric, S. (2002) Application of an on-line weld monitoring system. In: *Proc. of 1st Int. Conf. on Advanced Technologies for Developing Countries* (Slavonski Brod, Croatia, Sept. 12–14, 2002), 1–6.
17. Eryomenko, V.N., Lesnik, N.D., Pestun, T.S. et al. (1971) Kinetics of aluminium spreading on iron. In: *Physical chemistry of surface phenomena in melts*. Kiev: Naukova Dumka, 203–206.
18. Eryomenko, V.N., Lesnik, N.D., Pestun, T.S. et al. (1972) About the kinetics of spreading of aluminium-silicon melts on iron. In: *Wettability and surface properties of melts and solids*. Kiev: Naukova Dumka, 30–41.
19. Khorunov, V.F., Sabadash, O.M., Andreiko, A.A. (1998) Investigation of fusibility and chemical interaction in the K, Al, Si/F salt system fluxes for high-temperature brazing of aluminium. In: *Proc. of Int. Conf. on Brazing, High Temperature Brazing and Diffusion Welding* (Aachen, Germany, May, 1998), 200–202.
20. Sabadash, O.M., Khorunov, V.F. (2005) Materials and technology for flux brazing and soldering of aluminium and aluminium to steel. *The Paton Welding J.*, **8**, 62–67.
21. Khorunov, V.F., Sabadash, O.M. (2006) Reactive fluoride flux for brazing of aluminium and dissimilar joints. *Adgeziya Rasplavov i Pajka Materialov*, Issue 39, 68–75.
22. Sabadash, O.M., Khorunov, V.F. (2007) Reactive flux for brazing of aluminium. In: *Proc. of 2nd Sci.-Techn. Seminar on Welding and Related Processes in Industry* (17 April, 2007, Kiev). Kiev: Ekotekhnologiya, 48–49.
23. Bochvar, A.A., Sviderskaya, Z.N., Rytvin, N.I. et al. (1947) *New casting alloys. Zinc silumins*. Moscow: TsIIN TsM SSSR.

Received 13.11.2012

NEWS

Technology of Slag Crust Utilisation in Pipe Welding

Technology of flux waste processing after welding was developed, which includes separation with subsequent return of unused flux into production and manufacture of AN-60SM flux from the slag crust. Technology of flux manufacturing from the slag crust does not envisage the power-consuming and ecologically hazardous process of flux melting in furnaces. The flux is made by multi-stage crushing of the slag crust, magnetic separation, semifinished product screening and drying.

AN-60SM flux to DIN 32522–81 is of FMS 168 ACM SHP 53-403-40(2-16) class. Slag base is SiO_2–MnO–CaO–CaF_2. Basicity (by IIW formula) is 0.85. Bulk density is 1.3–1.8 kg/dm^3. The metal of weld produced with this flux (St3 + Sv-08A) has the following mechanical properties: yield point — 375 MPa, ultimate tensile strength — 500 MPa. Impact toughness *KCU* at +20 °C is equal to 125 J/cm^2, *KCV* at –20 °C is equal to 40 J/cm^2 (steel 10Kh–SND + Sv-10GN).

Application. Utilisation of flux wastes from welding fabrication allows reducing the purchased quantities of initial flux. AN-60SM flux made from the slag crust is suitable for welding instead of general-purpose fluxes AN-348 A, OSTs-45, ANTs-1 in shipbuilding, tank construction, general and chemical engineering.

Technical and economic advantages. AN-60SM flux ensures 1.5–2 times higher resistance of weld metal to porosity than AN-348A type fluxes (diffusible hydrogen content below 3 cm^3/100 g of weld metal).

Introduction of the technology of slag crust processing allows saving up to 50 % of the initial flux cost due to reuse of regenerated flux in production.

Technology of flux production based on slag crust recycling does not require power-consuming furnace melting of flux accompanied by harmful evolutions into the atmosphere.

State of development. This technology was introduced in Novomoskovsk and Khartsysk pipe plants. AN-60SM flux was introduced in welding parts in Kremenchug Wheel Plant, Kyiv Shipbuilding-Shiprepair Plant, Makeevka Plant of Metal Structures, Snezhnyansk «Khimmash» Plant, etc. Ukrainian specification for AN-60SM flux has been developed.

DEVELOPMENT OF THE TECHNOLOGY OF BRAZING DIAMOND–HARD ALLOY CUTTERS

B.V. STEFANIV
E.O. Paton Electric Welding Institute, NASU
11 Bozhenko Str., 03680, Kiev, Ukraine. E-mail: office@paton.kiev.ua

Brazing temperature influence on performance of diamond–hard alloy plates (DHAP) and diamond–hard alloy cutters (DHAC) was studied. It is established that application of copper-zinc and copper-manganese filler metals for brazing the composite cutter is not optimum because of the high heating temperature that leads to marked degradation of physico-mechanical properties of DHAP diamond layer because of graphitization. Technology of brazing DHAP with hard alloy mandrel (HAM) was developed that ensures the required properties of the diamond layer as a cutting tool. Technology of DHAC brazing (DHAP + HAM) was developed allowing performance of DHAC brazing with HAM and preserving its service properties on a high level. A lot of attention was given to assessment of performance of DHAC diamond layer after heating for brazing by gauging of a certain rock. It is shown that the proposed technology of DHAC brazing with diamond layer cooling allows application of filler metals with more than 700 °C brazing temperature without loss of this layer performance. During investigations standard filler metals and those developed at the E.O. Paton Electric Welding Institute were tested. Generalization of a set of tests led to the conclusion that Ag–Cu–Zn–Ni–Sn–Mn and Ag–Cu–Zn–Ni–Mn–Pd system filler metal are the most promising. Developed technology has been applied for items and tested under the actual service conditions. 9 Ref., 2 Tables, 4 Figures.

Keywords: *brazing, brazing filler metal, superhard materials, diamond layer, diamond–hard alloy cutter, diamond–hard alloy plate, hard alloy mandrel, graphitization, drill bit, thermal stability*

Drilling of oil and gas wells in soft, medium-hard and hard rocks is performed with application of drill bits, cutters, inserts and other types of tools fitted with cutting elements in the form of two-layer diamond–hard alloy plates (DHAP) and diamond–hard alloy cutters (DHAC). In Ukraine DHAP are manufactured at V.N. Bakul Institute for Superhard Materials (ISM) of the NAS of Ukraine. They are two-layer plates [1] of 13.5 mm diameter and 3.5 mm height, in which one layer of 0.5–0.8 mm height is a diamond polycrystal, and the other layer is a hard alloy substrate. Therefore, making DHAC of the necessary size requires joining DHAP with hard alloy mandrel (HAM).

It should be noted that foreign companies, for instance Element Six, Smith, Hugnes, Reed, Security, Ulterra and De Beers manufacture DHAC of the required dimensions by cutter height and the operation of DHAP brazing to hard alloy substrate during their manufacturing is not required.

The objective of the work was development of the technology of brazing DHAP with HAM, providing minimum influence of heating on diamond layer properties, i.e. preserving the physico-technological characteristics of the diamond layer as the cutting tool. They, in their turn, influence the mechanical speed and feed range of the drill bit. This paper gives the results of studies on DHAP fastening to HAM by brazing. Studied were DHAC manufactured by leading foreign companies and local manufacturer.

DHAC of Syndrill grade of Element Six Company (Great Britain) and DHAP of ISM were studied to determine their thermal stability and wear resistance. The term thermal stability of DHAP and DHAC determines the limits of temperature and time of heating, at which the diamond-containing layer preserves its physico-mechanical properties, particularly, wear resistance values. This concerns both the process of plate sintering and their service. The higher the value of DHAP thermal stability the better are the prospects for their application for drilling oil and gas wells by diamond drill bits.

DHAP and DHAC heating was performed in a muffle furnace in the temperature range of 500–1000 °C for 1 to 20 min. Analysis of the obtained results shows that temperature and time of soaking have a great influence on DHAP and DHAC thermal stability (Figure 1). For locally manufactured DHAP heating at temperature above 650 °C and soaking for 3 min leads to diamond layer degradation. Much better results on thermal stability, compared to DHAP, were obtained

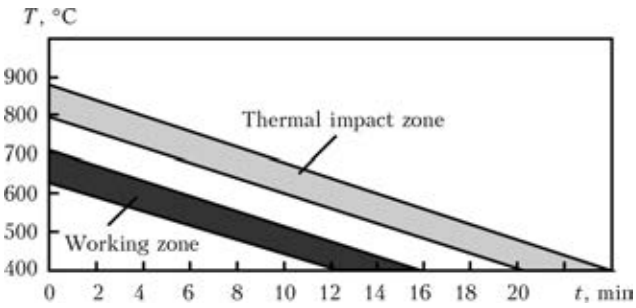

Figure 1. Areas of DHAP and DHAC thermal stability: *1* — series-production technology of ISM; *2* — technology of Element Six Company (Syndrill grade)

for Syndrill DHAC of Element Six. Their thermal stability is equal to 850 °C at heating for 3 min.

To determine the differences in thermal stability of DHAP of ISM and Syndrill DHAC of Element Six microstructural examination of diamond-containing layer was conducted (Figure 2). Investigation results revealed that the cause for low thermal stability of DHAP samples (ISM) is the high cobalt content in the diamond layer. Conducted examination in electron microscope Zeiss EVO 50 XVP showed that samples of Syndrill DHAC have a uniform distribution of cobalt in diamond-containing layer and its

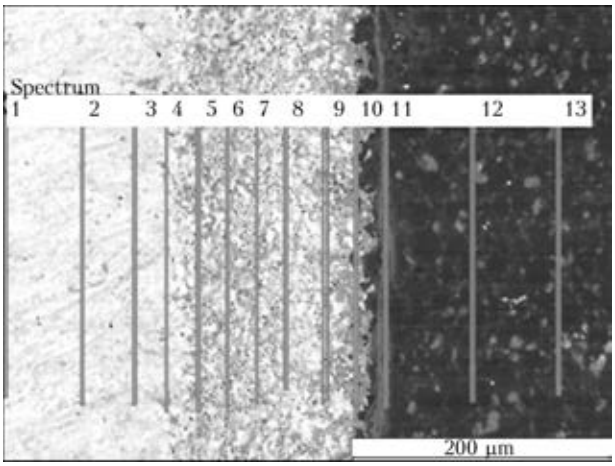

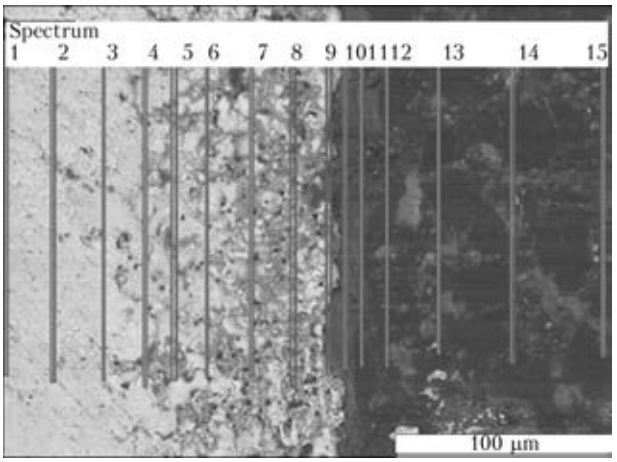

Spectrum number	C	Co	W
1	28.72	4.24	67.04
2	30.70	4.04	65.26
3	31.00	3.19	65.81
4	35.78	2.73	61.49
5	44.06	3.61	52.33
6	48.21	3.36	48.43
7	46.95	3.23	49.82
8	38.77	2.74	58.49
9	34.18	3.73	62.09
10	40.71	6.97	52.32
11	93.01	2.34	4.65
12	95.95	1.70	2.35
13	95.11	2.53	2.36
Average value	51.01	3.42	45.57
Root-mean-square deviation	25.63	1.28	24.96
Maximum value	95.95	6.97	67.04
Minimum value	28.72	1.70	2.35

a

Spectrum number	C	Co	W
1	13.28	12.72	73.99
2	8.25	11.66	80.10
3	10.50	11.30	78.19
4	21.96	9.62	68.42
5	19.36	9.82	70.83
6	15.23	8.16	76.61
7	14.22	6.60	79.18
8	12.60	8.33	79.07
9	6.69	11.95	81.36
10	10.07	26.01	63.92
11	71.73	9.62	18.64
12	89.85	4.06	6.09
13	87.66	3.84	8.50
14	88.58	4.97	6.45
15	93.54	3.60	2.87
Average value	37.57	9.48	52.95
Root-mean-square deviation	36.13	5.51	33.01
Maximum value	93.54	26.01	81.36
Minimum value	6.69	3.60	2.87

b

Figure 2. Microstructure and element content of spectra (wt.%) of Syndrill DHAC (*a*) and of DHAP ISM (*b*)

amount is equal to 7 wt.% unlike local DHAP, in which cobalt content is 26 wt.%. Increase of cobalt and lowering of carbon content have a negative influence on thermal stability and wear resistance (lowering their values). It should be taken into account when joining DHAP (ISM) to HAM.

At DHAP heating up to a critical temperature (670–700 °C) [2] physico-mechanical properties of the diamond layer abruptly degrade, because of diffusion interaction between the diamond particles and cobalt. Graphitization of polycrystalline synthetic diamonds and cracking, caused by the difference in thermal expansion coefficients of diamond and cobalt, take place, resulting in fracture of the diamond layer.

Earlier studies of the processes of DHAC brazing were conducted at V.B. Bakul ISM [3]. Experimental retrofitting of DHAC brazing technology was performed using copper-zinc filler metals of grades L63, LNKoMts 49-9-0.2-0.2, LNMts 60-9-5, MNMts 68-4-2, LMtsZh 51-1.5-0.75 with the temperature range of melting from 880 up to 1000 °C. However, melting temperature of these filler metals is by 150–250 °C higher than that of destruction of synthetic diamonds that required application of special measures on diamond layer cooling in brazing. The greatest difficulties at optimization of DHAC brazing technology consisted in heating of DHAP substrate surface up to a temperature ensuring filler metal spreading, at intensive simultaneous cooling of the diamond layer.

As in the opinion of the authors of this work, temperature of DHAP diamond layer should not be higher than 700–720 °C, and temperature of brazing DHAP substrate surface should be not less that 930–950 °C, temperature gradient by DHAP height should be of the order of 80–90 °C/mm. Analysis of the process of brazed seam formation and its condition after shear testing showed that the best and most stable results were obtained with application of LNKoMts filler metal. However, the authors do not give any data on wear resistance of brazed joints that is the main characteristic in drill bit operation.

At DHAP joining with HAM actually brazing of two hard alloys is performed, as the diamond coating is located on DHAP outer surface. Graphitization temperature of each grade of synthetic polycrystalline diamonds depends on many factors, including degree of purity (quantity of impurities of metals-catalysts), heating environment and time of soaking at elevated temperature [4]. Such features of synthetic diamonds should be taken into account at selection of filler metal composition, and its temperature interval of melting. PWI conducted extensive investigations in this direction [5–7].

Investigation of DHAC and DHAP thermal stability (see Figure 1) showed that the diamond layer in local DHAP degrades at the temperature of about 650–680 °C. As the currently available filler metals have liquidus temperature above 700 °C, the method of brazing with forced cooling was developed for joining DHAP with HAM. This requirement was realized in a specially designed unit of ingenious design (Figure 3), which allows performing simultaneous or separate heating of DHAP and HAM, measuring temperature on the surface of DHAP diamond layer, as well as changing the temperature of DHAP and HAM heating and cooling.

Calculation of the inductor for brazing presents considerable difficulties. As a result of the skin effect, current density is non-uniformly distributed across the section of inducing current wire. Actually, most of the inductors for brazing, particularly those at radio frequencies (UHF) are made proceeding from experimental data with subsequent retrofitting after testing them in operation. When designing the inductor, we tried to apply an enclosing structure, when the inductor is located outside the item being brazed, and follows the component configuration in the brazing zone. Enclosing inductors are characterized by the highest efficiency and provide more uniform heating [8].

At design of parts to be brazed, we envisaged the possibility of mounting an inductor of such a configuration that would ensure heating of the required zone. Inductor position was selected allowing for the mass and thermophysical proper-

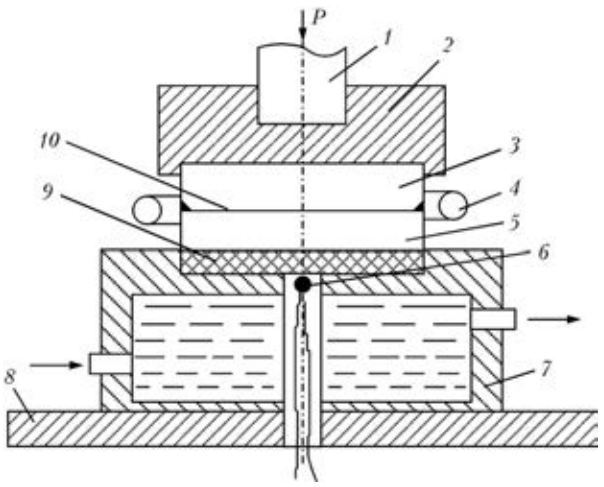

Figure 3. Schematic of device for induction brazing of DHAC: *1* — support; *2* — ceramic insert; *3* — HAM; *4* — inductor; *5* — DHAP; *6* — thermocouple; *7* — cooler; *8* — base; *9* — diamond layer; *10* — seam

Table 1. Shear strength of joints of hard alloy plates VK8 + VK8

Sample number	Filler metal grade or system	T_b, °C	Compression force P, kg	Shear strength τ_{sh}, MPa
1	Ag–Cu–Zn–Ni–Mn	700	3217	225
2	Ag–Cu–Zn–Ni–Mn–2Pd	730	3575	250
3	PM-50	850	4032	282
4	PM-72	950	3675	257
5	PSr-40	620	3500	245
6	Ag–Cu–Zn–Ni–Mn–5Pd	750	4500	315
7	Ag–Cu–Zn–Sn–Mn–Ni	750	5634	394

ties of materials so that the parts being joined reached the brazing temperature simultaneously.

DHAP + HAM heating temperature was determined using thermocouples of chromel-alumel type of two-channel meter-regulator of TRM 202 type. As a result of conducted experiments inductor location relative to mated composite parts of DHAC was selected. Heating was conducted from a more massive part, considering that the less massive part can be heated both by induction currents, and due to heat transfer from the massive part (Figure 4). To improve heating efficiency the gap between the inductor and heated surface of the parts was selected to be minimum in the range of 5–7 mm.

Heating duration in brazing essentially influences the quality of brazed joints. Short time of heating (less than 5–10 s) is insufficient for completion of the process of cleaning by the flux of the surfaces to be brazed and achievement of the same temperature by all the elements participating in brazing. At longer time of heating oxidation of filler metal and brazed metal takes place, leading to deterioration of the results (defects) of brazed joints.

As a result of conducted experiments on optimization of technologies and modes of heating, a graph of temperature distribution in the body of parts being brazed, was plotted. Figure 4 shows the curves of temperature distribution at induction heating of hard alloy substrate under the condition that at 0.1 cm depth the temperature is equal to 700 °C. It follows from the given data that the smaller the depth of current penetration, the higher is the surface temperature and the lower the temperature in deeper-lying layers. In our case, an inductor was selected, which provides uniform temperature field of the brazed parts at heating.

Selection of optimum composition of filler metal in DHAC manufacture, requires determination of shear strength and wear resistance of brazed joints. At the first stage at brazing of samples for shear testing filler metals given in Table 1 were applied. The Table also gives the results of testing performed using a special device in R-05 rupture machine at ISM.

At the second stage — at determination of wear resistance — DHAP + HAM were joined. For this purpose DHAC was made using the above filler metals, and wear resistance testing of DHAC diamond layer was performed in a special facility, which simulates the actual service conditions. The essence of this method [9] consists in that friction of tested sample against an abrasive surface is performed and then its wear intensity is determined. In other words, gauging

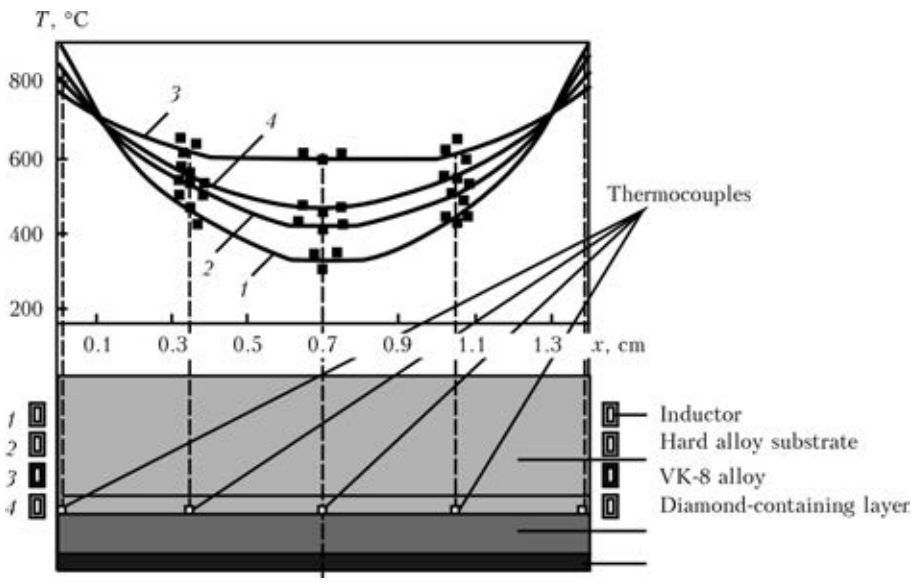

Figure 4. Influence of inductor position (*1–4*) relative to the blank on temperature distribution across the section of hard alloy substrate

Table 2. Wear resistance testing of DHAC hard alloy plates

DHAC sample number (DHAP + HAM)	Filler metal alloying system	DHAP cooling	Feed range, m (rock is sandstone)	Extent of wear on back edge h, mm
1	Ag–Cu–Zn–Cd (PSr-40)	Yes	50	0.15–0.20
2	Ag–Cu–Zn–Ni–Mn	Same	50	0.18–0.20
3	Ag–Cu–Zn–Ni–Mn–5Pd	No	30	Complete wear
4	Ag–Cu–Zn–Ni–Mn–5Pd	Yes	50	0.15–0.22
5	Cu–Zn–Mn–Ni–Sn–Cr (PM-50)	No	20	Complete wear
6	Cu–Zn–Mn–Ni–Sn–Cr (PM-50)	Yes	50	1.5–2.0
7	Cu–Mn–Ni–Si–Fe (PM-72)	Same	15	Complete wear
8	Ag–Cu–Zn–Sn–Mn–Ni	»	50	0.15–0.22

of that rock for which the sample is intended is performed.

DHAC brazing without cooling by various filler metals leads to complete wear of the diamond layer. Results of wear resistance testing showed that at brazing with filler metals of PM-50 and PM-72 grades DHAC are characterized by the lowest wear resistance even with cooling, and they cannot be applied in manufacture of drill bits, even though at studying of hard alloy material wetting these filler metals showed one of the best results and satisfactory shear strength.

DHAC wear resistance in the presence of cooling system could be increased up to the required level at application of filler metals of Ag–Cu–Zn–Cd, Ag–Cu–Zn–Ni–Mn, Ag–Cu–Zn–Ni–Mn–5Pd and Ag–Cu–Zn–Sn–Mn–Ni systems, having a lower melting temperature (610, 700, 740 and 720 °C, respectively). They ensure the required extent of wear not greater than 0.3 mm that allows them to be used in manufacture of drill bits, designed for well drilling on soft, medium-hard and hard abrasive rocks. Investigation data are given in Table 2.

Conclusions

1. Influence of temperature-time cycle of brazing on DHAC diamond layer and its performance (thermal stability and wear resistance) was established.

2. Developed technology of brazing DAHP + HAM provides lowering of heat impact on the diamond layer and allows preservation of its service properties at a high level

1. *TU 88.1244–91*: Diamond–hard alloy cutter inserts. Kiev.
2. Novikov, N.V. (2005) *Tools from superhard materials*. Moscow: Mashinostroenie.
3. Artyukhov, V.P., Pruss, O.P. (1997) Examination of brazing processes of diamond–hard alloy cutters. *Sverkhtv. Materialy*, **2**, 38–43.
4. Najdich, Yu.V., Umansky, V.P., Lavrinenko, I.A. (1988) *Strength of diamond-metallic contact and brazing of diamonds*. Kiev: Naukova Dumka.
5. Khorunov, V.F., Maksymova, S.V., Stefaniv, B.V. (2010) Manufacture of drill bits for production of dispersed methane in mine working. *The Paton Welding J.*, **6**, 41–43.
6. Khorunov, V.F., Maksymova, S.V., Stefaniv, B.V. (2010) Effect of tin additions on structure and technological properties of brazing filler metals of Ag–Cu–Zn system. *Ibid.*, **7**, 16–21.
7. Khorunov, V.F., Maksymova, S.V., Stefaniv, B.V. (2012) Effect of palladium on structure and technological properties of Ag–Cu–Zn–Ni–Mn system brazing filler alloys. *Ibid.*, **9**, 20–25.
8. Vologdin, V.V., Kushch, E.V. (1979) *Induction brazing*. Leningrad: Mashinostroenie.
9. *STP 28.5 05417377 100–2003*: Method for assessment of wear resistance of diamond–hard alloy inserts.

Received 29.11.2012

EXPERIENCE OF KHERSON SHIP-BUILDING PLANT IN APPLICATION OF PLASMA CUTTING

Zh.G. GOLOBORODKO
OJSC «Kherson Shipyard», 1 Karantinny Ostrov Str., 73019, Kherson, Ukraine
E-mail: repair@kherson-shipyrd.com

The peculiarities of application of plasma cutting in manufacture of ship-hull parts were considered. The positive and negative phenomena were mentioned. The influence of composition of plasma-forming medium on the main technological characteristics of cutting process was analyzed. Aim of the work is to present the experience of the Kherson Ship-Building Plant (Kherson Shipyard) on application of plasma cutting using plasma-forming medium with addition of a small amount of water. The design of plasmatron PMR 74M was described. The addition of water results in increase of cleanness and decrease of roughness of the cut surface. The explanation to the observed effect was given. The replacement of acetylene-oxygen cutting by plasma one in the plasma-forming media, such as air + water, allows 3–5 times improving the efficiency of cutting, decreasing thermal deformations and increasing accuracy of the parts being cut, providing simplicity of control of cutting process, possibility of automation with application of flexible industrial systems. This technology was realized at the automated area of the enterprise in the production lines by using the machines of the type «Kristall», NPC devices 2R32T on the basis of microcomputer. 7 Ref., 1 Table, 8 Figures.

Keywords: *plasma cutting, ship-hull parts, design of plasmatron, purity of cut surface, addition of water, efficiency, thermal deformations, automation, production lines*

The prospects of development of ship building in Ukraine are connected with modernization of technologies. The first stage of ship building is the manufacture of hull parts, the number of which amounts to tens of thousands per one hull. One of the main technological operations defining the quality of welding of parts and welding of a ship as a whole is thermal cutting, which is used to treat about 80 % of applied metal in ship building. As to the labor consumption, these works amount up to 20 % of the whole volume of works of hull-treated workshop [1].

The main method of thermal cutting is plasma cutting, which considerably surpasses the gas-oxygen one according to its efficiency and quality. According to the regulations of the Russian Maritime Register it is necessary during manufacture of parts to be sure that there is no excessive saturation of cut surface with gases (nitrogen, hydrogen) to avoid deterioration of quality of welds. The appropriate quality of cut surface along the free edges should be provided [2].

The wide practice of industrial application of plasma cutting in manufacture of ship-hull parts showed that use of high-enthalpy gases (hydrogen, helium, oxygen, etc.) for plasma formation results in considerable change in the whole process of plasma cutting. On one hand its high efficiency is achieved, on the other — the service life of electrodes of plasmatron is decreased and stability of arc burning is violated.

The elimination of undesired factors is achieved due to application of high-enthalpy gases not in the pure form, but in the mixtures with heavier gases, i.e. the transition from single- to multicomponent gas media.

Plasma-forming medium has a direct effect on all the main assemblies of the equipment for plasma cutting. Change in quality composition of the plasma-forming medium allows considerable changing in the main technological characteristics of the process and, in the first turn, the quality of cutting. The role of the composition of plasma-forming medium in the cutting technology is determined as follows [3]:

- composition of plasma-forming medium at the preset geometry of a nozzle and current of cutting determines the intensity of arc column field both inside as well as outside the nozzle. Therefore, due to the change of composition of a medium the amount of heat energy evolving in the arc can be regulated within the wide ranges;
- composition of plasma-forming medium significantly influences the maximum permissible value I/d, which allows controlling the density of current in arc, heat flow in the cut cavity and, as a result, the cut width and speed of cutting.

As a result of change in composition of a medium the most favorable conditions for re-

moval of molten metal from the cut cavity can be created, preventing the formation of a flash on the lower edges of a sheet being cut and making it easy to remove.

In some cases the considerable addition of heat energy due to chemical interaction of plasma-forming medium with a metal being cut should be also considered. The additional input of chemical reaction into the general heat balance can reach the value commeasurable with electric power of arc.

The composition of plasma-forming medium influences also the physical and chemical processes on the walls of a cut, the degree of saturation of cut walls with different gases, and also the depth of gas-saturated layer depend on it. Great influence on the selection of plasma-forming medium have the composition of metals being cut, and thickness of sheets have a great influence on the selection of plasma-forming medium. The higher the heat conductivity of a material and the larger the thickness of a sheet, the more rigid are the requirements to the composition of plasma-forming medium and, moreover, the range of used mixtures becomes more narrow.

In cutting of steels the compressed air as the most widely applied and economically efficient gas found the widest application as a plasma-forming medium [4–6].

The application of cheap and acceptable compressed air as plasma-forming medium in combination with high efficiency and flexibility of the process, suitable for cutting of almost all metals, provides considerable advantages as compared to other plasma-forming media. However, some disadvantages of plasma cutting in plasma-forming medium of air, where increase of hardness of metal of cut edges relates, do not provide perpendicularity of cut edges. Non-perpendicularity of 1.5–2.5 mm for each side increases with reduction of thickness of a metal being cut out. The change in chemical and structural composition and also increase of porosity of welds, produced along the edges after plasma cutting, narrow the area of its application. The reason of pores formation in welding of parts, sections and ship hulls of low-carbon and low-alloyed steels is nitrogen, located in the cut of edges in the state of oversaturated solution. The efficient method to decrease nitrogen concentration in the metal of edges is its bonding into thermodynamically stable compounds in air-plasma cutting.

The character of metallurgical processes running in the cut cavity is mainly determined by chemical properties of plasma gas. It is rationally to investigate the plasma jet with addition of gases possessing reduction properties. First of all hydrogen, being a strong reducer, and water-containing mixtures are related to such gases. The use of the latter is more preferable in many cases on the reasons of safety and availability. The advantages of application of water-air mixtures for plasma cutting are low cost, availability, easy achievement of reduction or oxidation properties of plasma gas, possibility of change in character of metallurgical processes running in the cut cavity.

The peculiar place in plasma-forming media is occupied by water, composition of which includes hydrogen and oxygen. The power parameters of arc allow referring water to water-containing mixtures and quality of cutting indicates that oxygen, released as a result of dissociation of water, actively interacts with the metal being melted. In particular, during cutting of low-carbon steels the speed of cutting during use of water is the same as in water-containing mixtures, and quality of cutting is the same as in oxygen-containing ones.

Water can be used as plasma-forming medium independently in a form of vapor or as addition to plasma gas. High intensity of arc column, high penetration ability of arc, high efficiency of use of electric power of arc are achieved by adding of hydrogen.

The use of water as plasma-forming medium did not receive a wide industrial application. During water-electric cutting the complications with arc exciting arise. Besides, applied graphite electrodes are consumed quickly and an additional device is required for vertical movement of graphite electrode in the direction of the nozzle unit during the process of cutting, making the design of plasmatrone more complicated [3]. All these factors make the process of cutting during use of water as a plasma-forming medium not reliable and not sufficiently technological.

Such foreign companies as ESAB (Sweden), Messer (Germany) and other apply the process of plasma cutting under the layer of water. During this process the plasma jet falls directly into the water pool, the formation of smoke is absent, deformation of parts, levels of light radiation and noise reduce considerably. Under these conditions water sufficiently improves the sanitary-hygienic characteristics of the process, provides improvement of quality of edges of the parts being cut.

The application of plasma cutting under the layer of water requires special layout tables with the system for water level control. Water should be softened to increase the life of nozzles. The water preparation should be performed to avoid oxidation of cut edges and remove products of

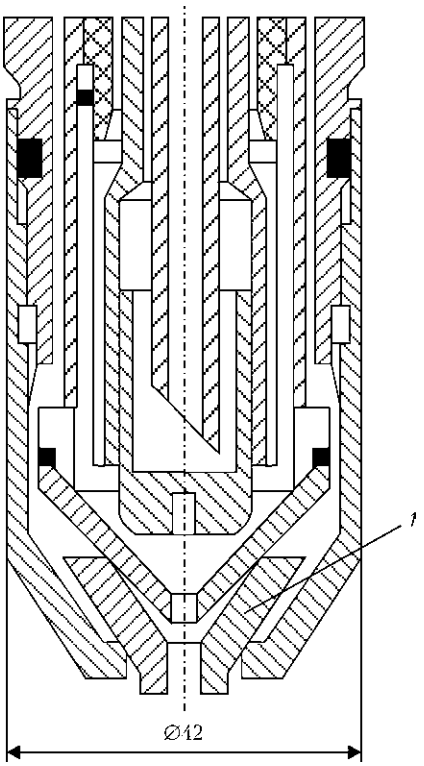

Figure 1. Scheme of plasmatron PMR 74M

plasma-chemical reactions running in the water. During cutting under water the operator can not observe the position of plasmatron and quality of cut edges. The application of special stabilizers of height and system of emergency stop of the process during casual throwing down of tiny parts are required. At the modern lines of thermal cutting with application of moving layout frames the application of the mentioned method of cutting is practically impossible.

At present, at the Kherson Shipyard the plasma-forming media for plasma-cutting of shiphull steels are used with addition of small amount of water to plasma gas. A part of water is supplied from the cooling system from modernized plasmatron PMR 74M (Figure 1) to the nozzle composed of two separate conic nozzles, included one into another (Figure 2). The outer nozzle of smaller sizes has six tangential grooves from the inside (0.15 × 0.93 mm), and 24 radial grooves (0.1 × 0.3 mm) from the outside for water supply. A part of water is supplied along the tangential grooves to the nozzle channel (into the plasma jet), and along the radial ones around the nozzle. To provide injection of water into the plasma jet the diameters of outer and inner nozzles are not equal between each other.

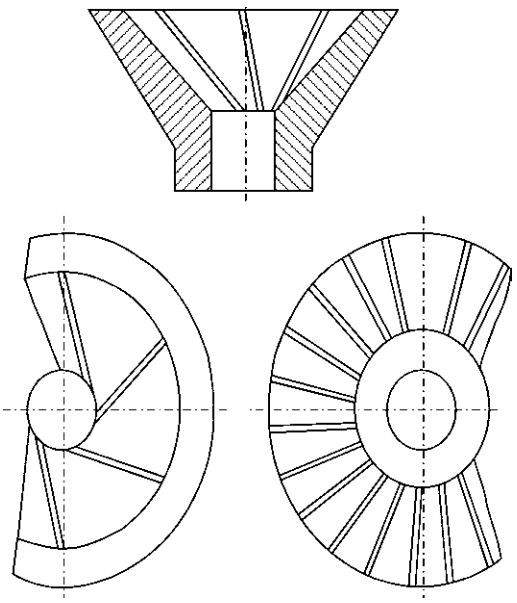

Figure 2. Scheme of nozzle unit for water supply

The water is supplied inside the channel clockwise with swirling, i.e. in the same direction as swirling of gas, squeezing additionally the plasma jet.

During adding of water into plasma the system is formed composed of nitrogen, oxygen and hydrogen. In this system plasma chemical reactions of bonding nitrogen with simultaneous obtaining of such products as NH_3, N_2H_4, NO, NO_2 and also other insoluble compounds of nitrogen in the cut edges [7]. The water is supplied along the radial grooves to the outside around the nozzle forming the air-water shower.

In the process of cutting the use of the considered design of a nozzle creates a double effect. The water supplied inside of the nozzle channel is partially evaporated, dissociates into hydrogen and oxygen, which during mixing create combined plasma-forming medium. Besides water squeezes and compacts the plasma jet in the nozzle channel, providing higher power characteristics.

Water, which is supplied concentrically to plasma column, is also partially evaporated and creates water-steam screen, limiting the access of air to the cutting zone. The gases being formed in the process of cutting are partially precipitated by water. The appearance of operating plasmatron with addition of water to air is shown in Figures 3 and 4.

The addition of small amount of water to plasma gas increases the quality of cut edges. Power parameters of arc allow attributing water to water-containing media, and quality of cutting indicates that oxygen, releasing as a result of dissociation of water, actively interacts with the metal being melted. During cutting of low-carbon steels the speed of cutting at adding of water is the same as in water-containing media and quality of cutting is the same as that of oxygen-containing ones.

Figure 3. Plasmatron PMR 74M for cutting (plasma-forming medium — air + water)

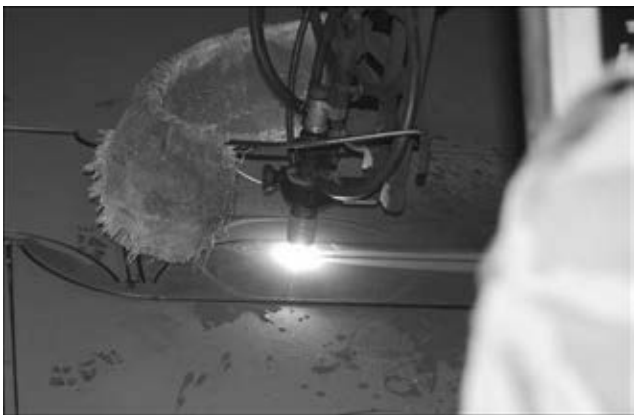

Figure 4. Process of cutting (plasma-forming medium — air + water)

The power of arc during plasma cutting in plasma-forming media with addition of water is increased due to the growth of voltage U_a, whereas the current I_a (in use of vertical external characteristics of the power source) almost does not change. Such effect of water adding can be explained by thermal-physical properties of hydrogen. During dissociation of hydrogen the considerable amount of energy is absorbed, the losses of which are compensated by growth in arc voltage; as a result of recombination of atomic gas at the surface of metal this power is transferred to the anode. At comparatively low values of voltage (130–150 V) in air-plasma cutting the cut acquires a significant conicity due to its width in the upper part of the sheet being cut out. As a result of this fact the amount of molten metal increases as compared to the cut, the edges of which are close to the parallel ones. The increase in U_a (170–180 V) during plasma cutting decreases the width of cut and volume of molten metal per unit of a cut length in the air + water plasma-forming medium. The flame of plasma is elongated, reaching 200 mm. During experimental verification the non-perpendicularity of edges amounted to not more than 1.0–1.2 mm on the side, which corresponds to the second grade according to the GOST 14792–80 for the thickness of 5–12 mm.

One of the characteristics defining the quality class of the parts being cut out is roughness of cut surface according to the GOST 14792–80. The character and depth of grooves, formed on the surface of a cut, characterize the fitness of parts to service having free edges under the conditions of dynamic loads.

The addition of water into plasma-forming medium results in increase of cleanness of cut surface of structural steel. The cut surface is smooth, has a silver color, projections and cavities have smooth transitions, drop of height values amounts to 10–20 μm (Table; Figure 5).

The roughness of cut surface is decreased from 120–90 μm at usual methods of cutting to 20–

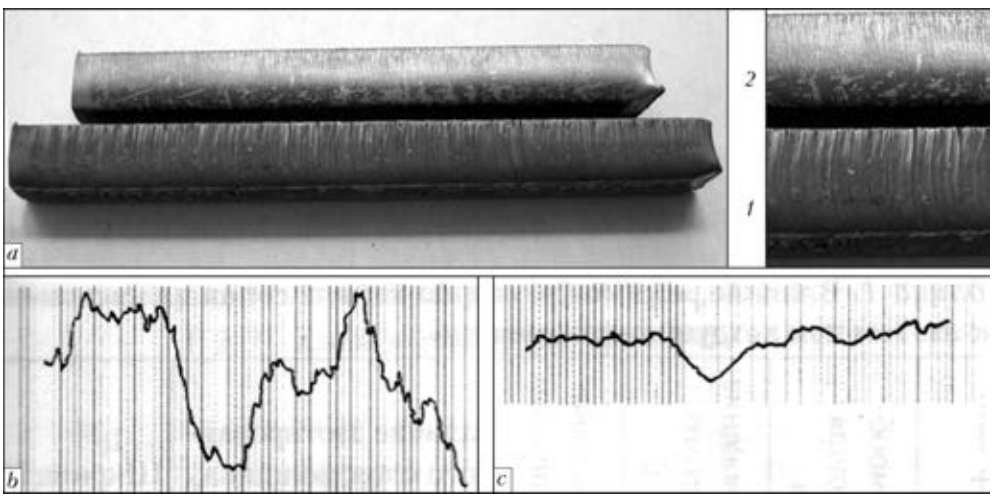

Figure 5. Appearance (*a*) and profilograms (*b*, *c*) of the surface of plasma cut in plasma-forming media: *1*, *b* — air; *2*, *c* — air + water

Dependence of roughness and microhardness of the cut surface on the cutting method

Cutting method	Microhardness, MPa	Width of HAZ, mm	Roughness, μm	Quality class	Speed of cutting, mm/s
Acetylene-oxygen	270	1.2–2.0	100–120	3	7.5
Plasma (plasma-forming medium — air)	620	0.6	80–100	2	33.3
Plasma (plasma-forming medium — air + water)	366	0.46	10–20	1	33.3
Machining (polishing)	150	–	5–10	–	–

10 μm during cutting with addition of water which corresponds to the first class of the surface according to the GOST 14792–80.

The parts, manufactured using thermal cutting, should be subjected to additional operations of treatment, straightening, lining. At present, in practice a number of technological procedures is applied to prevent and decrease thermal deformations: at the technological cards of layout the beginning and direction of cutting is indicated; succession of cutting out of parts; places where transition pieces were left; fixation of a sheet to the layout table, etc.

However application of mentioned procedures to prevent thermal deformations does not provide the production of parts according to the requirements RD 5.9091–80 «Manufacture of steel parts of hulls of metal ships». At the same time these procedures of struggling against deformations negatively influence the efficiency and quality of manufacture of parts.

During plasma cutting in plasma-forming media a part of water from the cooling system of plasmatron is supplied along the radial grooves outside around the nozzle forming air-water shower for localization of place of heating and reducing the thermal deformations. This cooling influences also the structure and mechanical properties of HAZ metal.

The presence of water prevents distribution of heat beyond the limits of water shower curtain surrounding the plasma jet and directly cooling the cut edges during movement of plasmatron. The concurrent cooling of cut edges provides minimal deformations from the plain and on the rib. The straightening of parts according to the RD 5.9091–88 is not required. The replacement of acetylene-oxygen cutting by plasma one in the air + water plasma-forming media allowed increasing efficiency of cutting (on the thickness of up to 14 mm) by 3–5 times; decreasing thermal deformations and increasing accuracy of the parts being cut out; providing simplicity in control of cutting process, possibility of automation with application of flexible industrial systems. The system includes complex of correlated technical, software, information and organization means, providing designing of geometry of flat parts; layout of parts on customer sheets; designing of technology of cutting out of parts; automatic cutting out of parts; automatic transportation of billets and parts; control of process using computer.

The flexible automated area (FAA) at the Kherson Shipyard has two production lines with machines of the type «Kristall» equipped with the NPC devices 2R32T on the basis of microcomputer. The control system of FAA including local computational network is realized on the basis of domestic computer technologies (Figure 6).

Using optimal modes of plasma cutting applying the offered plasma-forming media it is

Figure 6. FAA with machines of the «Kristall» type (for thermal cutting)

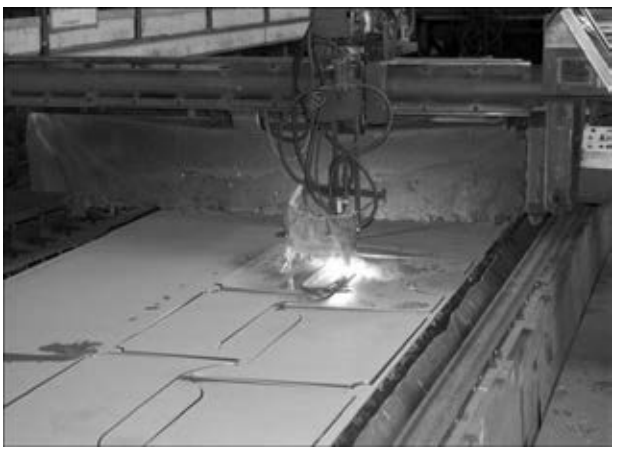

Figure 7. Plasma cutting in plasma-forming media with addition of water

Figure 8. Appearance of billets after plasma cutting

possible to obtain high quality characteristics of cutting (Figures 7 and 8).

As to the accuracy they are comparable with oxygen cutting excluding somewhat higher nonperpendicularity of cut edges. At the same time the depth of HAZ and deformations of the parts being cut out are smaller than during other methods of cutting. The developed modes of plasma cutting with addition of water provide elimination of pores in the weld metal during welding and allow reducing the thickness of the metal being cut out to 3 mm.

The roughness of the cut surface (see Figure 8) corresponds to the 1st grade according to the GOST 14792–80, free edges according to the regulations of the Russian Maritime Register do not require additional mechanical treatment.

Conclusions

1. The use of two-component plasma-forming mixtures is based on the fact that by selection of corresponding components and their correlations in the mixture the most optimal parameters of arc both from the power point of view, as well as from the point of view of stability of arcing, are provided.

2. In all mixtures containing hydrogen, the speed and quality of cutting depends mainly on the consumption of hydrogen and to the less degree on the consumption of the second component of mixture. Arc voltage depends also mainly on the volume of hydrogen in the mixture and practically does not depend on the fact, in what composition of mixture the hydrogen is included. Therefore, both thermal physical and electrophysical parameters of arc are determined by the presence of hydrogen in the mixture.

3. When using the oxygen in mixtures, the efficiency of plasma-forming mixture depends considerably on the character of chemical interaction of oxygen with the metal being cut out. The application of oxygen-containing plasma-forming mixtures allows using both electric as well as chemical energy. In this case cutting is partially the process of melting and partially the process of burning out of metal from the cut cavity.

4. The application of water-air mixtures in plasma cutting will allow decreasing the concentration of gases dissolved in the cut edges, changing electric and thermal characteristics due to H_2 dissociation accompanied by the consumptions of power, the losses of which are compensated by the growth of intensity of arc column during simultaneous redistribution of heat and density of current as compared to the arc stabilized by air.

1. Golovchenko, V.S., Dobrolensky, V.P., Misyurov, I.P. (1975) *Thermal cutting of metals in shipbuilding*. Leningrad: Sudostroenie.
2. (2004) *Rules for supervision of shipbuilding construction and manufacturing of materials and products for shipbuilding*. Vol. 3. Saint-Petersburg: RMRS.
3. Bykhovsky, D.G. (1972) *Plasma cutting*. Leningrad: Mashinostroenie.
4. Vasiliev, K.V. (1974) *Plasma-arc cutting*. Moscow: Mashinostroenie.
5. Esibyan, E.M. (2000) Air-plasma cutting: state-of-the-art and prospects. *The Paton Welding J.*, **12**, 4–15.
6. Lashchenko, G.I. (2012) Quality of cutter in plasma-arc cutting. *Svarshchik,* **4**, 34–39.
7. Goloborodko, Zh.G., Kvasnitsky, V.V. (2002) Investigations of plasma cutting in plasma-forming media with addition of water. *Zbirnyk Nauk. Prats UDMTU*, **5**, 37–46.

Received 13.11.2012

LASER WELDING OF LOW ALLOYED STEELS: INFLUENCE OF EDGE PREPARATION

M. SOKOLOV and A. SALMINEN
Lappeenranta University of Technology, Lappeenranta, Finland
E-mail: mikhail.sokolov@lut.fi

The objective of the research is to investigate an increase in efficiency of the high power laser welding process by the effect of two factors: joint edge surface roughness, and air gap between the plates. Welding of St3 low alloyed steel 20 mm thick was performed with high power fiber laser with a wavelength of 1070 nm at a power of 14 kW. Optimum roughness levels and recommended air gap between the plates to ensure maximum penetration depth and highest quality of weld are presented. 26 Ref., 5 Figures

Keywords: *laser welding, low alloyed steel, fiber laser, high power, absorptance, penetration depth, gap, roughness of edge surface*

Methods to increase the absorption and, therefore, efficiency of the welding process, are an important component of modern deep penetration laser welding, as the absorption affects the process parameters: power level needed for the welding process, production speed, and weld quality. The absorption level also determines whether deep penetration or keyhole welding is achieved. The keyhole is a metal vapor cavity that is formed when the power density at the laser–metal spot of contact achieves a sufficiently high level (~10^6 W/cm^2). Material melts along the front wall of the keyhole as the laser beam moves, and the molten material is then transported via the side wall to the back wall, where it solidifies and forms a narrow weld. The laser beam is reflected multiple times on the walls of the keyhole (Figure 1).

The absorption level is not a fixed determinant but is a function of the material properties, surface treatment and environment parameters. All these factors have a critical impact during formation of the initial keyhole [1–3].

Possible way of increasing the efficiency of the process is using preheating techniques. Use of the preheating requires typically more work phases than laser beam welding and it increases the complexity of the welding process considerably. Use of hybrid techniques, despite the significant advantages (like higher process stability, less porosity and cracking, greater flexibility) has a perceptible disadvantage: high complexity of the equipment setup, and more parameters that should be controlled and optimized comparing to laser beam welding [4–7]. Main purpose of the study is to find a relatively easy way to increase the efficiency of the laser beam welding in the workshop conditions. Therefore, the influence of the edge surface roughness and the effect of the pre-set air gap were investigated.

The relationship between absorption and edge preparation has been widely investigated in CO_2 laser welding. Arata and Miyamoto presented

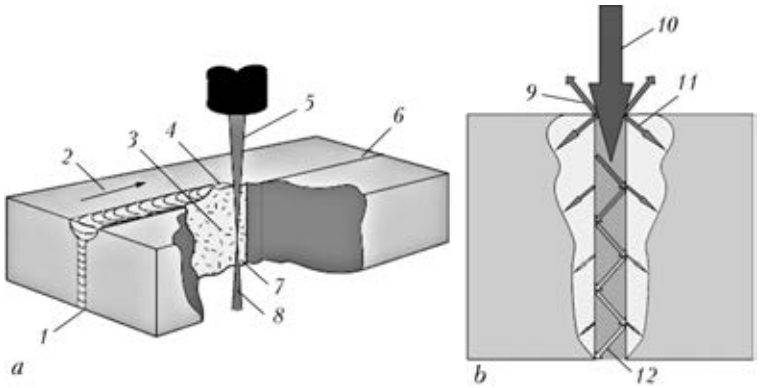

Figure 1. Keyhole welding process [4]: *1* — weld bead; *2* — welding direction; *3* — HAZ; *4* — keyhole; *5*, *10* — laser beam; *6* — weld edge; *7* — molten metal; *8* — laser beam exiting the workpiece; *9* — reflected radiation; *11* — absorbed radiation; *12* — multiple reflections on the keyhole walls

comprehensive results for the CO_2 laser absorption characteristics of metals in 1972 [8]. It was recorded that the absorption has a tendency to increase with the surface roughness, however, when the surface melts, the absorption decreases to a constant value. Some studies of laser beam welding have suggested that the influence of the edge surface roughness on the absorption is insignificant [6, 7]. However, results from other sources have indicated an increase in the absorption in roughened surfaces compared to fine polished ones [1, 9–12].

Laser welding research with Nd:YAG and high power fiber lasers to date has tended to focus on optimizing beam and mechanical parameters, and relatively little attention has been paid to surface preparation of the joint edges [13–20]. Bergstrom et al. [21] reported on the correlation between the absorption level and surface roughness with Nd:YAG laser surface treatment. It was found that the absorptance of the surface increases with roughness once a certain threshold has been exceeded. This phenomenon was explained by multiple scattering events.

It has been suggested that the absorption increase with increase in edge surface roughness may be explained by increase in the air gap size between the plates during butt joint laser welding [22, 23].

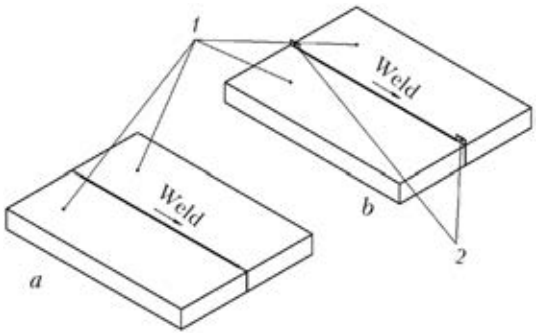

Figure 2. Welding setup for butt joint laser welding (*a*) and butt joint laser welding with pre-set air gap (*b*): *1* — steel plate; *2* — steel strip

The aim of this article is to contribute to the research data of thick section laser welding by investigating the influence of edge preparation on the weld quality and performance.

Experimental. Welding experiments with the high power fiber laser IPG YLR 15000 were performed on the St3 structural steel plates in the Laser Welding Laboratory of Saint-Petersburg State Polytechnic University, Russia. Randomly chosen pairs of samples were selected for chemical analysis. The alloying composition of the St3 steel according to GOST 380–94 [24] was as fol-

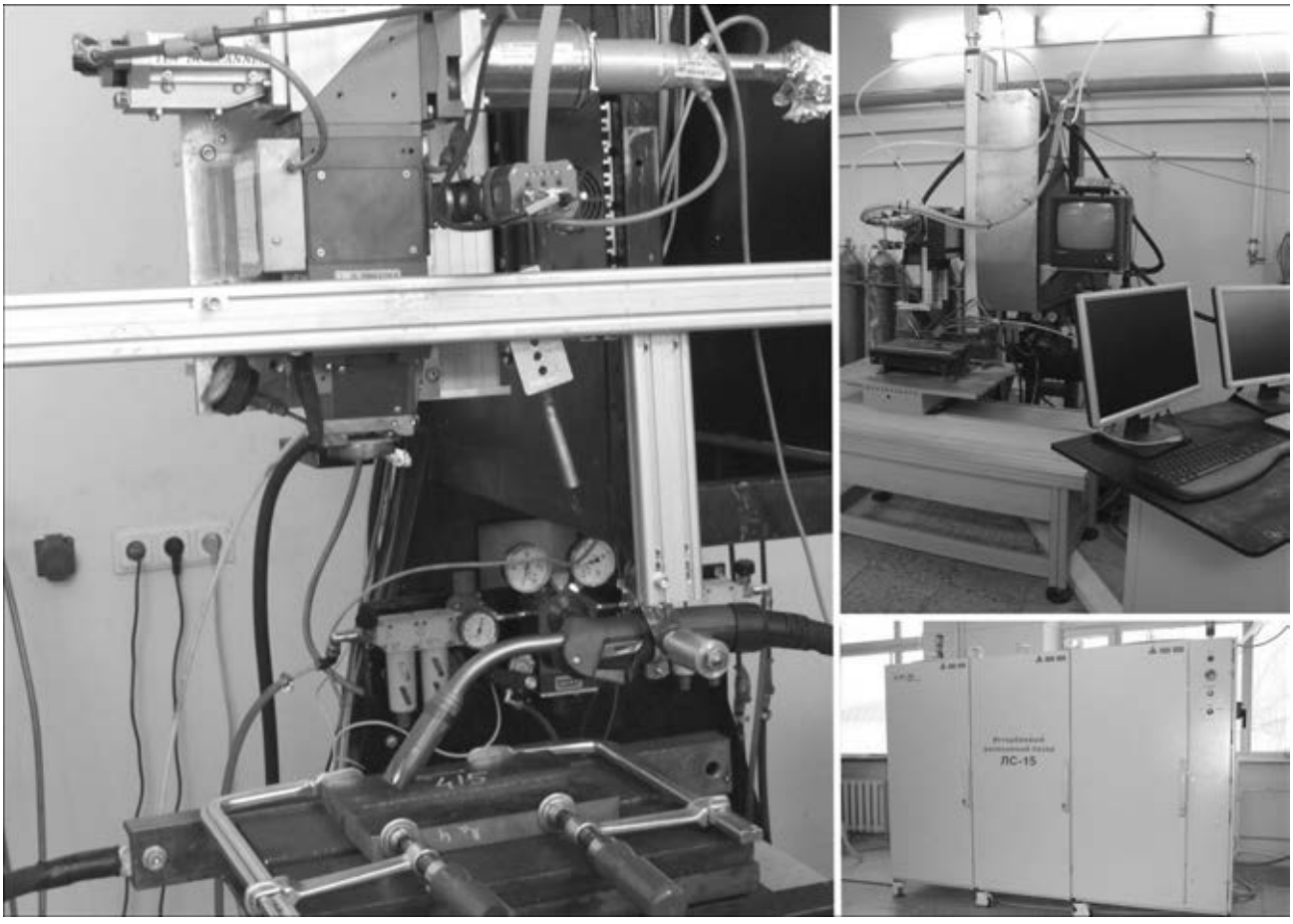

Figure 3. Thick section laser welding setup at focal length of 400 mm and focal point diameter of 0.4 mm

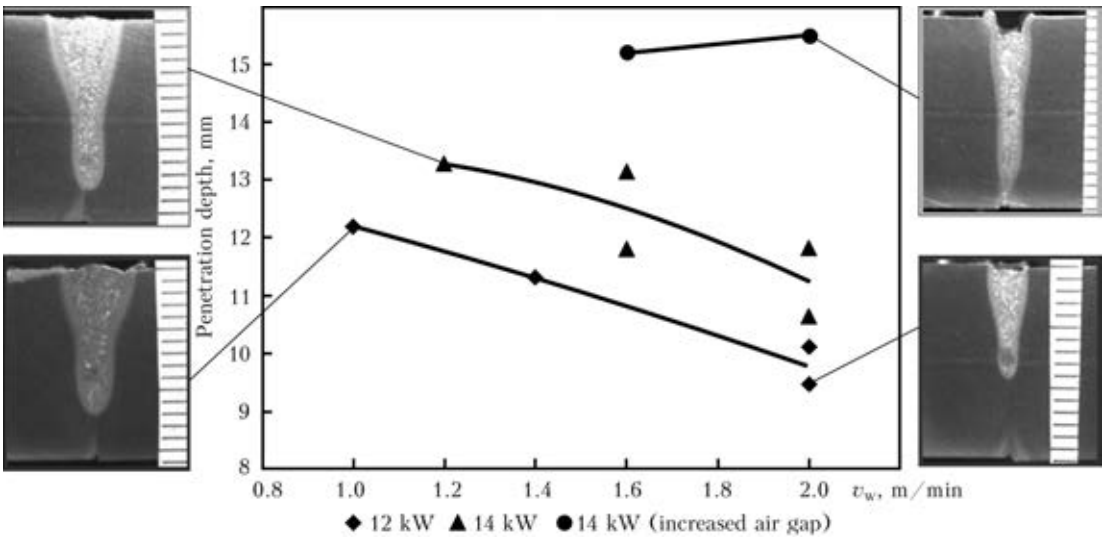

Figure 4. Depth of penetration of St3 steel 16 mm thick at different parameters of laser welding

lows, wt.%: 0.16C, 0.19Si, 0.44Mn, 0.01P, 0.01S, 0.03Cr, 0.01Ni, 0.02Cu, 0.03Al, 0.01N. Plates 20 mm thick were cut from the root surface into test pieces of 200 × 75 mm with water jet cutting machine, then processed to the desired roughness level with milling machine, and cleaned of the oxide layer by low-speed sandblasting. The surface roughness of the joint edges was measured with the contact roughness measuring device Taylor–Hobson Surtronic 10 Ra, with a measuring range of 0.1–40 μm, according to EN 10049:2005 [25], rounded to the nearest standard value.

Two variants of the setup were used: butt joint and butt joint with a pre-set air gap. The carbon steel strip was used (Figure 2), and the width of the air gap was 0.2 mm.

The equipment setup was, as shown in Figure 3, with the laser welding head mounted on the positioning system. In all sets of experiments the steel specimens were tightly fixed flat on the jig. Argon (20 l/min flow rate) was used as a shielding gas, delivered to the weld through the MIG/MAG welding torch. The weld penetration levels and weld quality levels were investigated according to ISO 13919-1:1999 [26].

The experimental plan was divided into two sets. In the first set, St3 steel plates of t = = 16 mm with roughness Ra = 2 μm were welded at welding speed v_w = 1–2 m/min, laser power P_L = 12–14 kW and focal point position $f_{p.p}$ = –7.5 mm.

Two-level factorial design (edge surface roughness (numeric) and pre-set air gap (cate-

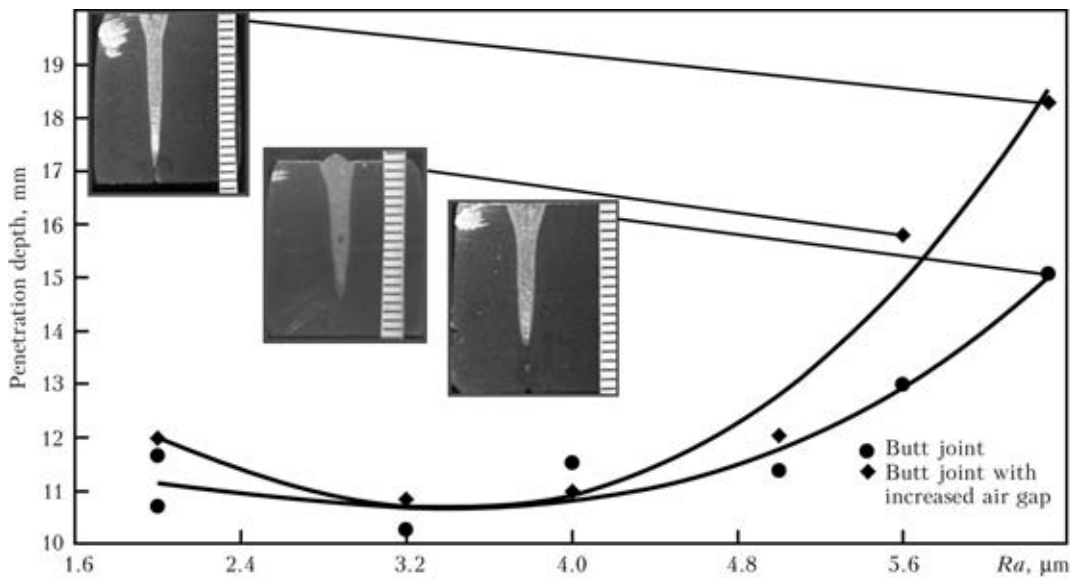

Figure 5. Depth of penetration of St3 steel 20 mm thick in laser welding at P_L = 14 kW, v_w = 2 m/min, $f_{p.p}$ = –7.5 mm, different roughness and air gap levels

goric)) was used in the second set of experiments on St3 steel plates 20 mm thick. Welding parameters were based on the results of the first set of experiments and remained constant (v_w = = 2 m/min, P_L = 14 kW, and $f_{p.p}$ = −7.5 mm).

Results and discussion. The results of the first set of experiments are shown in Figure 4. Interestingly, the additional gap increased the penetration depth significantly but caused an incompletely filled groove defect.

The results of the second set of experiments (Figure 5) show the minor changes in penetration depth or geometry shape of the weld at *Ra* = = 3.2–5.0 μm. Addition of the 0.2 mm steel strip to increase the gap between the plates does not change the trend at these roughness levels. At *Ra* = 5 μm an increase in the number of imperfections was recorded for the case of the pre-set air gap. Maximum penetration level of 15 mm was achieved with *Ra* = 6.3 μm. In combination with the 0.2 mm strip, the penetration depth increased to 18.3 mm. In both cases, the welds were of the confident stringent level for partial penetration with no critical imperfections.

Conclusions

In butt joint laser beam welding of St3 structural steel at edge surface roughness from 2.0 to 6.3 μm, maximum penetration depths were achieved at *Ra* = 6.3 μm. Addition of the 0.2 mm stainless steel strip to increase the gap between the steel specimens gave a positive result at *Ra* = = 6.3 μm, namely penetration depth increased to 18.3 mm. At the other roughness levels tested, the additional gap did not cause any significant changes in the weld characteristics. These finding suggest several conclusions:

1. The observed increase in penetration depth at *Ra* = 6.3 μm with increased air gap may be explained by changes in the re-reflection patterns that cause an increase in the absorption at the edge surfaces. With further increase in the roughness level and air gap, significant part of the laser beam may «fall through» the gap, and the absorption decreases.

2. The influence of the edge surface roughness might vary during the welding process, as the material melts in front of the keyhole. It means that the edge preparation has significant influence on the process only during the keyhole initiation, when the first re-reflections take place as the edge surface roughness with the increased air gap changes the pattern of the re-reflections. Therefore the absorption increases, the initial keyhole becomes deeper and more stable, while during the process the effect is no longer critical.

Both optimum edge surface roughness levels and increased air gap between the plates in butt joint laser welding should be taken into account at the stage of product design. However, a number of important limitations need to be considered: the welding setups, equipment and materials used in the experiments. Based on current knowledge, further experimental investigations are needed to ascertain the phenomena underlying the correlation between absorptivity and roughness level. Pre-determined edge surface roughness may be used with pre-heating techniques to promote an additional increase in the absorption. The relationships and causalities of these factors require further investigation in future studies. The findings of this study support the development of clear recommendations for edge surface roughness in thick section welding with high power lasers.

1. Duley, W.W. (1998) *Laser welding*. NY: John Wiley & Sons.
2. Ion, J.C. (2005) *Laser processing of engineering materials*. Oxford: Butterworth-Heinemann.
3. Xiangzhong, J. (2008) A three-dimensional model of multiple reflections for high-speed deep penetration laser welding based on an actual keyhole. *Optics and Lasers in Eng.*, 46(**1**), 83–93.
4. (2008) *Metallurgy and mechanics of welding: Processes and industrial applications*. Ed. by R. Blondeau. Saint-Etienne: ENSM.
5. Le Guen, E., Fabbro, R., Carin, M. et al. (2011) Analysis of hybrid Nd:YAG laser-MAG arc welding processes. *Optics & Laser Technology*, 43(**7**), 1155–1166.
6. Kah, P., Salminen, A., Martikainen, J. (2010) Laser-arc hybrid welding processes (Review). *The Paton Welding J.*, **6**, 32–40.
7. Bayraktar, E., Moiron, J., Kaplan, D. (2006) Effect of welding conditions on the formability characteristics of thin sheet steels: Mechanical and metallurgical effects. *J. Materials Proc. Techn.*, 286(**3**), 20–26.
8. Arata, Y., Miyamoto, I. (1972) Some fundamental properties of high power laser beam as a heat source: Report 2. *Transact. of JWS*, **3**, 163–180.
9. Covelli, L., Jovane, F., De lorio, L. et al. (1988) Laser welding of stainless steel: Influence of the edges morphology. *CIRP Annals–Manufac. Technology*, **37**, 545–548.
10. Ricciardi, G., Cantello, M. (1994) Laser material interaction: Absorption coefficient in welding and surface treatment. *Ibid.*, 43(**1**), 171–175.
11. Grigoryants, A.G., Shiganov, I.N., Misyurov, A.I. (2006) *Technological processes of laser treatment*. Moscow: Bauman MSTU.
12. Steen, W.M. (2003) *Laser material processing*. 3rd ed. London: Springer.
13. Kinoshita, K., Mizutani, M., Kawahito, Y. et al. (2006) Phenomena of welding with high-power fiber laser. In: *25th ICALEO Proc.*, 535–542.
14. Katayama, S., Kawahito, Y., Kinoshita, K. et al. (2007) Weld penetration and phenomena in 10 kW fiber laser welding. In: *26th ICALEO Proc.*, 360–369.
15. Salminen, A., Lehtinen, J., Harkko, P. (2008) The effect of laser and welding parameters on keyhole and melt pool behavior during fiber laser welding. In: *27th ICALEO Proc.*, 416–425.

16. Salminen, A., Piili, H., Purtonen, T. (2010) The characteristics of high power fibre laser welding. *J. Mechanical Eng. Sci.*, 224(**5**), 1019–1029.
17. Salminen, A., Purtonen, T. (2009) The effect of welding parameters on keyhole and melt pool dimensions and behavior during fiber laser welding. In: *Proc. of 12th Nordic Conf. on Laser Materials Processing*.
18. Kaplan, A., Wiklund, G. (2009) Advanced welding analysis methods applied to heavy section welding with a 15 kW fiber laser, In: *Proc. of IIW Int. Welding Conf.*, **53**, 295–300.
19. Katayama, S., Kawahito, Y., Mizutani, M. (2010) Elucidation of laser welding phenomena and factors affecting weld penetration and welding defects. *Physics Proc.*, **5**, 9–17.
20. Sokolov, M., Salminen, A., Kuznetsov, M. et al. (2011) Laser welding and weld analysis of thick section S355 structural steel. *Materials & Design*, 32(**10**), 5127–5131.
21. Bergström, D., Powell, J., Kaplan, A. (2007) The absorption of light by rough metal surfaces – A three-dimensional ray-tracing analysis. In: *26th ICALEO Proc.*, 704–713.
22. Malashenko, A.A., Mezenov, A.V. (1984) *Laser welding of metal*. Moscow: Mashinostroenie.
23. Sokolov, M., Salminen, A., Somonov, V. et al. (2012) Laser welding of structural steels: Influence of the edge roughness level. *Optics & Laser Technology*, 44(**7**), 2064–2071.
24. *GOST 380–94*: Common quality carbon steel. Grades.
25. *EN 10049:2005*: Measurement of roughness average *Ra* and peak count *RPc* on metallic flat products.
26. *ISO 13919-1:1996*: Welding. Electrons and laser beam welded joints. Guidance on quality levels for imperfections. Pt 1: Steel.

Received 07.12.2012

NEWS

Procedure for Evaluation of Technical State and Technology for Repair of Load-Carrying Structures of Transport Vehicles

It is a pressing problem to extend designed service life of transport vehicles. To solve it, it is necessary to estimate the actual technical state and residual life of load-carrying structures after they have exhausted their designed service life, and substantiate a package of the research, technical and organisational actions aimed at ensuring safe operation during the newly established service life. Statements and requirements were formulated for the scientific approach to ensuring safe operation of structures, based on the up-to-date notions of calculations and design, allowance for service loading and operating time of components, estimation of properties of materials, technical diagnostics, improvement of quality of the joints, application of new technological processes, including strengthening treatments.

Analysis of the technical state, actual operating time and service loading of load-carrying structures of the rolling stock makes it possible to establish types, causes and recurrence of premature damages, develop technical solutions for repair of the load-carrying structures with a 10–15 years extension of their designed rated service life, repair the load-carrying structures of an experimental batch of the train cars by extending their specified service life, develop a project of repair of the load-carrying structures of the inventory fleet of vehicles by the results of operation of the experimental batch of the cars, and train the Customer's staff in operating procedures.

The end product is a 10–15 years extension of the design service life of the rolling stock load-carrying structures, the cost of repair operations being no more than 40 % of the cost of a load-carrying structure.

In industrialised Western countries the problem of extension of life of the load-carrying structures is addressed, as a rule, through their reconstruction, and involves considerable expenses. Western Germany and USA pay attention to experimental-analytical estimation of the residual life of traction rolling stock and span structures of road bridges to plan their replacement and reconstruction.

In the solution suggested, estimation and guaranteed assurance of the residual safe operation of the load-carrying structures that have exhausted their design service life are a logical continuation of the development of the probability-statistical approach to fatigue calculation. This approach was developed in the 1980s of the last century by the E.O. Paton Electric Welding Institute and introduced in the 1990s into the design practice in the form of methodical guidelines of the USSR State Standard. It permits a differential allowance for the effect of factors of design embodiments of components and their service loading in calculation of the fatigue life of welded structures, and provides a substantial improvement of accuracy of the fatigue calculations. General provisions were worked out for the guaranteed residual safe operation and extension of lifetime of the load-carrying structures of subway cars, «Ukrzaliznytsya» traction rolling stock and industrial vehicles, allowing for probable upgrading and new criteria of the limiting state.

The guaranteed residual safe operation and extension of lifetime of the structures are provided through optimisation of the repair solutions, based on improvement of the calculation methods, use of the new, more substantiated criteria of the limiting state, and upgrading of assemblies by using the advanced technologies.

INTERNATIONAL QUALIFICATION SYSTEM FOR TRAINING OF WELDING PERSONNEL IN UKRAINE

P.P. PROTSENKO
Inter-Industry Training and Attestation Centre of the E.O. Paton Electric Welding Institute, NASU
11 Bozhenko Str., 03680, Kiev, Ukraine. E-mail: office@paton.kiev.ua

Stages of formation of the qualification system of Ukraine for training of welding personnel, which is harmonised with educational programs of the International Institute of Welding (IIW) and European Welding Federation (EWF), are described. The unified qualification system in Ukraine is recognised by the European and International accreditation bodies. The 10 years' experience in training of domestic specialists is available. Over 200 specialists were educated following different IIW programs for a number of leading enterprises. An important task for the future is to form the harmonised certification (attestation) system for welding personnel from welder to engineer, which should be unified for all the IIW member countries. It is planned to develop the system of compulsory advanced training for all levels of the personnel, based on the one- or two-week courses with periodicity of 2–3 years. The Training Centre of the E.O. Paton Electric Welding Institute has all possibilities to widen the list of the programs for periodic advanced training of technicians and engineers. 5 Tables, 1 Figure.

Keywords: *training of personnel, qualification systems, welding personnel, attestation and certification, education centre*

The key task of modern welding production is increase in competitiveness of products, which can be achieved due to technological advantages of a manufacturer. They are determined, primarily, by the presence of the qualified personnel, rather than by the advanced equipment and materials available at the competitors'. Professional training of the personnel capable of implementing advantages of modern welding technologies has certain peculiarities related to specific features of the welding process and high requirements to welding products.

These peculiarities are covered by the educational programs developed by the International Institute of Welding (IIW) and European Welding Federation (EWF), which formed the unified harmonised system for training of all categories of the personnel, starting from skilled welding operators and ending with certified engineers. The quantity of countries joining this harmonised international system for training of welding personnel is growing every year. Up to now it has been used in 37 countries: Australia, Austria, England, Belgium, Bulgaria, Brazil, Hungary, Germany, Holland, Denmark, India, Iran, Spain, Italy, Canada, China, Nigeria, Norway, Poland, Portugal, Russia, Romania, Singapore, Serbia, Slovakia, Slovenia, USA, Thailand, Ukraine, Finland, France, Croatia, Czechia, Switzerland, Sweden, South Africa, and Japan.

Owing to the use of the unified educational programs and the centralised system for monitoring of organisation and conducting of the qualification exams, these countries mutually recognise diplomas, certificates and licences issued by the authorised national bodies (ANB). They are recognised also in other countries-IIW members, which includes more than 50 countries. The unified qualification system makes it possible to determine conditions for the guaranteed level of quality of manufacturing of the welded structures independently of a country where they are manufactured. The qualification system is recognised by the European and international accreditation bodies, as it corresponds in full to the international standards of the ISO 3834 series (implemented as harmonised national standards of Ukraine — DSTU ISO 3834) specifying requirements to the quality of welding.

The new versions of standards ISO 3834:2005 «Requirements to the Quality of Fusion Welding of Metallic Materials» and ISO 14731:2006 «Coordination of Welding Operations. Tasks and Functions» (enforced as a harmonised national standard of Ukraine — DSTU ISO 14731) specify requirements to the welding personnel of different qualification levels. International Welding Engineer (IWE), International Welding Technologist (IWT) and International Welding Specialist (IWS) are recommended as personnel to perform the functions of coordination of welding operations. Inspection of welding, as specified in standard ISO 3834:2005 (Part 5), is

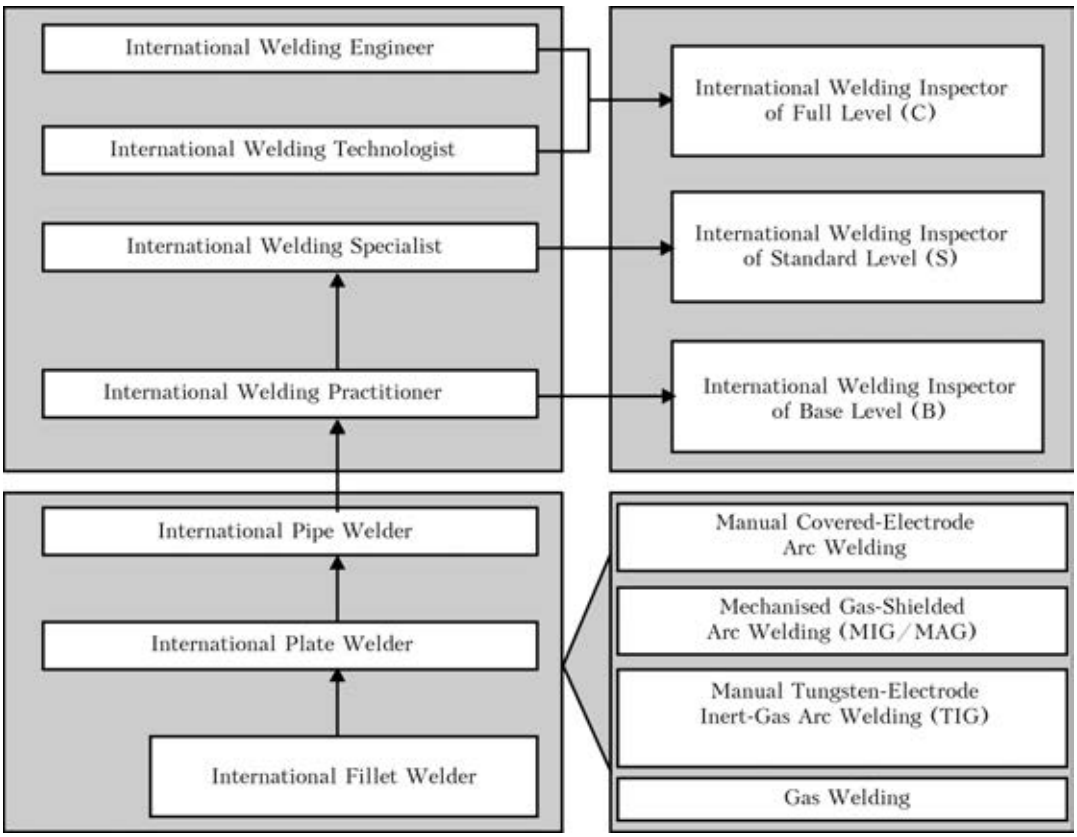

Qualification system for training and re-training of welding personnel

within the competence of International Welding Inspector Personnel (IWIP).

The fist domestic specialists with these qualifications in Ukraine were trained 10 years ago. In 1998, a group of welding engineers of Ukraine passed re-training following the EWF programs «European Welding Engineer». Organisation of these courses became possible owing to participation of the German Welding Society (SLV), having the corresponding accreditation of EWF, i.e. being one of ANBs, the functions of which include organisation of the harmonised international system for training of welding personnel in their countries. Ukraine also joined this system in 2002, obtaining the corresponding accreditation of IIW for organisation of training of specialists in all of the above four international qualifications, plus International Welding Practitioner (IWP) and International Welder (IW). The ANB functions in Ukraine are performed by the Inter-Industry Training and Attestation Centre (IITAC) of the E.O. Paton Electric Welding Institute of the NAS of Ukraine. In addition to Ukraine, Russia also has such accreditation.

Therefore, in Ukraine, along with the national qualification system for training of welding personnel, also the international one is in effect, which is in full correspondence to requirements of standard ISO 3834:2005.

The IIW-EWF qualification system is in a category of post-diploma education. In this connection, the conditions of access to education that include requirements to the level of education are specified for each category of the approved qualifications. Requirements to the conditions of access to the IIW-EWF training courses in different countries are adjusted based on the effective national professional education systems. The education access conditions for Ukraine are given in the Tables.

As of November 2008, over 150 specialists received training following different IIW programs. These are representatives of the Dnepropetrovsk Steelwork Plant, Zaporozhstal, Krayan, Zaporozhkran, Kremenchug Steel Casting Works, Kryukov Car Building Plant, Lugansk Pipe Works, Lukoil, Motor-Sich, Novokramatorsk Machine Building Works, Stirol, Ukrstalkonstruktsiya, Kharkov Car-Repair Plant and many others. Among them were also the citizens of Algeria, Germany, Israel, Iran, Kazakhstan, Russia, Uzbekistan and France.

Training of International Welding Inspectors is of special importance for quality assurance in welding production. In 2008, IITAC of the E.O. Paton Electric Welding Institute trained the first five specialists of this level for the Kryukov Car Building Plant. Partially, training was perfor-

International Welding Engineer (IWE)

Complete education course (440 h)	Shortened education course (340 h)	Short education course (120 h)
Diploma of master, engineer or bachelor in mechanics, electrical engineering or metallurgy	Diploma of master, engineer or bachelor in welding	Diploma of master, engineer or bachelor in welding, and working for the last four years as welding engineer

International Welding Technologist (IWT)

Complete education course (340 h)	Shortened education course (270 h)	Short education course (100 h)
Diploma of bachelor or technician in mechanics, electrical engineering or metallurgy	Diploma of bachelor or technician (junior specialist) in welding	Diploma of bachelor or technician in welding, and working for the last four years as welding technologist

International Welding Specialist (IWS)

Complete education course (230 h)	Shortened education course (200 h)	Short education course (170 h)
Technical education, and working for the last two years in industry	Diploma of technician in welding, and working for the last two years in industry	Diploma of bachelor, technician or instructor in welding, and working for the last three years at a post corresponding to IWS

International Welding Practitioner (IWP)

Complete education course (146 h)	Short education course (32 h)
Certificate of welder, and working for the last two years in welding production	Certificate of welder, and working for the last three years in welding production at a post corresponding to IWP

International Welding Inspector (IWIP)

Qualification	Complete education course	Short education course
International Welding Inspector of full level (IWI-C)	Diploma of bachelor in mechanics, electric engineering or metallurgy (course — 220 h)	Diploma of master, engineer or bachelor in welding, and working for the last three years in welding production (course — 100 h)
International Welding Inspector of standard level (IWI-S)	Technical education, and working for the last two years in industry (course — 160 h)	Diploma of bachelor or technician, and working for the last two years in welding production (course — 70 h)
International Welding Inspector of base level (IWI-B)	Vocational education (course — 110 h)	Certificate of inspector of welding operations, and working for the last two years in welding production (course — 50 h)

med in the territory of the Plant without discontinuing work.

The next important task initiated by IIW is formation of the harmonised system, unified for all the IIW member countries, for certification (attestation) of welding personnel from welder to engineer, similar to that in effect at EWF. Also, it is suggested developing the system for compulsory advanced training of welding personnel of all the levels, based on the one- or two-week courses, which every specialist should take once in two-three years. By now IITAC of the E.O. Paton Electric Welding Institute has every possibility for widening the list of the proposed programs for periodic further training of technical and engineering staff involved in welding production, as well as for rendering services on their certification.

Received 17.04.2012

DEVELOPMENT OF THE TECHNOLOGY FOR BRAZING OF TITANIUM ALLOYS USING FILLER ALLOYS BASED ON THE Al–Mg SYSTEM

V.V. VORONOV
E.O. Paton Electric Welding Institute, NASU
11 Bozhenko Str., 03680, Kiev, Ukraine. E-mail: office@paton.kiev.ua

It should be noted that, despite a large number of the investigations performed on brazing of titanium using aluminium filler alloys, brazing of titanium by using the Al–Mg system based filler alloys have not received acceptance in the territory of Eastern Europe and, particularly, in Ukraine. However, the quantity of publications covering developments of new aluminium alloys for brazing of titanium alloys is growing, this being indicative of the demand of the industry for commercial medium-melting point filler alloys for brazing of titanium and its alloys. The purpose of the present study was to develop the technology for brazing of titanium alloys by using the Al–Mg system based filler alloys. Presented are the investigation results on brazing of the samples of titanium alloy VT1-0 using aluminium filler alloys by radiation heating in vacuum. Structural and chemical heterogeneity of the brazed joints was investigated. It was found that aluminium filler alloys based on the Al–Mg system are suitable for producing sound brazed joints on titanium alloys. The dense and defect-free joints were made in brazing of models of sections of lamellar-ribbed heat exchangers by using filler alloy AMg6, the strength of the joints being sufficient for this type of the items. Brazing filler alloy TiBrazeAl-665 was found to be suitable as well. 4 Ref., 3 Figures.

Keywords: *brazing, brazing filler alloys, titanium alloys, aluminium alloys, lamellar-ribbed heat exchangers, honeycomb structures, microstructure, mechanical properties*

In fabrication of heat exchangers, honeycomb structures and other complex engineering items the use of light Ti- and Al-base alloys provides the maximum decrease in their weight and increase in strength, corrosion resistance and other operational properties. Brazing is the most promising method for fabrication of such structures.

Brazing of lamellar-ribbed heat exchangers is a complex technological process related to the need to simultaneously produce the seams of a large length (the seams in heat exchangers can be hundreds or even thousands of metres long), as well as to the impossibility to correct defects formed inside a structure. Therefore, considering the above-said, as well as high reactivity of titanium at increased temperatures, the most promising method to fabricate heat exchangers of titanium alloys is vacuum brazing [1, 2].

The composition of a filler alloy plays an important role in the process of brazing of lamellar-ribbed heat exchangers. Erosion activity of a filler alloy can be minimal, as heat exchangers are made from thin-sheet elements. In addition, the temperature and time of brazing of heat exchangers should be such that they prevent undesirable changes in structure and properties of the base metal [1–3]. The choice of aluminium filler alloys is based on their relatively low cost, good wetting and spreading of these filler alloys on the titanium substrate [3, 4] at a comparatively low temperature, as well as a low level of erosion of the base metal in brazing.

Despite a large amount of the performed experimental studies on brazing of titanium by using aluminium filler alloys, brazing of titanium with this type of the filler alloys have not received acceptance in the territory of Eastern Europe and, particularly, in Ukraine. However, at present the quantity of the publications covering developments of new aluminium filler alloys for brazing of titanium alloys is growing, this being indicative of the demand of the industry for commercial medium-melting point filler alloys for brazing of titanium and titanium alloys.

The purpose of the performed experimental studies was to develop the technology for brazing of titanium alloys by using filler alloys based on the Al–Mg system. Alloy VT1-0, which is practically a non-doped Ti-base alloy with a good thermal conductivity for titanium alloys, was chosen as a material for fabrication of the lamellar-ribbed heat exchanger elements. Aluminium alloy AMg6 (Al–6Mg–0.6Mn–0.4Si–0.4Fe–0.1Ti) and modern commercial filler alloy TiBrazeAl-665 (Al–2.5Mg–0.2Si–0.4Fe–0.2Cr) were selected as filler alloys. The experiments on brazing were carried out in vacuum furnace

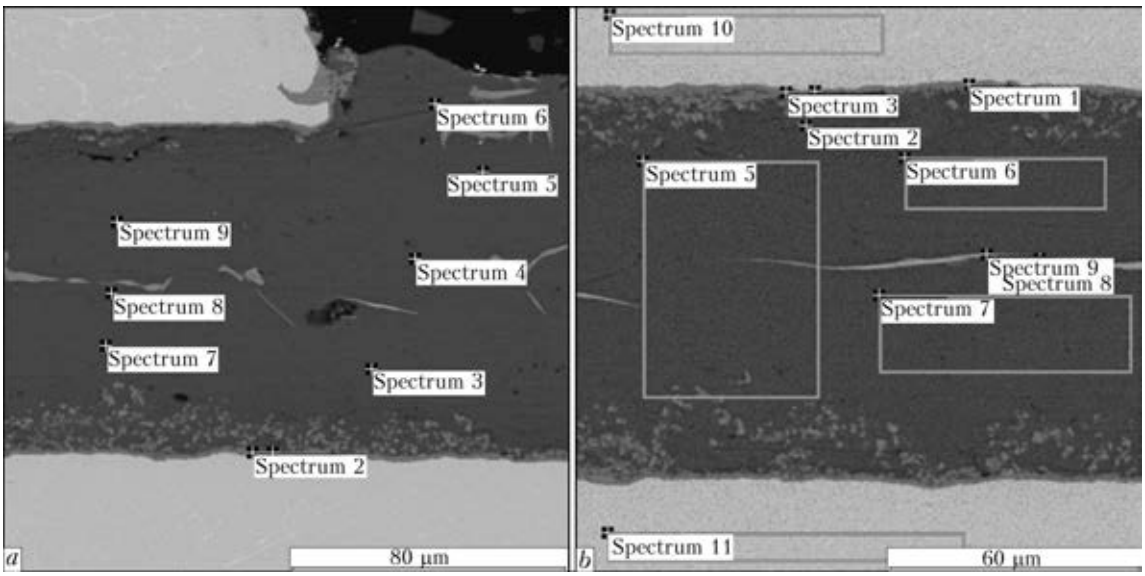

Figure 1. Microstructures of fillet region (*a*) and seam centre (*b*) of the brazed joint on titanium alloy VT1-0 made by using filler alloy AMg6 (T_{br} = 685 °C, t = 3 min, vacuum $5 \cdot 10^{-5}$ mm Hg)

SGV 2,4-2/15-I3, in vacuum of $5 \cdot 10^{-5}$ mm Hg. Brazing was performed in a titanium container with a getter to ensure additional cleaning of the brazing atmosphere.

Metallographic examinations of the brazed joints made by using the Mg-containing aluminium filler alloys (Figure 1) showed the presence of a continuous intermetallic interlayer at the filler alloy–base metal interface. Chemical composition (wt.%) of the interlayer varies from 49.53Al–48.81Ti–1.06Si–0.6Mn in the fillet region to 76.16Al–21.73Ti–0.79Mg–0.87Si–0.45Mn at the seam centre. In the first case it approximately corresponds to the composition of intermetallic compound $TiAl_2$, and in the second case — $TiAl_3$. The low (≈ 1.2 wt.%) manganese content of the seam can be explained by evaporation of magnesium from the seam metal during heating and melting of the filler alloy in vacuum, this causing destruction of the aluminium oxide film on the filler alloy surface.

The strength values of the brazed joints made by using Mg-containing filler alloy TiBrazeAl-665 and filler alloy AMg6 are almost identical and equal to 82–83 MPa. Resulting strength of the brazed joints is suitable for brazing of honeycomb and lamellar-ribbed structures, as well as for brazing of sheet items with a large contact area.

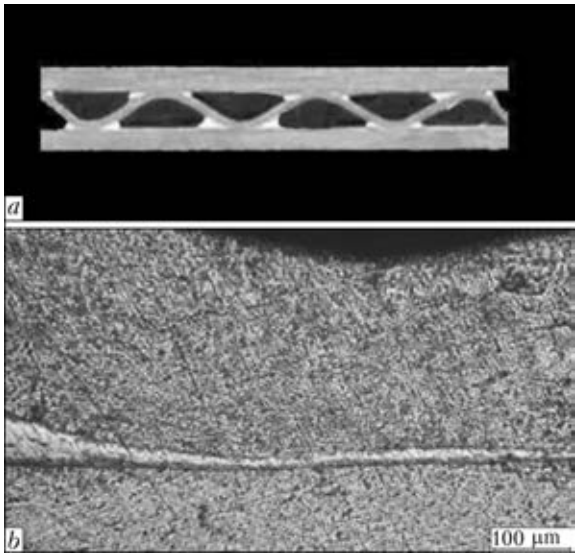

Figure 2. Fragment of a high-efficiency lamellar-ribbed heat exchanger (alloy VT1-0) made by using brazing filler alloy AMg6 (*a*), and microstructure (×100) of region of the joint (*b*) (vacuum $5 \cdot 10^{-5}$ mm Hg, container with getter, T_{br} = = 680 °C, t = 3 min)

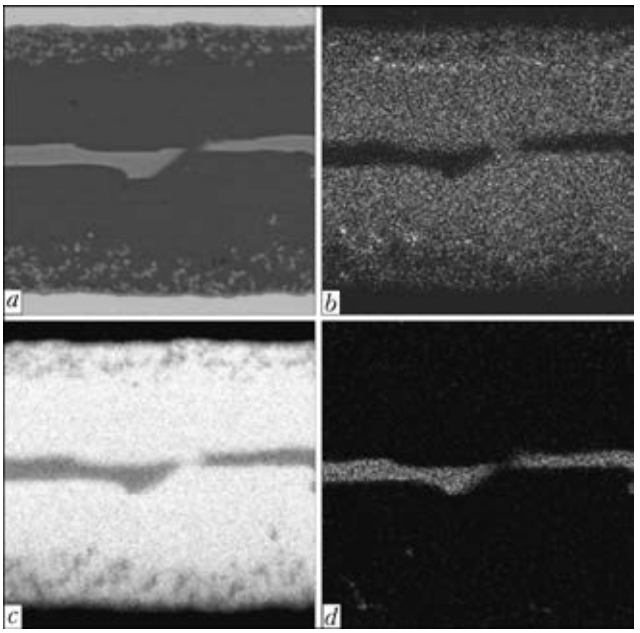

Figure 3. Microstructure of region of the joint (*a*), and distribution of magnesium (*b*), aluminium (*c*) and iron (*d*) in the brazed joint on titanium alloy VT1-0 made by using filler alloy AMg6 (T_{br} = 685 °C, t = 3 min, vacuum $5 \cdot 10^{-5}$ mm Hg)

The experiments on brazing of sections of lamellar-ribbed heat exchangers by using aluminium alloy AMg6 showed that the brazed seams are dense and defect-free (Figure 2, *a*). Analysis of microstructure of the brazed joints revealed that thickness of the intermetallic interlayer is maximal in a region of fillets of the joint and does not exceed 20 μm, and that there is almost no erosion in the base metal (Figures 2, *b* and 3, *a*, *c*).

The central part of the seam is a solid solution of magnesium in aluminium (the magnesium content is up to 1.2 wt.%). The light interlayer along the seam axis is formed by the phase enriched with iron (up to 8.66 wt.%).

Conclusions

1. Analysis of the investigation results shows that aluminium filler alloys based on the Al–Mg system (AMg6, TiBrazeAl-665) are suitable for ensuring sound brazed joints on titanium alloys.

2. In brazing of models of sections of titanium lamellar-ribbed heat exchangers by using filler alloy AMg6 at T_{br} = 680 °C for 3 min the dense and defect-free joints were produced, having a strength value sufficient for this type of the items.

1. Lashko, N.F., Lashko, S.V. (1977) *Brazing of metals*. Moscow: Mashinostroenie.
2. Shapiro, A.E., Flom, Y.A. (2007) Brazing of titanium at temperatures below 800 °C: Review and prospective applications. *http://*www.titanium-brazing.com/publications. DVS-Manuscript_1020-Copy2-19-07.pdf
3. Kimbal, C.E. (1980) Acoustic structures in producing titanium honeycomb acoustic cylinders. *Welding J.*, 59(**10**), 26–30.
4. Nesterov, A.F., Dolgov, Yu.S., Telkov, A.M. (1985) Brazing of titanium structures with aluminium filler alloys. In: *Filler alloys for brazing of modern materials*. Kiev: PWI, 39–45.

Received 16.11.2012

NEWS

Technology and Equipment for Manufacture of Spirally-Welded Pipes of 75–460 mm Diameter

In manufacture of pipes the coiled strips of 100 or 200 mm width are used. The process of pipe manufacture is continuous, consisting in forming of a metallic strip in special devices with a simultaneous welding of edges being joined and next automatic cutting of pipes for measured length without interruption of the welding process. The metals being joined: black low-carbon steel, zinc-plated or aluminized steel (almost without losses of anticorrosion properties), stainless steel, aluminium. To join edges, the arc welding is used if the process efficiency of 3–4 m/min is required, or high-frequency welding if the higher efficiency of 30–40 m/min is required. Using this type of welding no auxiliary consumables (gas, flux, wire) are required.

Technical characteristics of equipment

Pipe wall thickness, mm	0.5±3.5
Speed of pipe outlet, m/min	1±12
Efficiency, km of pipes per shift	0.1±1.5
Capacity of power sources, kW	20±250
Capacity of electric drive, kW	up to 8
Length of pipes, m	2±6 and more
Mains voltage, V	380

Field of application. Machine building, construction, agriculture.

Efficiency:

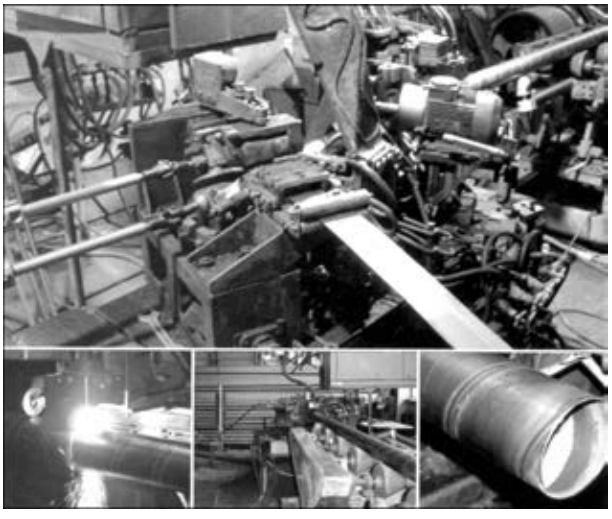

• in case of application of electric arc welding – 100–200 m of pipe per shift;

• in case of application of high-frequency welding – up to 1500 m of pipes per shift.

Payback. The term of payback of equipment depends on annual program of pipes output and is 1 ± 2 years.

RULES FOR JOURNAL AUTHORS

«Avtomaticheskaya Svarka» is Published Monthly Since 1948 in Russian, ISSN 005-111X;
«The Paton Welding Journal» is Published Since 2000 in English, ISSN 0957-798X
(Translation of «Avtomaticheskaya Svarka» Journal Into English)

Publication of Articles in Journal is Free of Charge, the Fee is not Paid

1. Standard volume of article shall be 8–10 pages of text including tables, references, 5–6 figures (the volume of review article can be increased up to 12–14 pages). Text shall be printed at 1.5 spacing by Times New Roman, 12 type size.

Information should be described briefly, without repetition of data of tables and figures in the text. References should be given for literature, tables and figures.

Figures should not have the data of secondary importance. Physical units and symbols should be presented using International System of Units SI.

Publication of article will be accelerated if to send it in electron form by E-mail in Word for Windows format. Illustrations shall be presented in separate files in format *.tif (300 dpi) for raster graphics or *.cdr (versions of not higher than 11.0, 600 dpi) for vector graphics.

2. The article should not have more than 5 authors (the rest ones, participating in the work, can be mentioned in footnote). Information about author should include affiliation and address, position, scientific title, address, telephone. In addition, the postal address of organization should be given in Russian and English (to take better from official site) and E-mail of one of authors (organization).

3. The article should be added with abstract and key words (from 7 to 10). The abstract (of 1400–1600 characters at a single space between words) should completely enough to describe the article content. It should include the aims and tasks, methods, results, field of application, conclusions.

4. Each article should have a bibliography list, including of not less than 8–10 references (own works of authors should amount to not more than one/fourth of the list; references to sources since 2000 are obligatory).

The literature cited in the article should be prepared in the following way:

for books: name, initials of author(s), full title, city, publishing house, year of edition, total number of pages;

for journal articles: name, initials of author(s), title of article, journal, year of publication, number, volume or issue, pages; foreign publications should be given in the language of original;

for articles in collection: title of article, authors, name of collection, number of issue (or volume), place of publication, publishing house (or publishing organization), pages of beginning and end of article; for internet-references: name of resource, access mode.

5. Manuscript of article should be signed by all the authors (or by one author on behalf of author's group). Manuscript should enclose the license agreement for transfer of the author's rights to the editorial board for the article publication. Form of agreement is given on site: www.paton.kiev.ua or can be sent by the editorial board by E-mail (by request). Non-conformity of materials to the above-mentioned requirements (items 1–5) may serve a reason to refuse a manuscript for publication.

6. Authors of the article can receive free of charge one copy of appropriate numbers of journals «Avtomaticheskaya Svarka» and «The Paton Welding Journal» (by request).

Contacts of Editorial Board of Journal «Avtomaticheskaya Svarka» and «The Paton Welding Journal»:
Tel.: (38044) 200-63-02, 200-82-77
E-mail: journal@paton.kiev.ua; www.paton.kiev.ua; www.rucont.ru

SUBSCRIPTION
FOR «THE PATON WELDING JOURNAL»

If You are interested in making subscription directly via Editorial Board, fill, please, the coupon and send application by fax or e-mail.

The cost of annual subscription via Editorial Board is $348.

Telephones and faxes of Editorial Board of «The Paton Welding Journal»:

Tel.: (38044) 200 82 77, 200 81 45

Fax: (38044) 200 82 77, 200 81 45.

«The Paton Welding Journal» can be also subscribed worldwide from catalogues of subscription agency EBSO.

SUBSCRIPTION COUPON

Address for journal delivery _____

Term of subscription since _____ **20** **till** **20**

Name, initials _____

Affiliation _____

Position _____

Tel., Fax, E-mail

Subscription to the electronic version of «The Paton Welding Journal» can be done at site: *www: rucont.ru*

We offer for the subscription all issues of the Journal in pdf format, starting from 2009. You can subscribe to individual issues or to the entire archive including all issues over a period of 2009–2011. The subscription is available for natural persons and legal entities.

ADVERTISEMENT
IN «THE PATON WELDING JOURNAL»

External cover, fully-colored:
First page of cover (190×190 mm) – $700
Second page of cover (200×290 mm) – $550
Third page of cover (200×290 mm) – $500
Fourth page of cover (200×290 mm) – $600

Internal cover, fully-colored:
First page of cover (200×290 mm) – $350
Second page of cover (200×290 mm) – $350
Third page of cover (200×290 mm) – $350
Fourth page of cover (200×290 mm) – $350

Internal insert:
Fully-colored (200×290 mm) – $300
Fully-colored (double page A3) (400×290 mm) – $500
Fully-colored (200×145 mm) – $150
Black-and-white (170×250 mm) – $80
Black-and-white (170×125 mm) – $50
Black-and-white (80×80 mm) – $15

- Article in the form of advertising is 50 % of the cost of advertising area
- When the sum of advertising contracts exceeds $1000, a flexible system of discounts is envisaged

Technical requirement for the advertising materials:
- Size of journal after cutting is 200×290 mm
- In advertising layouts, the texts, logotypes and other elements should be located 5 mm from the module edge to prevent the loss of a part of information

All files in format IBM PC:
- Corell Draw, version up to 10.0
- Adobe Photoshop, version up to 7.0
- Quark, version up to 5.0
- Representations in format TIFF, color model CMYK, resolution 300 dpi
- Files should be added with a printed copy (makeups in WORD for are not accepted)